Collapse Safety Assessment of Steel Multi-storey Buildings with Friction Sliding Braced Frames and Backup Moment Resisting Frames as a Dual System

Derek Millichamp

A Thesis

in

The Department

of

Building, Civil, and Environmental Engineering

Presented in Partial Fulfillment of the Requirements

for the Degree of Master of Applied Science (Civil Engineering) at

Concordia University

Montreal, Quebec, Canada

December 2021

Concordia University

School of Graduate Studies

This is to certify that the thesis prepared

By: Derek Millichamp

Entitled: Collapse Safety Assessment of Steel Multi-storey Buildings with Friction Sliding Braced Frames and Backup Moment Resisting Frames as a Dual System

and submitted in partial fulfillment of the requirements for the degree of

Master of Applied Science (Civil Engineering)

complies with the regulations of the University and meets the accepted standards with respect to originality and quality.

Signed by the final Examining Committee:

Dr. Anjan Bhowmick ______________________ Chair

Dr. Emre Erkman ______________________ Examiner

Dr. Anjan Bhowmick ______________________ Examiner

Dr. L. Tirca ______________________ Supervisor

Approved by: ______________________

Chair of Department or Graduate Program Director

____

Dean of Faculty

Date: ______________________

Abstract

Collapse Safety Assessment of Steel Multi-storey Buildings with Friction Sliding Braced Frames and Backup Moment Resisting Frames as a Dual System

Derek Millichamp

In the early 1980's, Concordia University's library building saw the first application of cross-braced Pall friction dampers (PFD). Although PFDs have evolved and improved, including the friction material used, development of the design procedure has been limited. Using a recently proposed force-based design method and considering detailed computational and modeling techniques, three types of seismic force resisting systems are presented herein: the bare Friction Sliding Braced Frame (FSBF), Friction Sliding Braced Frame with Continuous Columns including gravity columns (FSBF-CC) and Dual FSBF system (D-FSBF). Installing backup MRFs in parallel with a primary FSBF can provide the structure with load path redundancy and elastic-frame action, while taking advantage of the large energy dissipation capacity of PFDs.

The objectives of this research are three-fold: 1) to develop an accurate nonlinear model for PFD that is capable of bearing and failure, 2) to quantify the ductility-related force modification factor, R_d, for the proposed seismic force resisting systems: bare FSBF, FSBF-CC, and D-FSBF and 3) assess fragility and collapse safety of low-rise and middle-rise buildings braced with the proposed seismic force resisting systems subjected to crustal and subduction ground motions.

These objectives are carried out using 2-D numerical models developed in OpenSees for 4- and 8-storey prototype buildings located on Site class C in Vancouver, B.C. A force-based design method was developed in line with NBCC 2015 and CSA/S16-14 standard requirements. Considering the similarity with buckling restrained braced frames (BRBF), design was conducted for R_dR_o=4 and R_dR_o=5. All buildings were subjected to short duration crustal and long duration subduction ground motions, and a discussion regarding the slip length demand of PFD was provided.

From nonlinear response history analysis of 4 and 8-storey FSBF buildings (R_dR_0=4), it was found that the bare FSBF was structurally unstable and reached collapse prior to design level under the ground motion suites. Therefore, using the bare FSBF is not recommended. The 4-storey FSBF-CC building (R_dR_0=4) prevented collapse at design level, however experienced excessive residual drift, while the 8-storey FSBF-CC building reached collapse at design level under both crustal and subduction ground motions. Thus, the FSBF-CC system can be used only for low-rise buildings, but caution should be taken.

Using the Dual FSBF system composed of FSBF and a backup MRF, designed for an additional 25% base shear and two sets of R_dR_0 =4 and 5, it resulted that both 4-storey and 8-storey D-FSBF buildings showed sufficient margin of safety under both ground motion suites. Subsequently, when increasing the building height (e.g. the 8-storey building), the ductility-related force modification factor, R_d = 4 is recommended. The Dual FSBF system is recommended to brace low-rise and middle-rise buildings located in subduction zone, as Cascadia subduction zone, where megathrust earthquakes could occur.

Acknowledgement

I would like to thank my thesis supervisor Dr. Lucia Tirca for her unending support throughout the years. She has been the most formative figure in my understanding of the material presented herein, and her inexhaustible passion for research has been a true inspiration. She has provided me with the knowledge and abilities that have formed me into the engineer that I am today, and I am eternally grateful.

Furthermore, I would like to thank Concordia University and its staff. The majority of this research was conducted remotely during a global pandemic, and though I did not have the opportunity to build the relationships with my fellow colleagues as I would have wanted, I feel as though I was provided with the tools and services needed to complete my research effectively. Also, I would like to thank my colleagues and friends: Yudong Wang, Siamak Pejmanfar, Anastasia Athanasiou, and Lizhu Chen. It was a pleasure getting the know you and I hope we continue to cross paths in the future!

To my family, I would like to thank you for your support and encouragement. In a different world, under different conditions, with a different family, I would not be where I am today. To my mother, who has always taught me to approach things with a sense of childish enthusiasm and passion, to my father who has always grounded me, and to my sister who has always been there to make sure that I don't lose sight of the important people in my life; I would not be the person I am today without your love and patience.

Last, but certainly not least, to my partner Mel. I cannot even begin to describe how important your never-ending love and support has been over the last decade. With the greatest level of gratitude, I dedicate the entirety of the work presented herein to you. No one is more deserving of the credit. Without your encouragement, this research would never have entered the world in its current form, and it has been an honour and a privilege to have shared this journey with you. I love you!

Table of Contents

List of Figures

List of Tables

List of Symbols

m – Fatigue ductility exponent

$\ddot{u}_g$ – Ground acceleration

c - Damping

$\dot{u}$ – Velocity

k – Stiffness

u – Displacement

f_s – Elastic or inelastic force due to stiffness and displacement

E_S – Recoverable strain energy

E_D – Damping energy

E_Y – Yielding Energy

E_K – Kinetic Energy

E_I – Input Energy

μ – Coefficient of friction

μ_D – Dynamic coefficient of friction

μ_s – Static coefficient of friction

N – Normal Force

F_f – Force of friction

A_r – Real contact area of friction

σ_0 – Material penetration hardness

s – Shear through cold-weld junction

n – Number of asperities

r – radius/half-width of asperity

h - height of asperity

F_a – Friction force due to abrasion

F_p – Friction force due to penetration

μ_t – Ductility factor of first storey over roof displacement

χ – Moment-curvature

L_p – Length of plastic hinge

θ_p – Pre-capping plastic rotation

θ_{pc} – Post-capping plastic rotation

Λ – Cumulative plastic rotation

ϵ_i – Strain amplitude

$n(\epsilon_i)$ – number of cycles at the strain amplitude ϵ_i

$N_f(\epsilon_i)$ – Total number of amplitude cycles at amplitude ϵ_i necessary to cause failure

DI – Damage index

ϵ_0 – Fatigue ductility coefficient

$\Delta\epsilon_0$ – Rate of material degradation

ϵ_{0min} – Strain at which local buckling is initiate

L_m – Buckling wavelength of flange

L_v – Effective length of beam

λ_f – flange slenderness

$S_a(T_1)$ – First-mode spectral acceleration

$\Phi[]$ – Lognormal cumulative distribution function

m_R – Median of the fragility function

β_R – Logarithmic standard deviation

e – Prediction error (residuals)

$\hat{\sigma}_e$ – Standard deviation of the residuals

β_{RR} – Aleatoric uncertainty

β_{RU} – Epistemic uncertainty

$\beta_{D|S_a}$ – Seismic demand uncertainty

β_C – Capacity uncertainty

s^2 – Standard error

T_a – Fundamental period of structure

F_{slip} – Slip force in Pall Friction Dampers

C_r – Compressive resistance

φ – Factor for the resistance of steel

r – radius of gyration

λ – member slenderness

F_y – yield strength of steel

E – elastic modulus

Δ_{slip} – slip length for Pall Friction Damper

C_u – probable compressive strength of steel member

M_f – factored moment

M_r – moment resistance

Z – plastic modulus of steel

A – Area

T_r – tensile resistance

T_f – factored tensile load

R_{jb} – Joyne-Boore distance

t_d – Trifunac duration

$\bar{V}_{s30}$ – average shear wave velocity

T_m – mean ground motion period

T_p – principal ground motion period

M_w – moment magnitude of ground motion

PGA – peak ground acceleration

PGV – peak ground velocity

ζ – critical damping ratio

B_r – factored bearing resistance of steel

V_r – factored shear resistance of steel

A_b – area of bolt

A_{ne} – net effective area

t_g – thickness of gusset plate

W_w – Whitmore width

F_u – ultimate strength of steel

Chapter One

Introduction

1.1 General

In the aftermath of the 6.3 magnitude earthquake in Christchurch, New Zealand (2011), several unreinforced masonry buildings, timber buildings, and some reinforced concrete collapsed. Analysing the economic loss in New Zealand new attitudes and policies suggest a shift in perception in the importance of seismic resiliency. The city's reconstruction predominantly used steel structures such as Buckling Restrained Braced Frames (BRBF), Moment Resisting Frame (MRF), MRF with friction connections, Eccentrically Braced Frames (EBF), Rocking Frames, and Concentrically Braced Frames (CBF). Forensic engineering reports have shown that, with rare exception, steel buildings performed the best in comparison with reinforced concrete buildings (Clifton et al. 2011). This along with steel's ability to fast-track construction and reduced risk when affected by liquefaction (e.g. steel structures possess lower specific weight) has brought steel structures to prominence in Christchurch. (Bruneau and MacRae 2017).

Some of the most widely used seismic force resisting systems are the steel Concentrically Braced Frame (CBF), the Moment Resisting Frame (MRF), and newly proposed low-damage steel structures such as MRFs with sliding hinge joints and rocking frames. It is worth mentioning that CBFs are known for their high stiffness and moderate ductility, and MRFs for their high ductility. Among the energy dissipating devices used in steel structures is the Pall friction damper (Pall et al. 1980; Pall and Marsh 1982) which has been frequently employed in buildings in Canada (Aiken et al. 1988; Balazic et al. 2011; Pasquin et al. 2004). Primarily, these devices were employed to retrofit steel and concrete structures. Early development of Pall friction dampers (PFD) were characterised as a cost-effective device with a stable hysteretic shape with the ablility to improve the seismic performance of moment frames. However, a stable coefficient of friction and clamping normal force over a long period of time has proven to be difficult in practice and has limited the device's adoption (Symans et al. 2008). Furthermore, the traditional PFD lacks the ability to self-center without an external mechanism. To solve this issue, development of self-centering friction springs have been studied, however these devices have comparatively limited dissipative capacity compared to traditional friction devices due to their flag-shaped hysteretic response (Filiatrault et al. 2000; Nims et al. 1993). Currently, the National Building Code of Canada (NBCC 2015) and the CSA S16-14 (CSA S16 2014) standard do not have special provisions for the design of friction dampers. However, there are some guidelines in North America that were developed based on the energy-based design methods (ASCE 2000, 2013; FEMA 2000, 2003).

To solve the issues regarding large permanent deformation of BRBFs, dual systems have been introduced where a backup MRF is designed to provide redundancy and force redistribution through frame-action (Kiggins and Uang 2006; Sahoo and Chao 2015; Whittaker 1990). Although dual systems have been used in the past, they have now been adopted in modern North American codes (ASCE 2000; NBCC 2015), where the backup moment frame is designed for 25% design base shear. If combined with traditional friction devices, structures could be given the ability to maintain large hysteretic energy dissipation, while limiting residual drift, and adding little additional stiffness to the structure.

1.2 Objectives and Scope

The objectives and scope of this research are as follows:

- To present and validate a force-based design method for Friction Sliding Braced Frames (FSBF) that is compatible with the current NBCC (2015) and CSA/S16-14 standard requirements. This requires evaluation of the ductility-related force modification factor (R_d) and overstrength-related force modification factor (R_o) of the system.

- To develop a nonlinear model for friction dampers that is able to replicate the bearing phase at the limits of the devices designed slip length.

- To develop and compare the nonlinear seismic response of bare Friction Sliding Braced Frames (FSBF) against FSBFs with continuous columns including gravity columns (FSBF-CC) and Dual systems (D-FSBF) composed of FSBF and backup MRF, under crustal and subduction ground motions. Only low-rise and middle-rise buildings are considered.

- To assess the probability of exceedance of specific performance objectives by means of fragility analysis and collapse safety analysis of the seismic force resisting systems presented under the crustal and subduction-zone ground motions.

1.3 Description of Methodology

To achieve the aforementioned objectives, the following steps were carried out:

- A force-based design method was developed according to the NBCC 2015 and CSA/S16-14 standard requirements in order to design the FSBF and sizing the PFDs.

- 2-D nonlinear models were developed in OpenSees for FSBF, FSBF-CC, and D-FSBF for a 4 and 8-storey building configuration. Behaviour of the friction dampers were developed using parallel gap materials to simulate bearing, and a Bouc-Wen material to simulate the elastic-perfectly-plastic behaviour of PFD.

- All models and configurations were analyzed under two ground motion suites with 7 ground motions in each suite that were selected to have the soil properties, magnitudes, and distances realistic to the building location conditions in Vancouver, BC, Canada. Incremental scaling of these ground motions was done until collapse was exhibited. The investigated parameters are the structure's interstorey drifts, residual interstorey drifts, and floor accelerations.

- Using the collapse safety criteria and the methodology provided in FEMA P-695 (FEMA 2009) the proposed seismic coefficients (R_dR_o) were validated for the low-rise (4-storey) and middle-rise (8-storey) buildings. The failure criterion was defined and a secondary ductile fuse was proposed to act at a targeted slip force. The secondary ductile fuse is developed within the PFD-to-frame gusset plate bolted connections. In addition, the reparability limit state was proposed.

- The seismic performance of both low-rise and middle-rise buildings with focus on Dual FSBF was carried out by means of collapse safety analysis.

1.4 Thesis Organization

This thesis is organized into seven chapters:

- Chapter 1 includes the objectives, methodologies, and organization of the thesis.

- Chapter 2 contains the literature review beginning with a discussion on energy dissipation and friction theory. A brief discussion on the current state-of-the-art of Pall Friction

Dampers (PFDs) is then introduced starting with the earliest type of PFD inserted at the intersection of X-braces designed as tension-only braced frame. Later on, Pall developed the friction damper installed in-line with diagonal braces. Closely related, in behaviour, to the devices studied herein, the slotted-bolted connection was discussed to give a more complete history of these types of devices. A review of the literature on structural systems with continuous columns was also presented, as well as the benefits of dual systems. Modelling of moment frames in finite element analysis programs was presented as well as the literature on incremental dynamic analysis and fragility analysis.

- Chapter 3 presents the design methodology used for the design of FSBFs and describes the requirements employed from the NBCC 2015 and CSA/S16-14 standard that refer to the design of steel braced frames. The building descriptions for the studied 4 and 8-storey building prototypes were presented, including the loads and member sections. Modeling of PFD in OpenSees is described and the results for the 4 and 8-storey bare FSBFs at design level as well as IDA were also presented.

- Chapter 4 includes a discussion on the inclusion of a secondary ductile fuse by means of gusset plate failure to limit excess force triggered into the columns. Continuous column models and results are shown at design level and incremental dynamic analysis are presented for FSBF-CC models.

- Chapter 5 focuses on the design of the dual system (D-FSBF) according to NBCC and CSA/S16 standard. Building configuration and modeling approaches are presented. Design level results are shown, as well as the results at the defined reparability limit state and near collapse limit state. A discussion of the ductility reduction factor is included to show its effect on the building's response.

- Chapter 6 evaluates the structures through collapse safety analysis according to the methodology presented in FEMA P-695 (FEMA 2009) for all building types subjected to both crustal and subduction-zone earthquakes, typical for Vancouver, BC.

- Chapter 7 concludes the research and proposes future work.

Chapter Two

Literature Review

2.1 Energy Dissipation

The first design guidelines for displacement-dependent devices, such as Pall Friction Dampers, were introduced in FEMA 356 (FEMA 2000) and FEMA 450 (FEMA 2003). These guidelines were then incorporated into ASCE 41-13 (ASCE 2013) and ASCE 7-10 (ASCE 2000). These guidelines are energy-based (e.g. the Work-Energy method) and no force-based guidelines are presented, as per the approach used in building codes for conventional structural systems. Thus, the seismic forces required to design the PFDs are calculated by taking into consideration the damping amount provided by the energy dissipation devices.

Inelastic systems exhibit energy dissipation through both viscous and yielding damping mechanisms. The input energy into the building is due to ground motion and is defined by the equation of motion Eq. (2.1.1). Herein, the motion of a body is defined by the earthquake input energy, $m\ddot{u}_g$, where $\ddot{u}_g$is the ground acceleration of the ground motion; and the output energy is caused by the kinetic force which is dependent on acceleration, $m\ddot{u}(t)$, the velocity-dependant damping force, $c\dot{u}(t)$, and the stiffness proportional displacement-dependent force, $ku(t)$. For inelastic systems, the displacement-dependent force, $ku(t)$, can be replaced with an implicit force-deformation function as defined in Eq. (2.1.2).

Elastic System: $$m\ddot{u}(t) + c\dot{u}(t) + ku(t) = -m\ddot{u}_g(t) \qquad (2.1.1)$$

Inelastic System: $$m\ddot{u}(t) + c\dot{u}(t) + f_s(u) = -m\ddot{u}_g(t) \qquad (2.1.2)$$

Energy is based on a principle of work where force is integrated over its displacement. Since each term in the equation of motion (Eq. (2.1.1)) represents a corresponding force, integrating each term over displacement as per Eq. (2.1.3) describes the energy dissipated. Thus, in terms of energy, the recoverable strain energy is E_s (Eq. (2.1.4)), the energy dissipated by damping is E_D (Eq. (2.1.5)), energy dissipated by yielding is E_Y (Eq. (2.1.6)), energy dissipated through kinetic energy is E_K (Eq. (2.1.7)), and input energy E_I is as per Eq. (2.1.8) (Chopra, 2012).

Elastic systems do not have energy dissipation through a yielding mechanism but only through the kinetic, strain, and damping energy as shown in the Figure 2.1-1. Thus, supplemental damping, as in the modifcation of the term $E_D(t)$, will in turn decrease the other terms on the left hand side of Eq. (2.1.8), so that the output energy balances with the input balance. This phenomenon is shown in Figure 2.1-1 b), where the inclusion of a yielding mechanism changes values regarding strain, damping, and kinetic energy.

$$\int_0^u m\ddot{u}(t)du + \int_0^u cu(t)du + \left[\int_0^u f_s(u)du - E_s(t)\right] = -\int_0^u m\ddot{u}_g(t)\, du \qquad (2.1.3)$$

$$E_s(t) = \frac{[f_s(t)]^2}{2k} \qquad (2.1.4)$$

$$E_D(t) = \int_0^t c[\dot{u}(t)]^2 dt \qquad (2.1.5)$$

$$E_Y(t) = \left[\int_0^t \dot{u} f_s(u)dt\right] - E_s \qquad (2.1.6)$$

$$E_K(t) = \frac{m\dot{u}^2}{2} \qquad (2.1.7)$$

$$E_K(t) + E_D(t) + E_S(t) + E_Y(t) = E_I(t) \qquad (2.1.8)$$

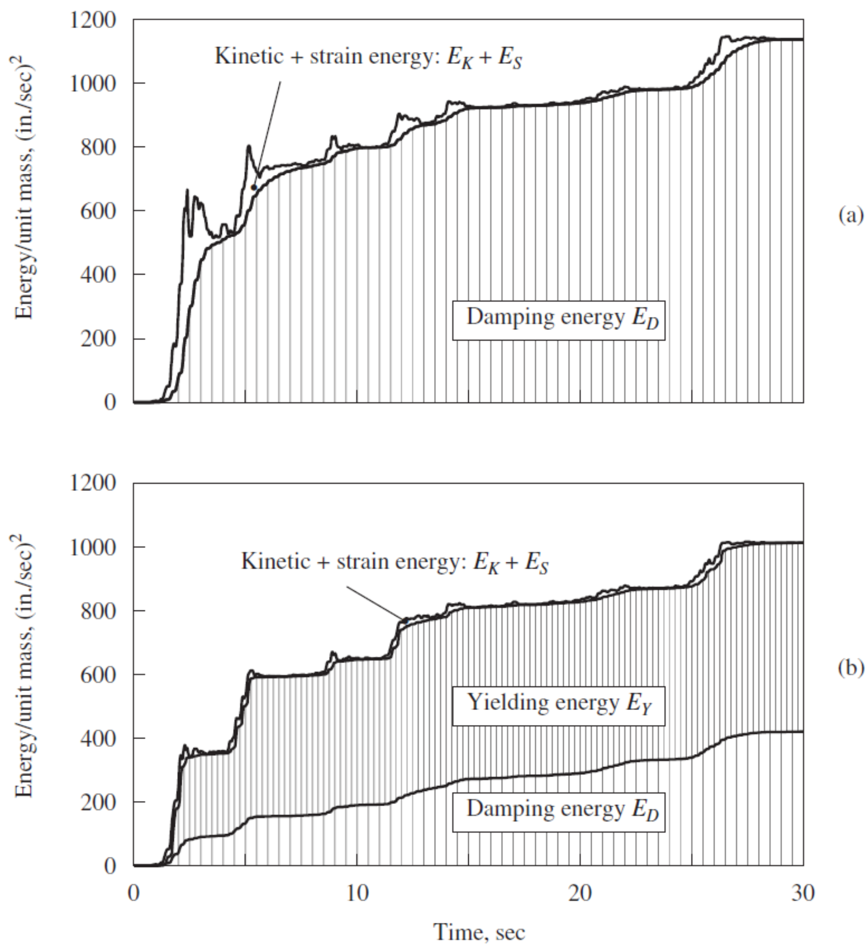

Figure 2.1-1. Energy dissipated over time: a) elastic system; b) inelastic system (Chopra, 2012)

2.2 Tribology – Friction Theory

Tribology is the study of the dynamic interaction between two surfaces, which includes friction, lubrication, and wear. Friction in particular follows three principal laws:

1. Amontons' First Law: Friction is proportional to the applied normal force.

2. Amontons' Second Law: Friction is independent of the apparent contact surface area.

3. Coulomb's Law: Friction is independent of relative velocity for very slow sliding velocity.

Furthermore, the study of friction makes a distinction between two components of dry friction, that is adhesion and plowing. Adhesion is due to the plastic deformation of microscopic impurities called asperities, and plowing is caused by the penetration of a hard metal into a soft metal. (Jaisee et al., 2021; Ludema et al., 1997). The most generalized model for friction, know as Coulomb Friction, is given by Eq. (2.2.1) and Figure 2.2-1, where k is the stiffness. Typically, the coefficient of friction, μ, is dependent on the state of motion; static or dynamic. The static coefficient of friction is typically lower than the dynamic coefficient of friction.

$$F_f = \mu N \tag{2.2.1}$$

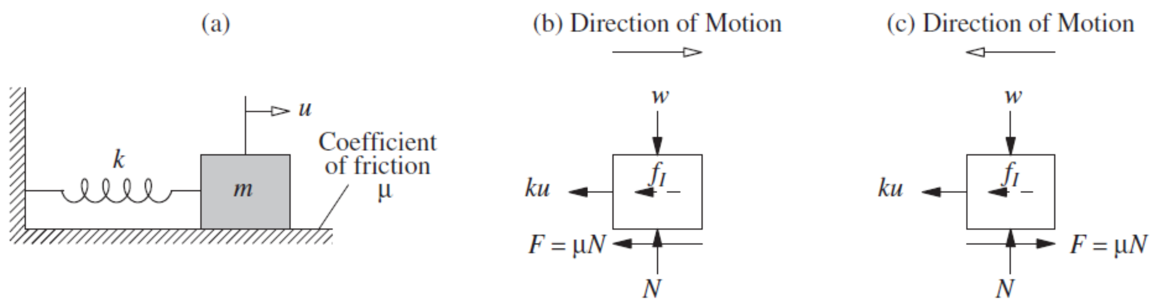

Figure 2.2-1. Basic Friction Model: a) SDOF Model b) and c) Freebody diagrams (Chopra 2012)

However, more elaborate models have been developed in order to create a more complete theory surrounding friction which includes the plowing and the adhesion components. Adhesion has been described by the real contact area, A_r, which is defined in Eq. (2.2.2) as the normal force, N, over the material penetration hardness, σ_0, multiplied by the force required per unit area to shear through the cold-weld junction, s. The cold-weld junction is considered to be the adhesion between the asperities of two surfaces in contact by a normal force (Bowden and Tabor 2001; Ludema et al. 1997). Plowing is defined by the Eq. (2.2.3) where n is the number of asperities, r is the radius/half-width of the asperity, and h is the height of the asperity. Combining the adhesive and plowing forces, the total friction force is provided in Eq. (2.2.4). Plowing is however negligible for the study of dry metallic friction and thus can be neglected where abrasion is considered to be dominant (Jaisee et al. 2021).

$$F_a = A_r s = \left(\frac{N}{\sigma_0}\right) s \tag{2.2.2}$$

$$F_p = nrh\sigma_0 \tag{2.2.3}$$

$$F = F_a + F_p = \left(\frac{N}{\sigma_0}\right) s + nrh\sigma_0 \tag{2.2.4}$$

2.3 Friction Dampers

Pall friction dampers used in structures have been in development since the 1980s and have seen a lot of variation and applications (Pall et al. 1980). A review article, (Jaisee et al. 2021) looked at the current state of the literature on friction dampers and collected 187 research papers between the years 1958-2020 as shown in Figure 2.3-1. Research in these devices has increased greatly since the early 1980s and peaked in 2015-2019.

2.3.1 Brief History on Pall Friction Dampers (PFD)

Pall friction dampers were first introduced for large panel structures between the vertical panel joints (Pall et al. 1980). These connections were referred to as Limited Slip Bolted Joints (LSB) as shown in Figure 2.3-2, where the LSBs were located at the panel joints located at the center of the building. An insert plate is anchored into the concrete of the panels at the joints and bolted once they are erected. High strength bolts were used to clamp the connection plate, the friction material, and the insert plate together. Slotted holes were used to allow adequate displacement and limit bolt bearing. Within this research, some basic friction damper behaviours were established such as the 3 macro stages of the behaviour of LSBs i) Elastic stage ii) Slipping stage and iii) Bolt Bearing stage as shown in Figure 2.3-3 a). In addition, the behaviour of 6 different materials that were tested under monotonic loading are shown in Figure 2.3-3 b).

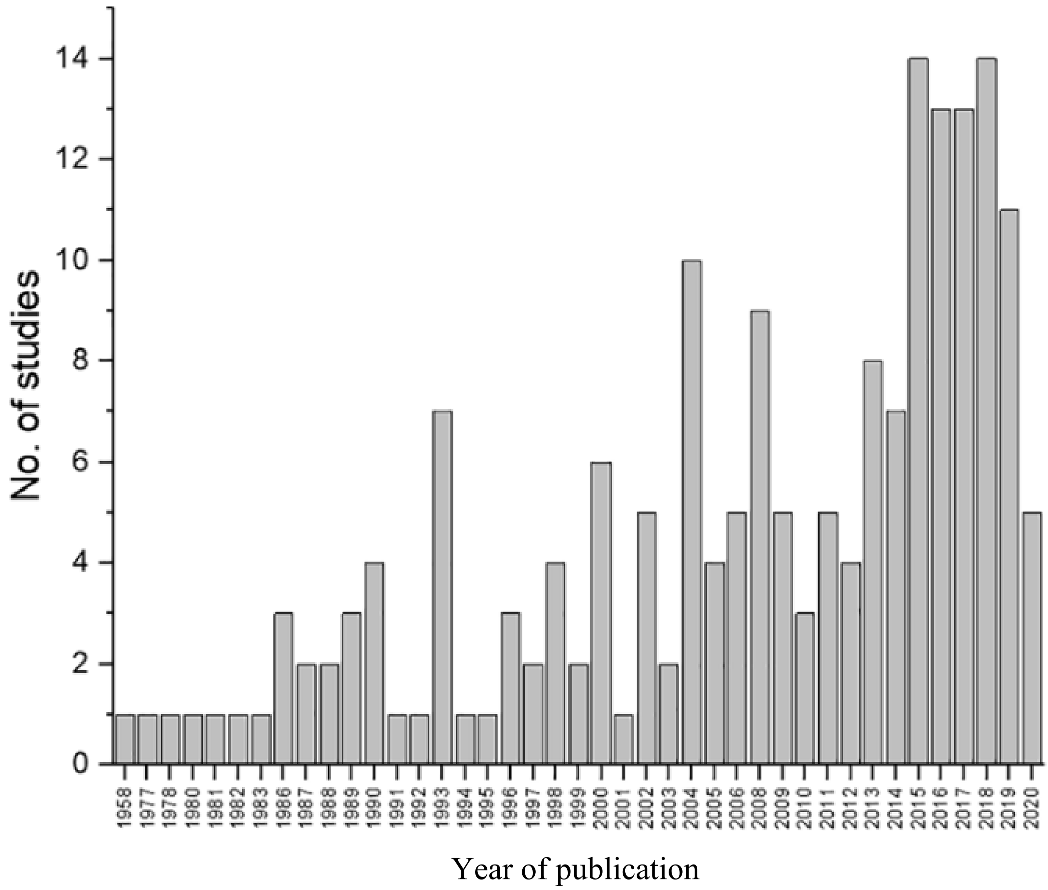

Figure 2.3-1. No. of publications over the years for friction dampers (Jaisee et al. 2021)

Figure 2.3-4 shows the hysteresis behaviour for different friction surface materials tested. It was observed that the break lining pads had a sufficiently high slip load, displacement, and very stable hysteresis response. This was seen as well in the monotonic behaviour in Figure 2.3-3 b). The second-best behaviour was found to be given by the sand blasted surface. The result for the overall structural system is relatively limited since analysis was only done under one ground motion. Furthermore, the optimal slip load was calculated using an energy-based design method where the storey shear flux between the joints in the vertical wall is induced by an inverted triangular load. This results in a single optimal slip force over the entire height of the building for each storey.

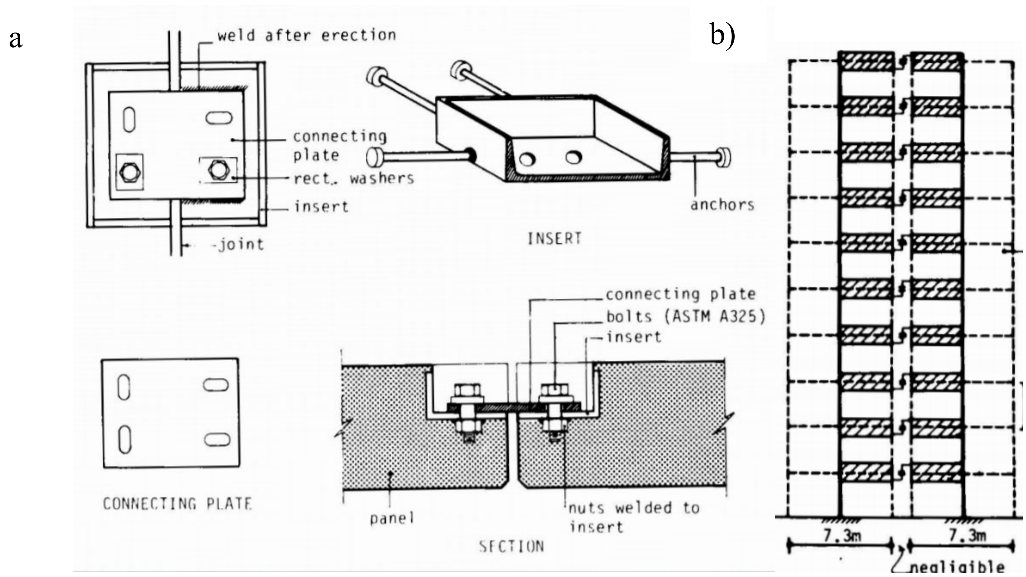

Figure 2.3-2. Limited Slip Bolted (LSB) Joints between vertical panels: a) LSB detailed drawing b) Building elevation with LSB (Pall et al. 1980)

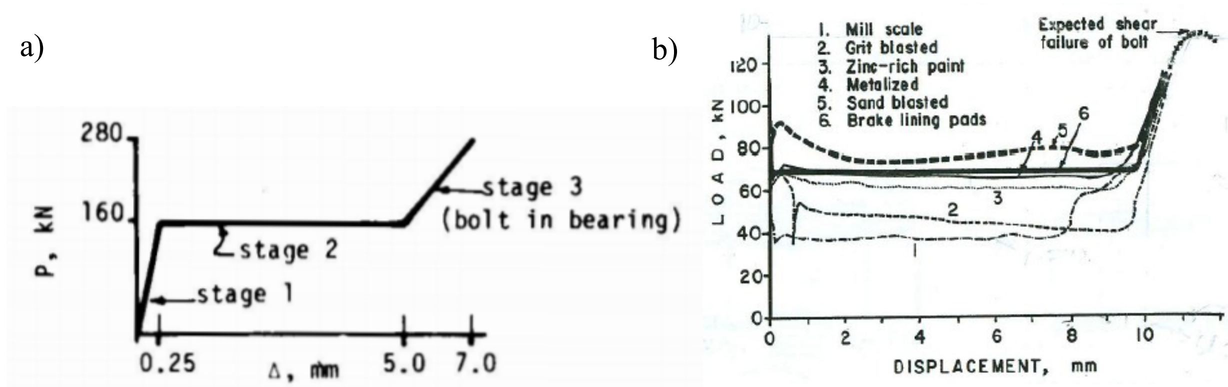

Figure 2.3-3. Monotonic response of LSB including bolt bearing phase: a) Idealized System b) Tests for different friction materials (Pall et al. 1980)

In (Pall and Marsh 1982), the authors discussed the first application of friction dampers in braced framed structures. They considered slender tension-only X-configuration braces with a friction device inserted at the brace intersection. The article focused on a comparison between three building types, Moment Resisting Frame (MRF), Braced Moment Frames (BMF), and Friction Damped Braced Frame (FDBF). The FDBF was equipped with the device shown in Figure 2.3-5 a) where the hysteretic behaviour is described by Figure 2.3-6 c). This device limits all friction dissipation to be located during the tension phase. Therefore, although the device response is not symmetric between compression and tension regions, since this is a tension-only device for tension-only braces, it is symmetric for both positive and negative displacement and contained in the tension region. A time step diagram of the device is shown in Figure 2.3-7.

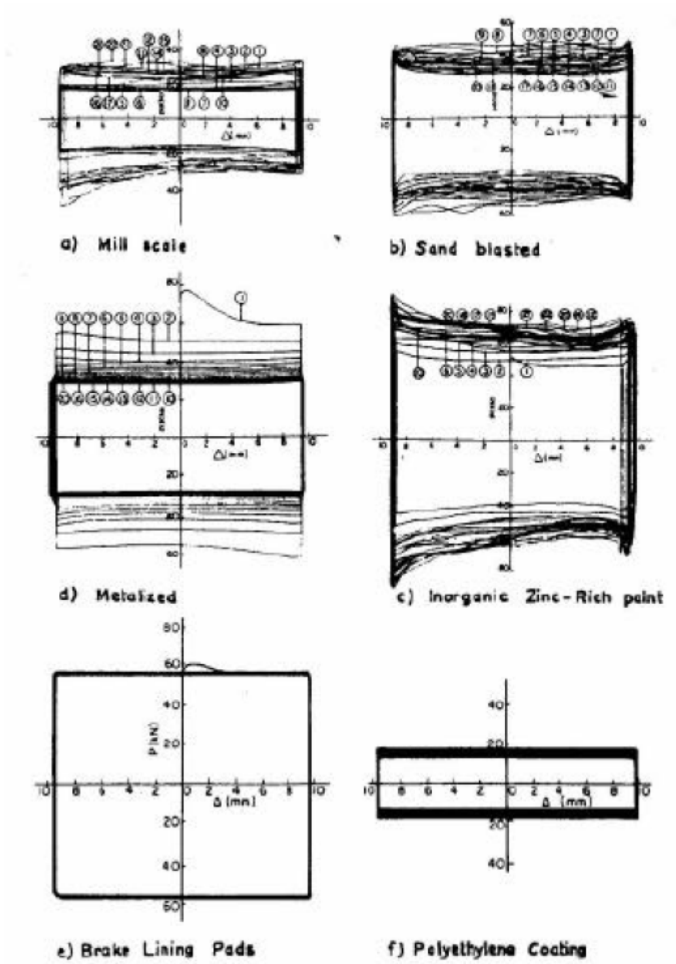

Figure 2.3-4. Hysteresis diagrams for different friction surface materials (Pall et al. 1980)

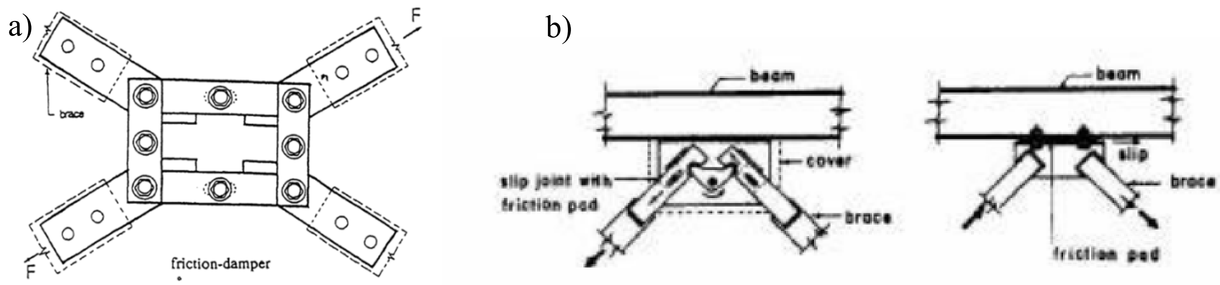

Figure 2.3-5. Friction devices for tension-only brace configurations: a) X-bracing (Jaisee et al. 2021) and b) chevron bracing (Pall and Marsh 1982)

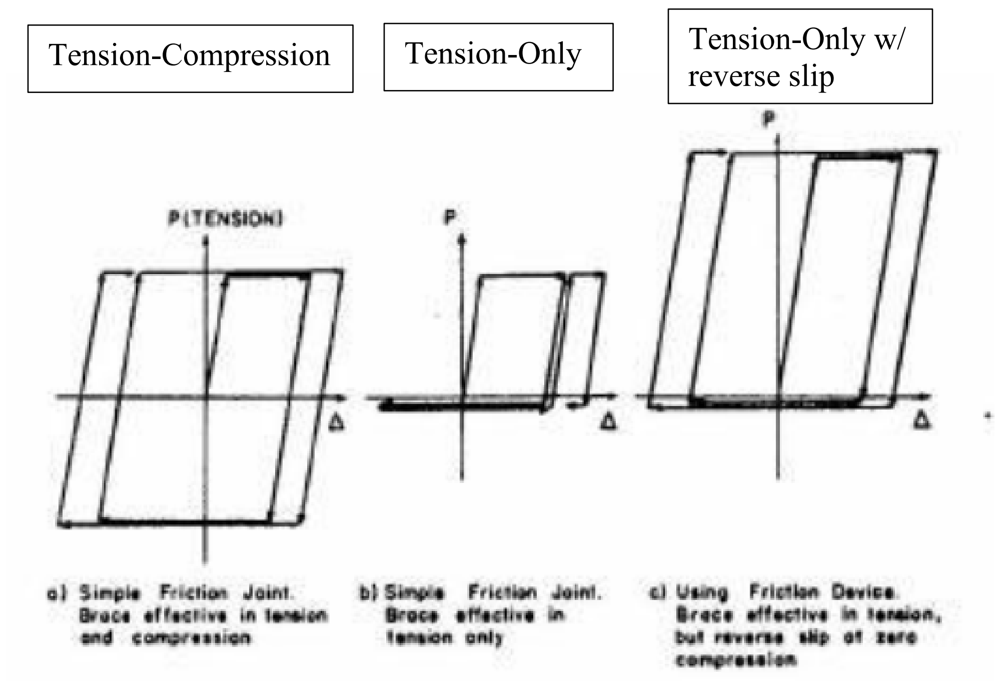

Figure 2.3-6. Hysteretic response of friction device: a) tension-compression b) tension-only c) tension-only braces with reverse slip at zero compression (Pall and Marsh 1982)

The FDBF has the same member sections as the BMF (e.g. the same braces, beams, and columns), and the MRF contained the same beams and columns as the other two systems. In other words, the friction devices were contained in a structure that also had a moment frame. Thus, little residual drift was observed in the time-history analysis. This, however, does not consider a situation where the devices are to be installed in a system without a parallel moment frame. For the one ground motion considered, it was observed that no sliding occurred in the Pall friction damper while yielding did occur in the beam members of the MRF and the BMF. It is useful to note that even as early as the first studies of these systems, the friction devices were installed within moment frames (Aiken et al. 1988; Balazic et al. 2011; Pall and Marsh 1982; Pasquin et al. 2004).

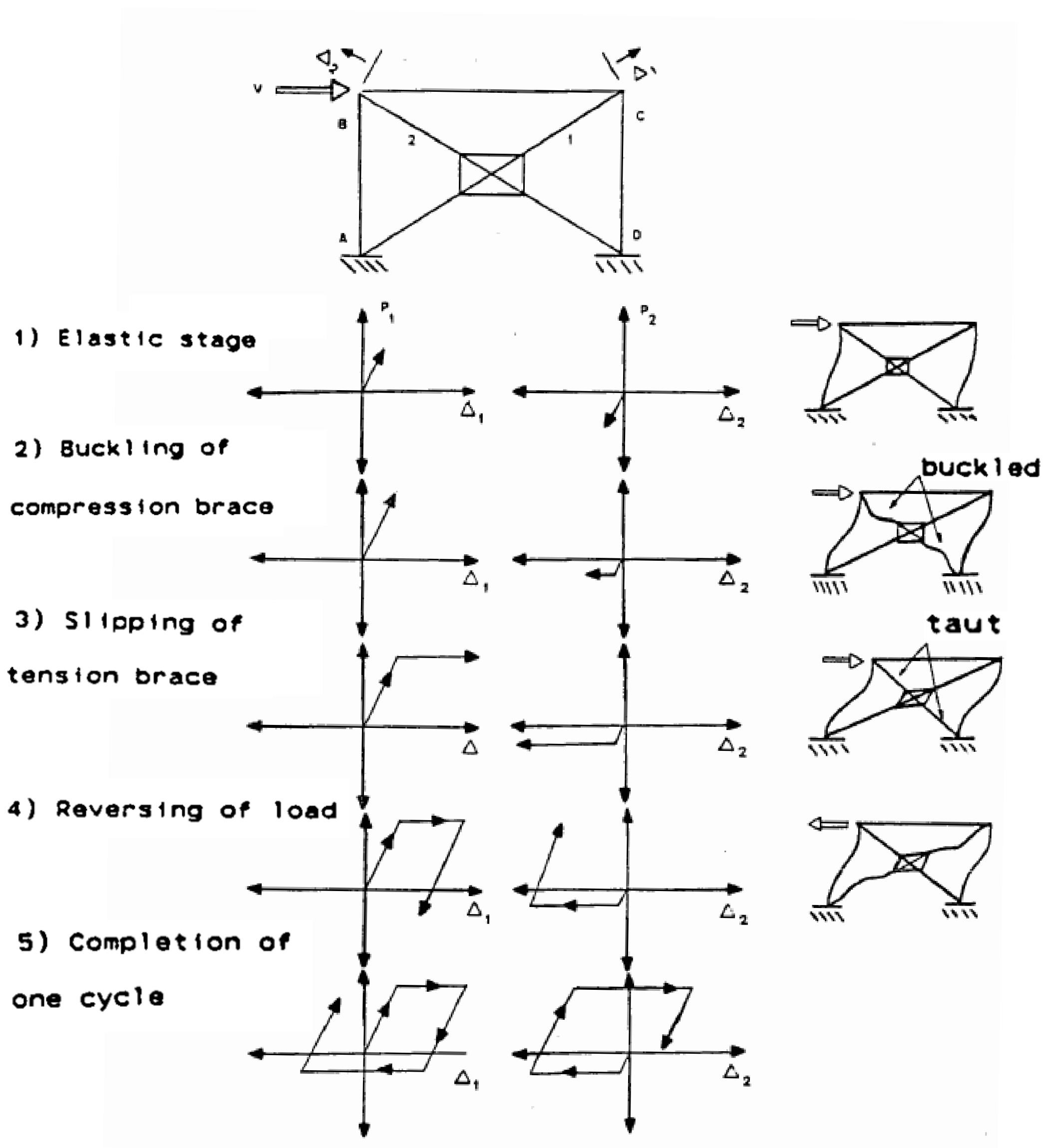

Figure 2.3-7. Phases of the x-brace configuration considering tension-only braces with reverse slip at zero compression (Filiatrault 1985)

Most of the previous literature, slip load of dampers was designed by optimizing seismic response parameters through an energy-based design method. In 2018, a force-based design method was proposed and a numerical model was developed to retrieve the interstorey drift demand, used as input in the testing of the full-scale friction damper sub-assembly carried out at Université Polytechnique in Montréal, Québec, Canada (Tirca et al. 2018). This study compared Friction Braced Frames (FBF) with and without a backup moment resisting frame design. The FBFs were designed for 100% of the design base shear and the back up moment frames were design for an additional 25%. Friction braced frames without MRF and with MRF are shown as the proportion of base shear assigned to the moment frame, α. Where non-MRF is $\alpha = 0$, and the dual system is $\alpha = 0.25$ shown in Figure 2.3-8. The results show large interstorey drift for non-dual friction braced frames, as well as large residual drift for both 4 and 10-storey buildings. The buildings designed with the backup MRFs for 25% of base shear shows a significant improvement in drift and residual drift for both buildings studied.

Experimental testing on a full-scale friction damper was conducted on the configuration shown in Figure 2.3-9 for crustal and subduction ground motion drift histories. The behaviour of the friction damper under the 2011 Tohoku subduction ground motion (300 s duration) is shown to be very stable and have little to no degradation.

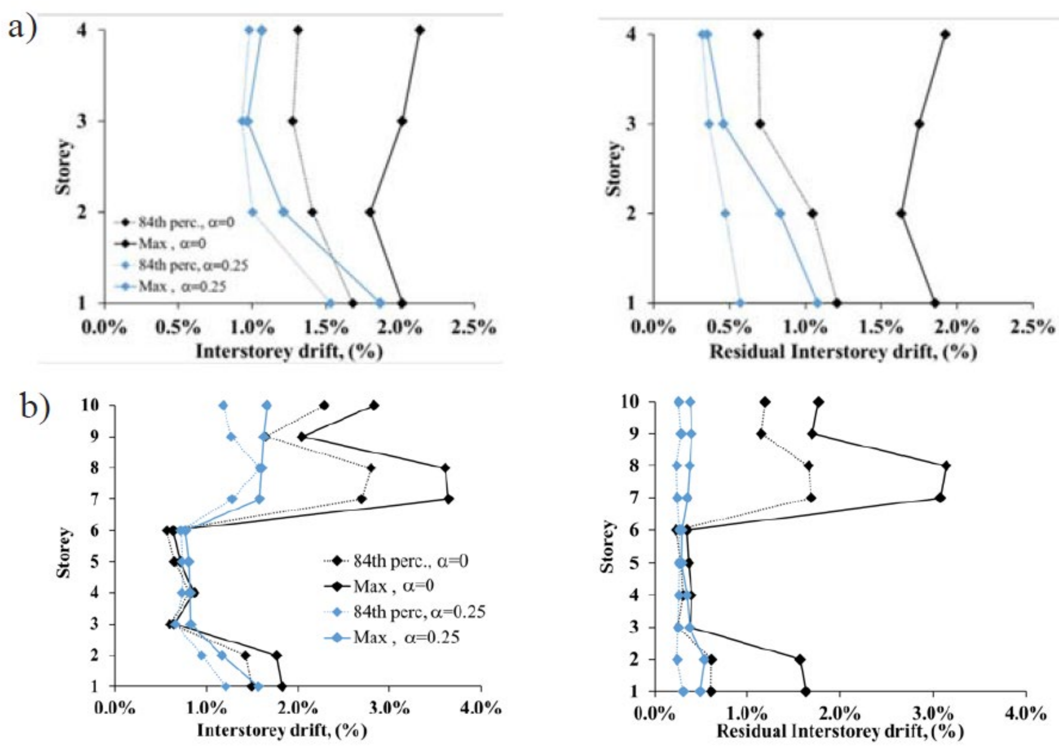

Figure 2.3-8. Simulated analysis results for peak interstorey drift and residual drift, with and without Backup Moment Frames: a) 4-storey b) 10-storey (Tirca et al. 2018)

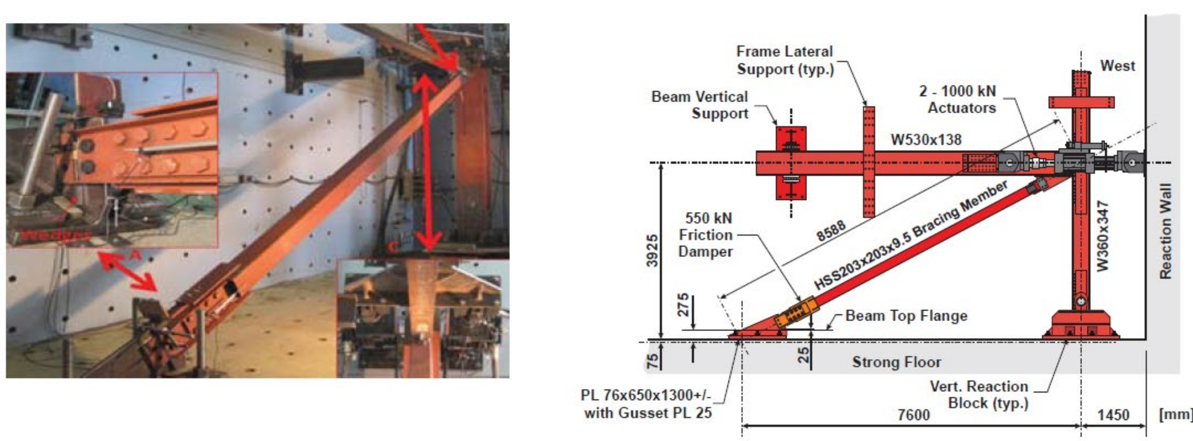

a) b)

Figure 2.3-9. Sub-assembly with Pall Friction Damper: specimen tested at École Polytechnique (a picture of full assembly b) testing setup schematic (Tirca et al. 2018)

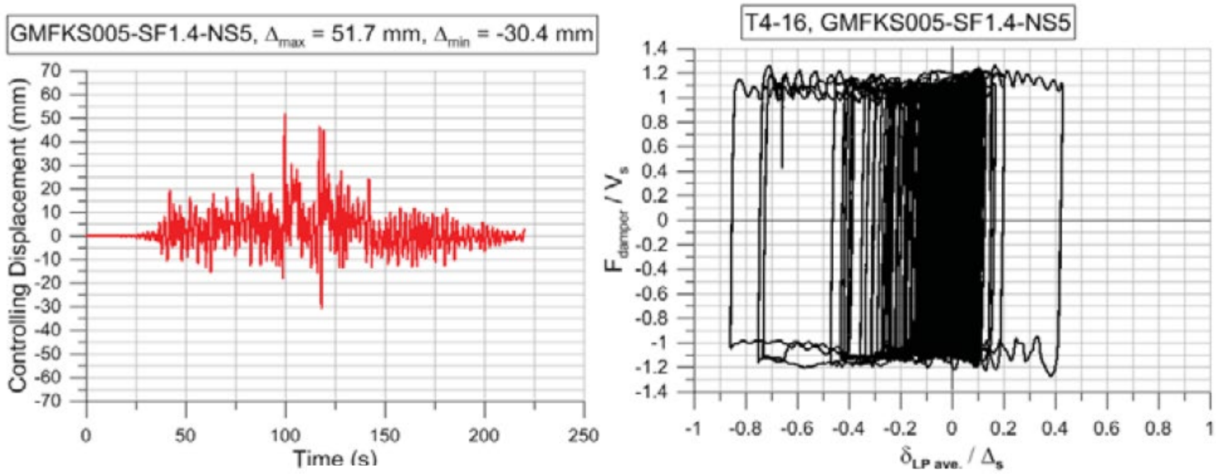

a) b)

Figure 2.3-10. Input and FD hysteresis under a Tohoku record (2011): a) displacement input resulted from numerical model and b) hysteresis of FD (Tirca et al. 2018)

2.3.2 Slotted Bolted Connections (SBC)

The earliest works on Slotted-Bolted Connections, SBC, presented the devices to be an economical, simple, and effective energy dissipation device via a stable hysteretic behaviour resulting in limited permanent damage (Fitzgerald et al. 1989; Roik et al. 1988). The simplest of these early devices was the 2-stage SBC proposed by (Fitzgerald et al. 1989), where two back-to-back channel sections with slotted holes were bolted to a slotted gusset plate with one or two high-strength bolts, as shown in Figure 2.3-11 b) and Figure 2.3-12. The high-strength bolts are bolted to the channels using Belleville spring washers and cover plates, where the cover plates and the channel interfaces generates the second friction stage. The first slipping stage is due to the sliding between the channels and gusset plate interface. This staging is shown in Figure 2.3-12 b).

These devices showed little deterioration during testing and were very stable. Furthermore, the observed friction slip forces were accurately predicted by simple equations regarding the normal forces by the bolts and the coefficient of friction. One of the limitations of this study is that bolt

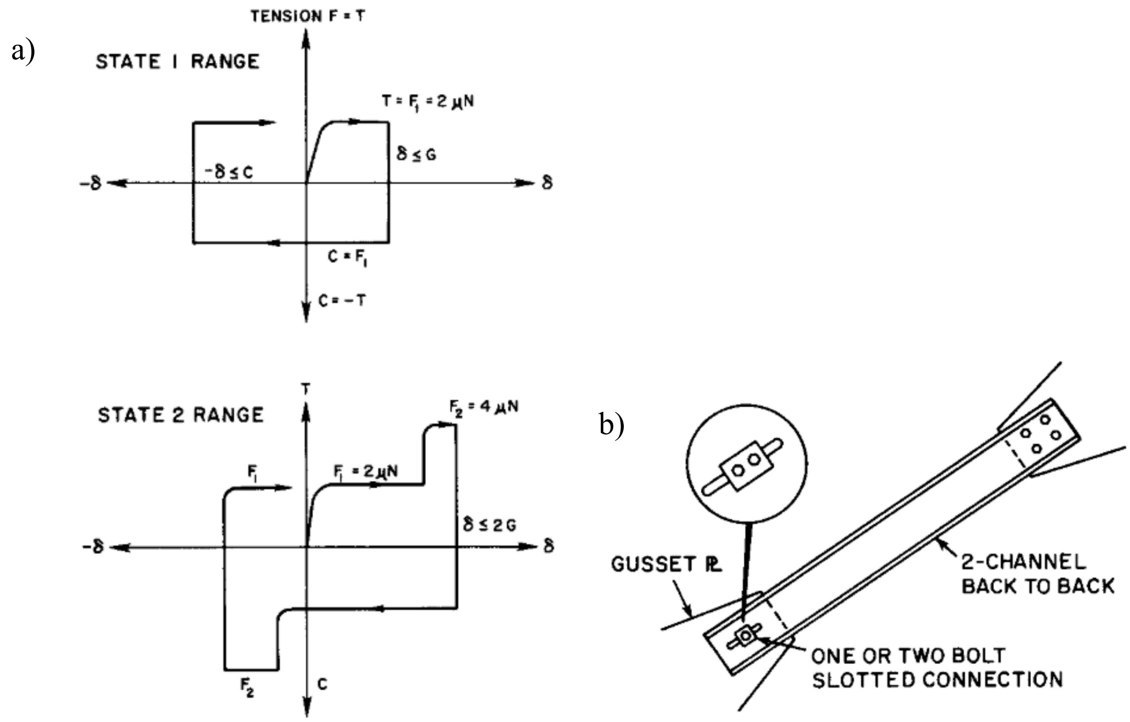

Figure 2.3-11. Slotted-Bolted Connections: a) Hysteresis for Both Slipping Stages, b) Gusset-Brace Friction Device (Fitzgerald et al. 1989)

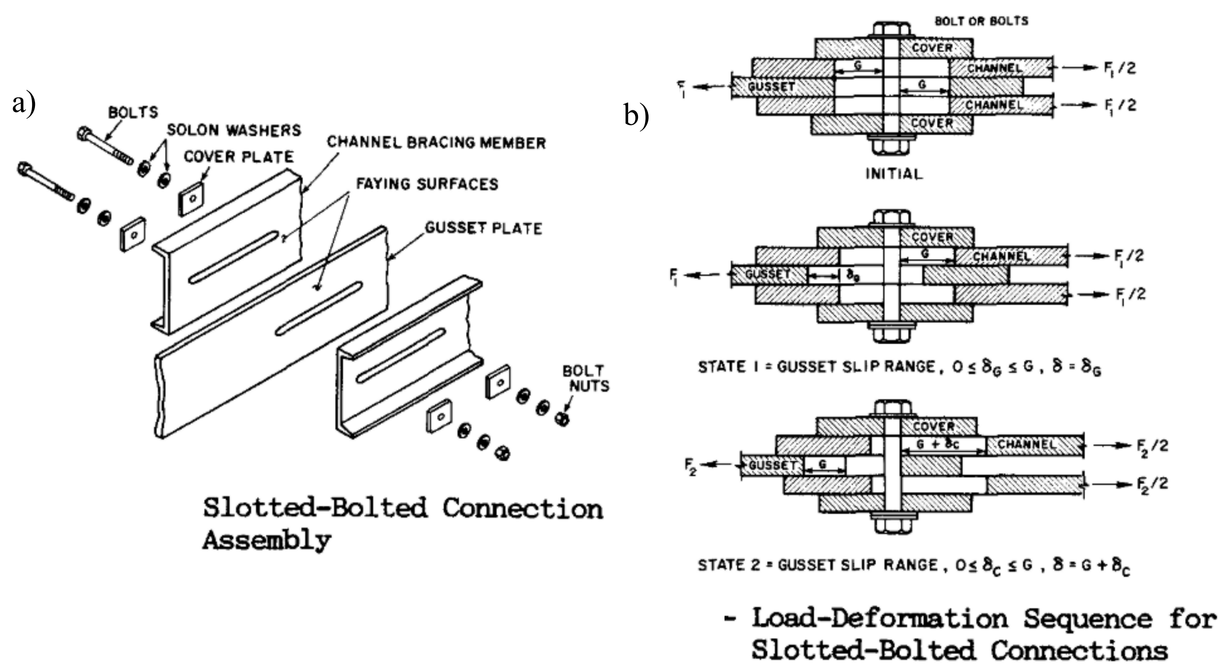

Figure 2.3-12. Slotted-Bolted Connection: a) assembly b) slipping stages (Fitzgerald et al. 1989)

bearing phase, when both stages of slipping had their slot lengths exhausted, was never tested to observe behaviour near failure.

In 1988, (Roik et al. 1988) published work on a Three-Stage Friction-Grip Element. This research looked at friction elements that were designed to slip at different displacement lengths in order to simulate a progressive breaking mechanism. Three friction elements were put in parallel with different initial stiffnesses and slip lengths creating a less sharp transition from linear to non-linear (slipping) behaviour as shown in Figure 2.3-13. The response of the devices was observed first with a simulation of a 7-storey building with X-bracing, where columns were continuous over its entire height. Compared to a ductile frame, the frame with friction devices resulted in a significant

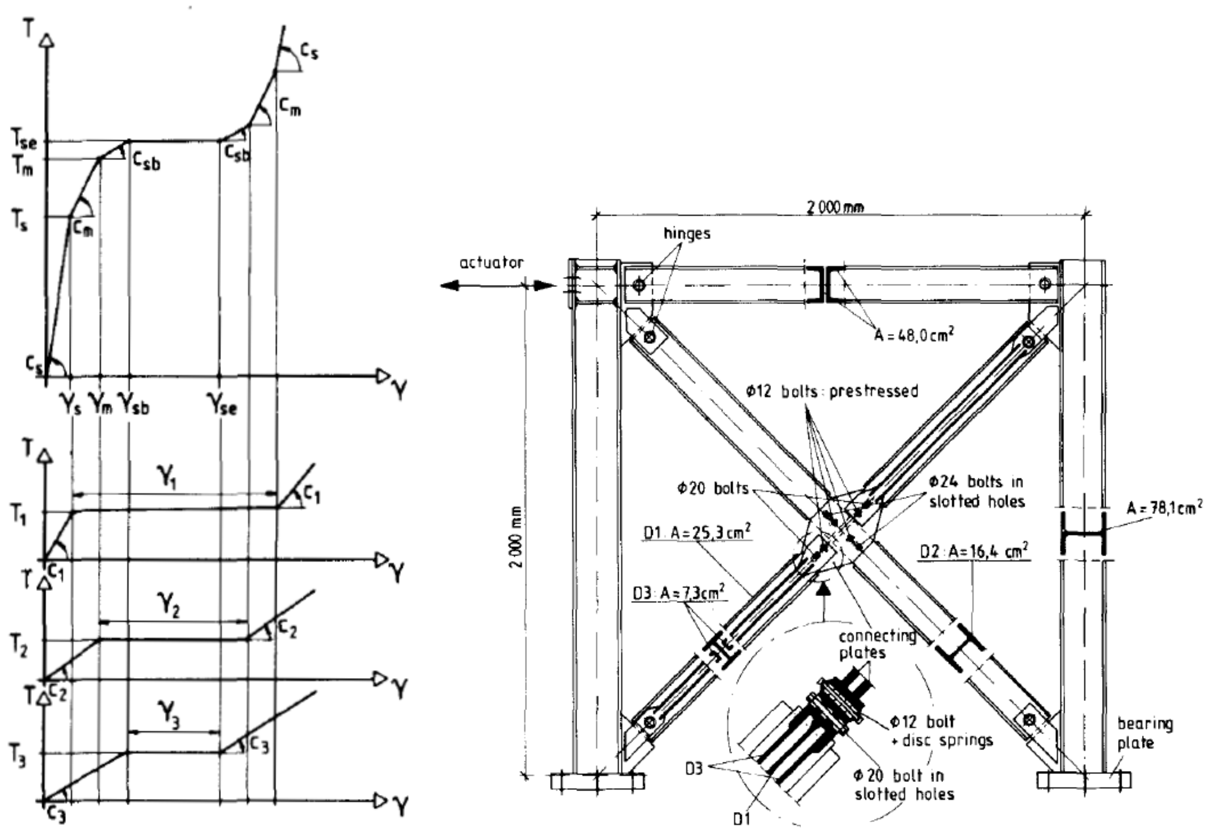

a) b)

Figure 2.3-13. a) 3-Stage Friction-Grip Elements: a) multi-linear curve, b) Prototype Frame Configurations Studied (Roik et al. 1988) decrease in total displacement under El Centro earthquake. A scaled down test of the specimen shown in Figure 2.3-13 was done and compared with simulated results. The tests were done up to 200% the design limit to observe bearing of the bolts where failure did not occur, and bolt prestressing remained unchanged.

Based on a similar device, (Lukkunaprasit et al. 2004) looked at bolt bearing phases of Slotted-Bolted Connections (SBC) and the effects on connection stiffness of the different phases of slipping. Firstly, a simple slip stage device was tested up to the bolt bearing phase as shown in Figure 2.3-14. A very stable hysteresis diagram is observed and then a sharp increase in load as the bolts begin to press against the end of the slotted bolt holes was exhibited.

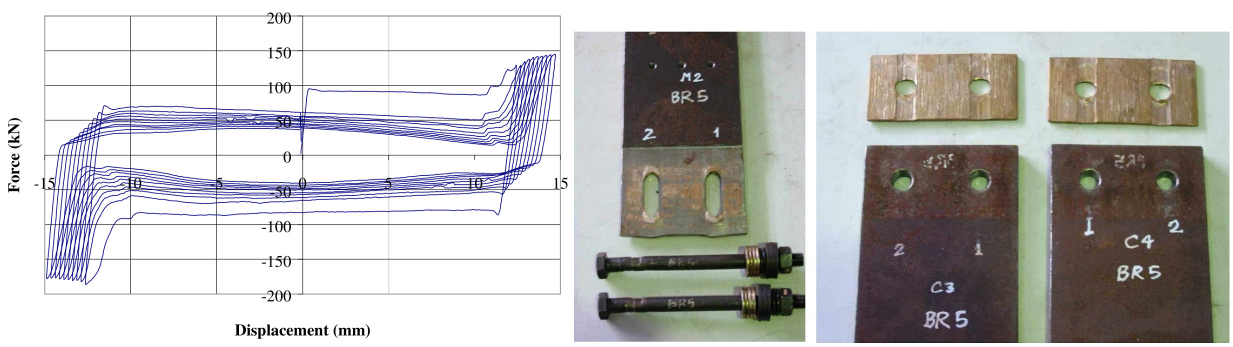

a) b)

Figure 2.3-14. SBC response: a) Hysteresis including bolt bearing, b) Test specimen of SBC under bearing showing bolt hole deformation (Lukkunaprasit et al. 2004)

Then a two-stage device, similar to that found in (Roik et al. 1988), was used as seen in Figure 2.3-13 b). This device was taken to have the second phase of the 2-stage device to occur at 50% of the slip length of the single-phase device. The effects of the second phase's slip force were observed for second slip force values of [0 ,60 ,90] percent of the brace's buckling strength coupled with the first slip force of either [20% or 40%]. Figure 2.3-15 shows these results for a single ground motion, Parkfield. The inclusion of a second slip phase does have a small effect on reducing the maximum interstorey drift however there seems to be little effect on the drift when the second slip force is altered between 60% and 90%.

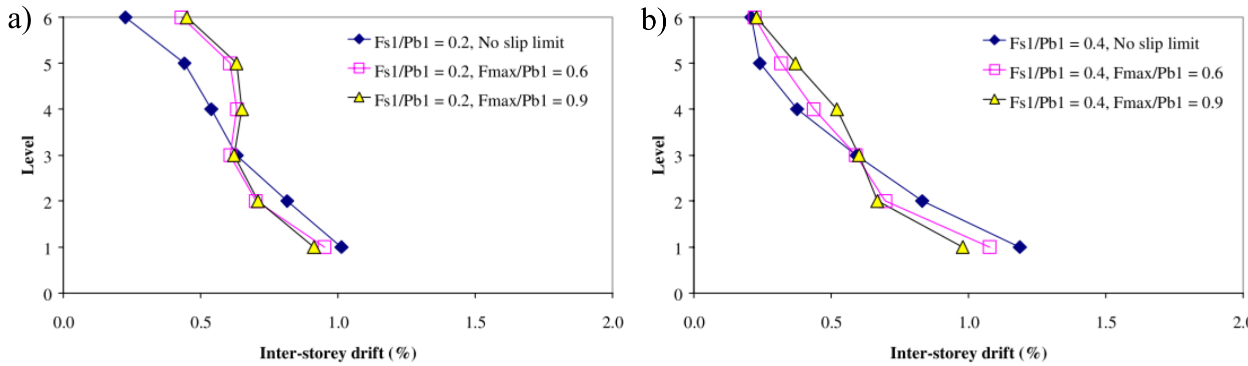

Figure 2.3-15. Interstorey drift response of: a) single-phase and b) two-phase SBCs for variable slip forces (Lukkunaprasit et al. 2004)

2.4 Effects of Dual Systems and Gravity Columns

2.4.1 Effects of Gravity Columns for Drift Mitigation

The effects of gravity columns, column stiffness, and column continuity have been studied to observe their ability to influence residual drift and interstorey drift (Ji et al. 2009; Macrae et al. 2004). The interest in research on continuous columns and column stiffness is focused on the reduction of soft storey mechanism typically found in CBFs. Theoretical models were developed by (Macrae et al. 2004) for different configurations of CBFs with continuous columns, and/or continuous gravity columns and compared with numerical models. Nonlinear pushover analysis was completed on a two-storey CBF structure, where only first storey yielding was achieved. Different ductility factors, μ_t, defined by the first storey displacement over the roof displacement at first storey yielding, were also considered. The observed parameter was the Drift Concentration

Factor (DCF) which is the maximum interstorey drift at any storey, as a percentage of storey height, divided by the maximum roof drift. Figure 2.4-1 shows the pushover results for various ductility factors when column stiffness is increased. Thus, identifying the column stiffness, whether that be by seismic or gravity columns, has a significant effect on drift. It was also observed that altering the stiffness of columns, such as making them continuous, had little effect on the fundamental period of the structure and thus mostly acts as a force redistribution mechanism to avoid soft-storey behaviour.

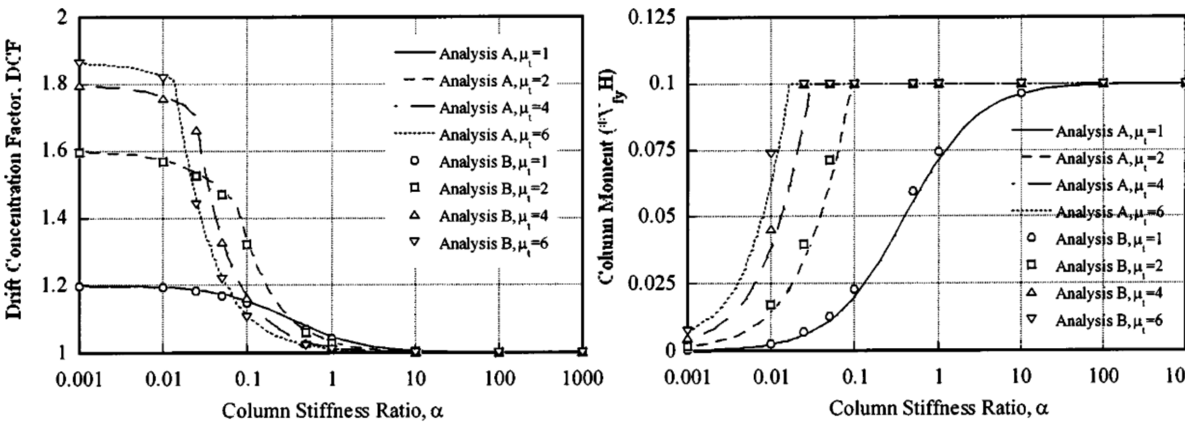

(a) Drift Concentration Factor, DCF (b) Column Moment, M_c

Figure 2.4-1. Effects of column stiffness via Nonlinear Pushover Analysis on: a) Drift Concentration Factor and b) Column Moments (Macrae et al. 2004)

The research conducted by (Macrae et al. 2004), looked into the effects of gravity columns in CBFs buildings and developed a theoretical model to estimate drift by including buckling behaviour of the braces. However, this research is limited by the simplification of the theoretical models where the braces were considered as elastic-perfectly plastic. Gravity columns were considered as continuous over the height of the building and designed to behave elastically even once all braces had yielded. The parameters verified by the study were: the effects of gravity column base restraints (e.g. fixed or pinned), the brace slenderness, and of the seismic ductility reduction factor in relation to interstorey drift and the total number of gravity columns. In Figure 2.4-2 the effects of adding N gravity columns to pinned and fixed-based structures are shown. For the pinned-base structure, an increase in the total number of gravity columns decreased the storey drift of the first storey and resulted in a relationship where adding more gravity columns generally improved the overall response of the structure. For the fixed-base case, increasing the number of gravity columns up to N = 4, for the 3-storey structure, effectively eliminates large interstorey drift of the first storey. However, increasing the number of gravity columns above N = 20, negatively affects the response of the structure. This relationship can be seen in Figure 2.4-2 for variable building heights where fixed-base structures have a critical number of columns which if surpassed results in an increase in drift, N = 4 for the 3-storey and N = 40 for the 6-storey.

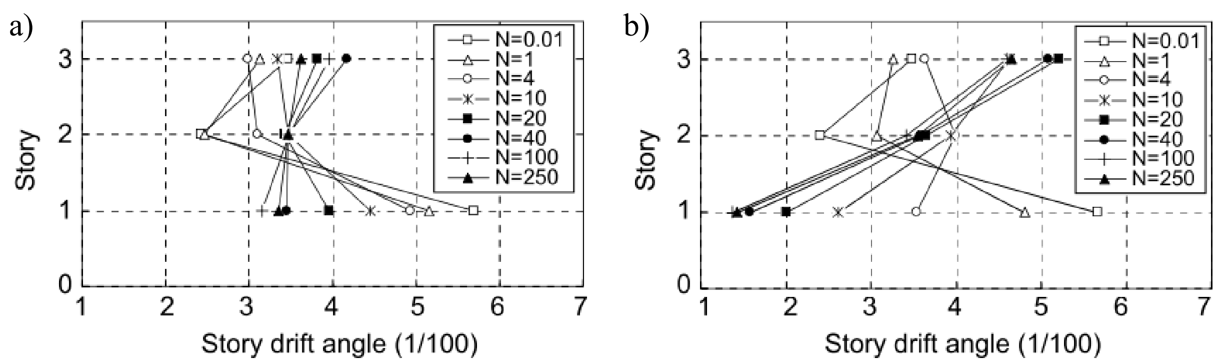

Figure 2.4-2. 84th Percentile Results for Variable Number of Gravity Columns for: a) Pinned bases and b) Fixed bases (Ji et al. 2009)

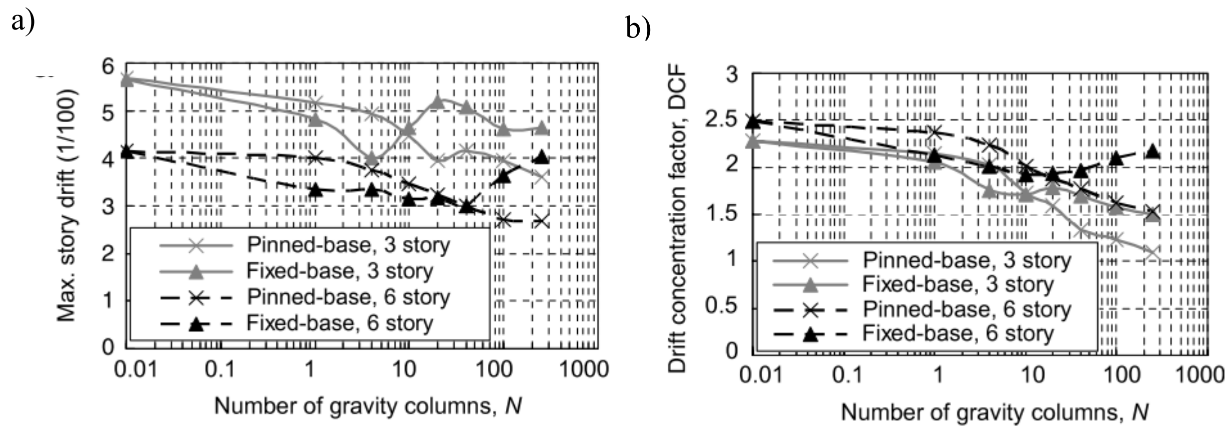

Figure 2.4-3. Effects of gravity columns on buildings of variable heights and column base fixity: a) Max drift and b) Drift Concentration Factor (Ji et al. 2009)

Ohira showed improvements of a 4-storey hospital building when continuous columns were selected for CBFs equipped with PFDs, as shown in (Ohira 2020). These results are shown in Figure 2.4-4.

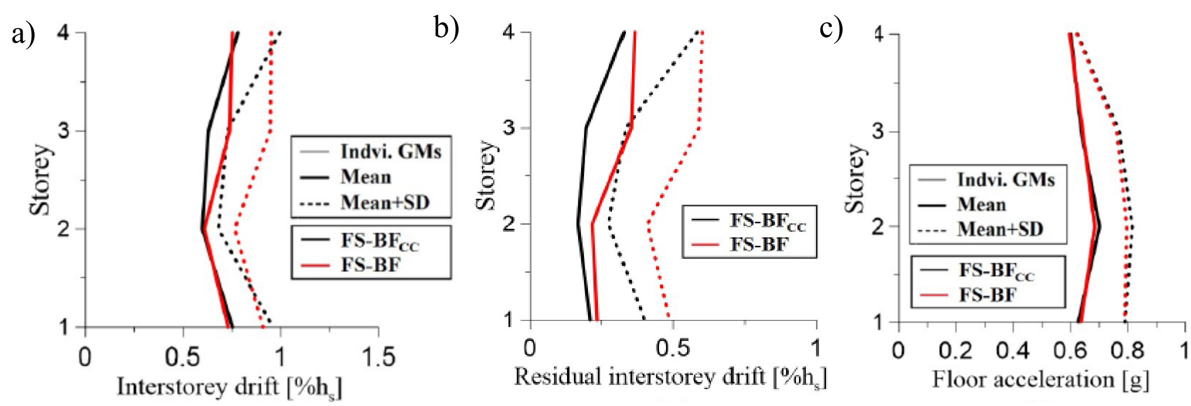

Figure 2.4-4. Response of 4-storey hospital building braced by FSBF: a) Interstorey drift b) residual drift c) floor acceleration for FSBF vs. FSBF with continuous columns for 4-storey hospital building (Ohira 2020)

2.4.2 Dual Systems

Early work on dual systems was concerned with a structural redundancy to avoid collapse during strong earthquakes (Whittaker 1990). Later dual systems were studied as a method to reduce residual drift in Buckling Restrained Frames, BRBs (Kiggins and Uang 2006). In the aforementioned study, chevron braced frames were designed for 3 and 6-storey buildings, as a conventional and a dual system. The backup moment frame (MF) was designed for an additional 25% design base shear and used as a restoring mechanism. It was found that the backup moment frame brought some reduction in maximum drift, 10-12%, but the reduction in residual drift was much more significant under nonlinear time-history analysis.

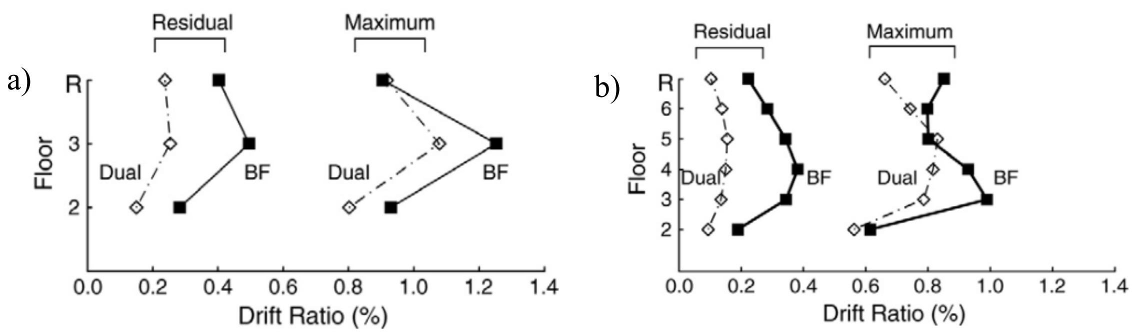

Figure 2.4-5. Maximum and residual drift for: a) 3-storey and b) 6-storey buildings (Kiggins and Uang 2006)

To better understand the influences of the backup MF on drift and residual drift response, (Sahoo and Chao 2015) looked into the stiffness of Buckling Restrained Braced Frames (BRBFs) and how the response of three types of frames, a conventional frame (V-Conv), a modified frame with stiffer column sections (V-Mod), and a conventional design with backup moment frame (V-Dual). Each frame type was designed for a 3 and 6-storey building with either fixed bases (FB) or hinged bases (HB), as well as pinned beam connections (PBC) or rigid beam connections (RBC). The paper's contributions among others included a relationship between stiffness and strength for dual systems and the development of an empirical equation to predict residual drift as a function of elastic storey stiffness (excluding BRB stiffness).

It was found, as shown in Figure 2.4-6, for systems with RBC, there was a 20 and 40% reduction in interstorey drift for the 3V-Mod and the 3V-Dual, respectively, compared to the 3V-Conv. Furthermore, in terms of drift, there was not significant difference between the RBC and HBC models. For the 6-storey structures, a 20% reduction in interstorey drift was observed for both 6V-Mod and 6V-Dual, compared to the 6V-Conv structure. In short, for reducing interstorey drift of the V-Conv structures, the V-Mod and V-Dual systems are similar in terms of overall outcomes.

For residual drift, the average response saw a reduction of 35 and 59% for the 3V-Mod (PBC) and 3V-Dual (PBC) models, respectively, in comparison with the 3V-Conv (PBC) models, and 14 and 45% for the corresponding RBC models. Demonstrating that the reduction in residual drift is much more effective if improvement of a pinned beam-column frame is done than for a frame with rigid beam-column connections. For the 6-storey structures, the mean residual drift was reduced by 60% for 6V-Dual (RBC) and 45% for 6V-Mod (RBC) compared to 6V-Conv (RBC). Thus, presenting evidence that a dual system is more effective at reducing residual drift than simply increasing column stiffness. The overall residual drift of the structures can be seen in Figure 2.4-6.

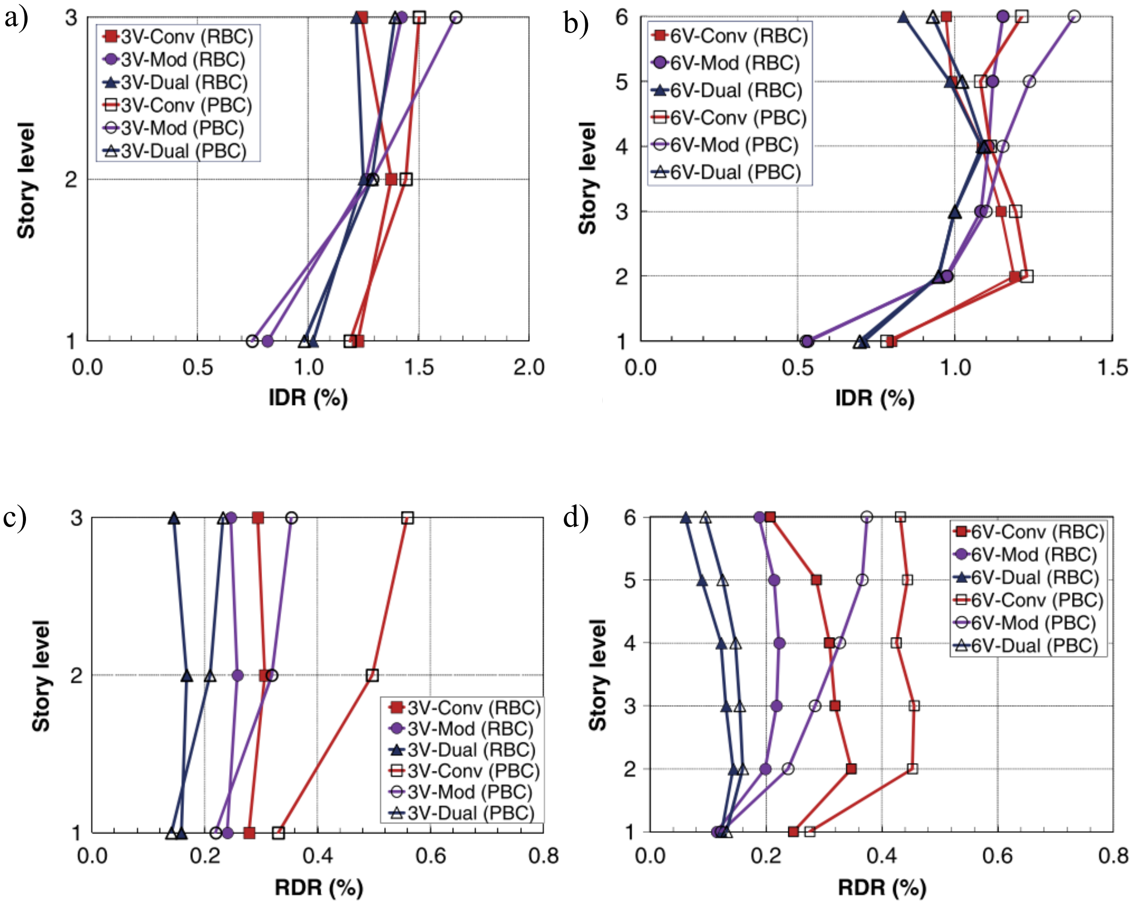

Figure 2.4-6. Response of BRBF (conventional, modified, and dual systems): a) Interstorey drift for 3-storey frames, b) interstorey drift for 6-storey frames, c) residual drift for 3-storey frames and d) residual drift for 6-storey frames (Sahoo and Chao 2015)

A parametric analysis was conducted, and the V-Conv, V-Mod, and V-Dual systems were compared to a V-Dual system with a 50% reduction in beam stiffness (RS) while maintaining the same strength, and a V-Dual system with an increased beam strength of 50% (IS) while maintaining the same stiffness. These results are shown in Figure 2.4-7. Reducing the stiffness and increasing the strength of the beams does not affect the interstorey drift response, however for the residual drift, it can be observed that an increase in strength results in an increase in residual drift, furthermore, a reduction in stiffness increases the residual drift even more. Thus, demonstrating the dependence of residual drift on stiffness and not strength.

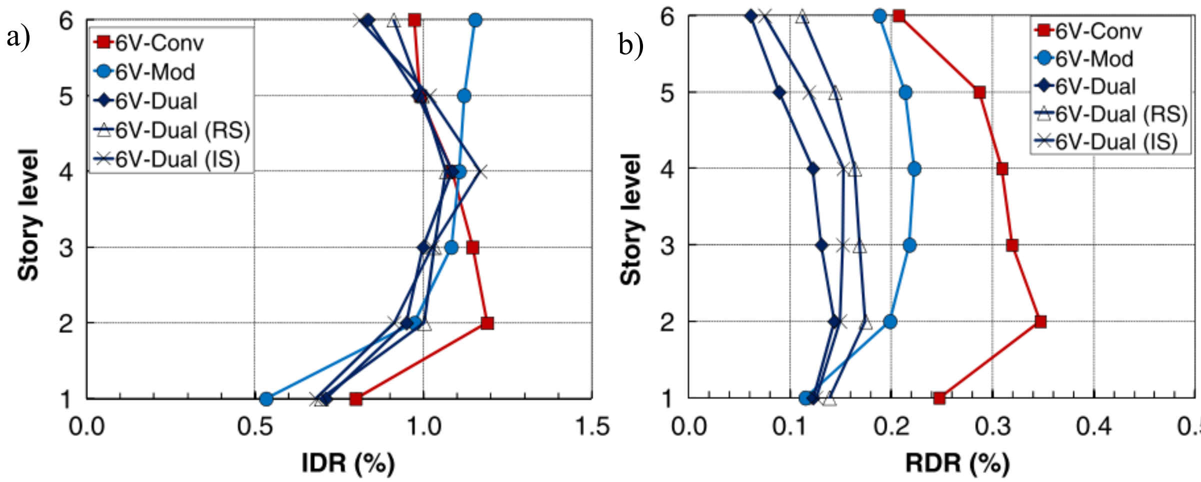

Figure 2.4-7. Response of BRBF under 20 ground motions with Rigid Beam Connections and Dual Systems with Reduced Stiffness (RS) and Increased Strength (IS): a) average IDR and b) average RDR (Sahoo and Chao 2015)

A displacement-based design procedure was developed by (Pettinga et al. 2007) for dual systems and judged if a secondary elastic moment frame would be effective and consistent in reducing residual drift. The research also looked into the validity of using 25% of the design base shear to design the members of the secondary elastic moment frame which has been a design requirement present in the NBCC since 1970. From the formulations developed, it was judged that a design based around 5-10% of design base shear would be acceptable. However, this may prove to be a distinction without a difference in the design of steel moment frames since sections are already predetermined based on standard member sections. However, the reduction in design base shear for the secondary frame is due to the fact that the solutions in this research are based on stiffness and not strength-based design. As previously observed (Sahoo and Chao 2015), stiffness is the contributing parameter to the effectiveness of the moment frame and not strength, even though these two parameters are not mutually exclusive in practical applications.

Wang (2018) also used a dual system to design an 8-storey building in Vancouver, BC (Wang 2018). The Dual system consisted of conventional CBF and backup moment frame designed for 25% additional base shear. It was found that there were good improvements in the seismic response while concentration of damage within a floor was mitigated.

2.5 Modeling of Moment Resisting Frames in OpenSees

In OpenSees (Open System for Earthquake Engineering Simulation) and in finite element analysis in a broader sense, the complexity of modeling of Moment Resisting Frames, MRFs, consists in the modeling of the beam elements in reference to their plastic deformation, and their deterioration in terms of strength, stiffness and other phenomenological behaviours (Lignos et al. 2011; Ribeiro et al. 2015; Tirca et al. 2016). Two principle beam modeling methods are typically implemented, the first being the Concentrated Plasticity Model which generally refers to the use of a zero-length rotational spring at both ends of a linearly elastic beam-column element (Giberson 1969), and the second being a Distributed Plasticity model of finite elements (Ribeiro et al. 2015). For Distributed Plasticity models, different types of integration methods are possible to permit proper evaluation of arbitrary hinge lengths, and convergence (Ribeiro et al. 2015; Scott and Ryan 2013). These models do not consider cyclical deterioration, this must be accomplished with an analytical model of specific beam behaviour. According to ATC guidelines (PEER/ATC 72-1 2010), there are 4 options for analytical models regarding cyclic deterioration such as: 1) explicit deterioration 2) skeleton curve 3) backbone curve with modification factors and 4) deformation limit.

OpenSees has built in functionality for force-based beam-column elements with two discrete plastic hinges with distributed plasticity, coupled with an elastic middle segment known as a *BeamwithHinges* element as seen in Figure *2.5-1*. The *BeamwithHinges* element uses a modified Gauss-Radau integration scheme and permits the use of deterioration models to be defined in the plastic hinge sections within a given plastic hinge length. The nonlinear behaviour of the plastic hinge length and its deterioration can be defined, among many others, by a moment-curvature relationship derived from a backbone moment-rotation relationship (Ribeiro et al. 2015) or a fibre-based cross-section model (Bosco and Tirca 2017).

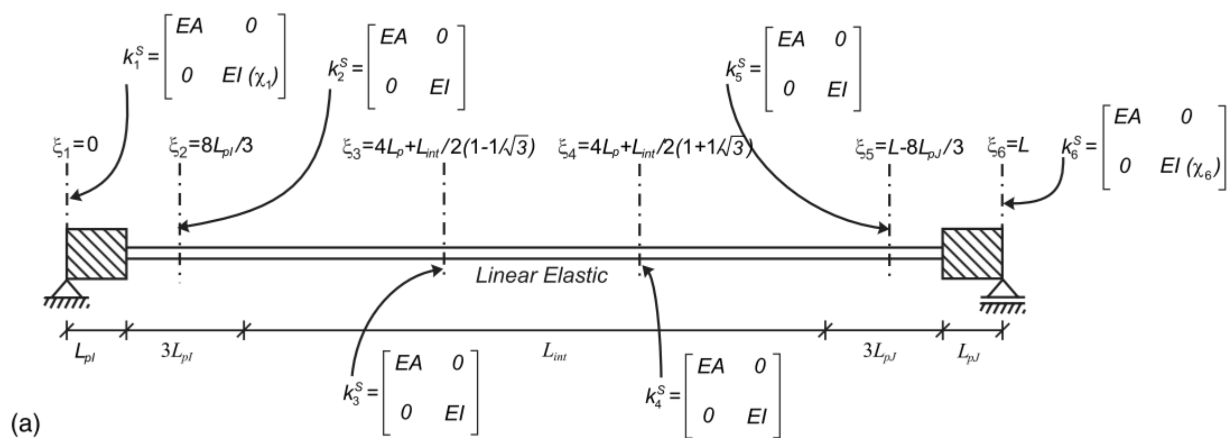

Figure 2.5-1: *BeamwithHinges* Element Using a Modified Gauss-Radau integration Scheme (Ribeiro et al. 2015)

To have proper local and global deformation results for moment-curvature definitions, research has shown that moment-curvature relationships derived from the direct scaling of moment-rotation relationships, $\chi_i = \frac{\theta_i}{L_p}$, cannot be properly identified (Scott and Ryan 2013). Thus, a methodology using moment-rotation constitutive law compared with experimental data was developed (Ribeiro et al. 2015). This allows a deterioration modeling of the plastic hinges to be implicitly defined by a backbone deterioration definition. For example, a modified Ibarra-Krawinkler model (Lignos et al. 2011) which was verified on a large set of experimental data can be used. This study looked at the effects of multiple geometric parameters such as beam depth, span to depth ratio, buckling length to depth ratio, width-to-thickness ratio of beam flange, and depth to thickness ratio of beam web. Done for both reduced and non-reduced beam sections, empirical equations were developed to define the pre-capping plastic rotation, θ_p, post-capping plastic rotation, θ_{pc}, and the reference cumulative plastic rotation, Λ, as shown in Figure 2.5-2. This method of backbone deterioration can be used in Concentrated Plasticity models or in Distributed Plasticity models.

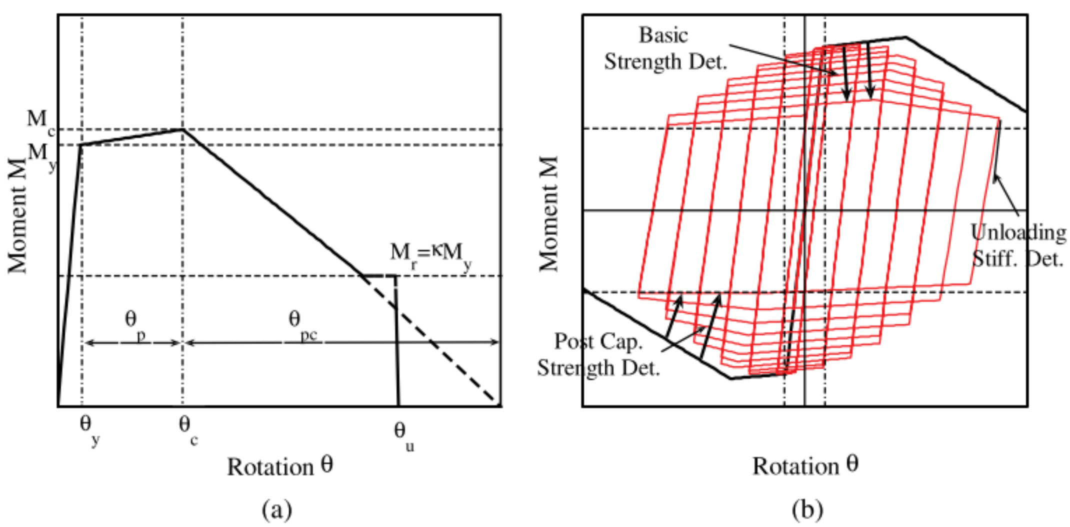

Figure 2.5-2. Backbone curve for Modified Ibarra-Krawinkler Deterioration Model and the hysteresis response (Lignos et al. 2011)

An alternative to the backbone deterioration model is to have an explicitly defined deterioration model using a fiber-based accumulation model (Bosco and Tirca 2017). By assigning a nonlinear material such as the Giuffre-Menegotto-Pinto steel material, *Steel02* in OpenSees, wrapped with a specific low-cycle fatigue material to the fibers of the cross-section permits the beam's hinges to deform inelastically and model low-cycle fatigue. Low-cycle fatigue, such as the *fatigue* material in OpenSees, works off of the Miner's rule for accumulating damage as defined by Eq. (2.5.1), where $n(\epsilon_i)$ is the number of cycles at the strain amplitude ϵ_i, $N_f(\epsilon_i)$ is the total number of amplitude cycles at the strain amplitude ϵ_i necessary to cause failure. Identification of the strain amplitude at each reversal can be defined by the Manson-Coffin relationship given by Eq. (2.5.2), where ϵ_0 is the fatigue ductility coefficient and m is the fatigue ductility exponent (Uriz and Mahin 2008).

$$DI = \sum_{j=1}^{n} \left(\frac{n(\epsilon_i)}{N_f(\epsilon_i)} \right)_j \qquad (2.5.1)$$

$$\epsilon_i = \epsilon_0 \left(N_f \right)^m \qquad (2.5.2)$$

To consider local buckling of the flange, the fatigue ductility coefficient is defined to have a minimum value of $\epsilon_0 = \epsilon_{0min}$ and a maximum value of $\epsilon_0 = \epsilon_{0min} + \Delta\epsilon_0$, where the rate of degradation is given by $\Delta\epsilon_0$, and the initiation of local buckling is given by ϵ_{0min}. The fatigue ductility coefficient is linearly distributed in the flange from the end of the flange to the web as shown in Figure *2.5-3*. Each fiber of the flange is then assigned a fatigue ductility coefficient, E_0, as given by Eq. (2.5.3) along side a *Steel02* material. The rate of degradation, $\Delta\epsilon_0$, is defined by Eq. (2.5.4) where the buckling wave length of the flange is L_m, the effective length of the beam is L_v, and λ_f is the flange slenderness, as defined by Eqs. (2.5.5), (2.5.6) and (2.5.7), respectively.

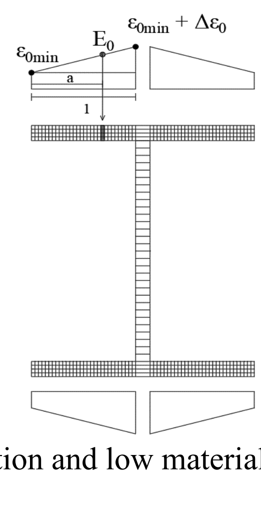

Figure 2.5-3. Fiber cross-section and low material cycle fatigue (Bosco and Tirca 2017)

$$E_0 = \varepsilon_{0,min} + a\Delta\varepsilon_0 \tag{2.5.3}$$

$$\Delta\varepsilon_0 = 0.217 + 0.770\lambda_f + 0.452\frac{b_f t_f}{dL_v} + 0.902\frac{L_m}{L_v} \tag{2.5.4}$$

$$L_m = 2\beta c; where\ \beta = 0.6\left(\frac{t_f}{t_w}\right)^{\frac{3}{4}}\left(\frac{d}{c}\right)^{\frac{1}{4}}\ and\ c = 0.5\left(b_f - t_w\right) \tag{2.5.5}$$

$$L_v = L + \frac{d_c}{2} - l_c \tag{2.5.6}$$

$$\lambda_f = \frac{b_f}{2t_f}\sqrt{\frac{F_{yf}}{E}} \tag{2.5.7}$$

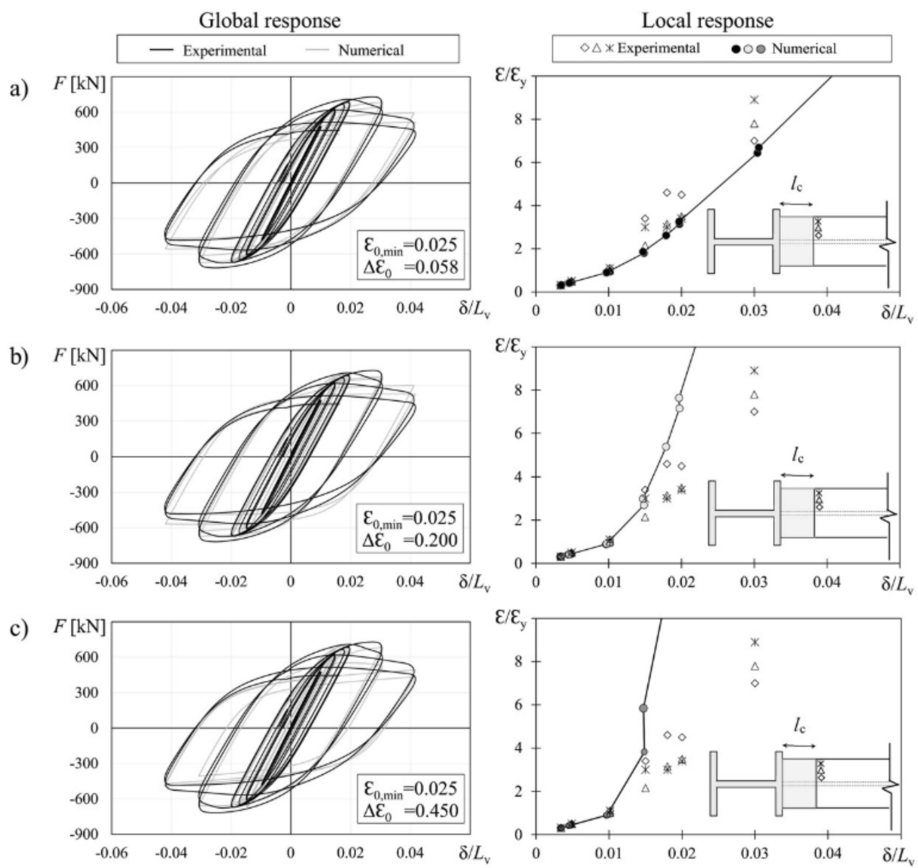

Figure 2.5-4. Global and Local Response of Experimental versus Numerical model: a) *BeamwithHinges* with Modified Gauss-Radau Integration scheme b) *BeamwithHinges* with two-point Gauss-Radau Integration and c) Beam with Distributed Plasticity (Bosco and Tirca 2017)

To demonstrate the efficacy of the fibre-based fatigue accumulation model coupled with the modified Gauss-Radau integration scheme, proposed by Bosco and Tirca (2017), a comparison was done between two integration schemes for the *BeamwithHinges* element in OpenSees (modified Gauss-Radau and Gauss-Radau), and a beam with distributed plasticity as shown in Figure 2.5-4. It can be concluded that the local response, as measure by the uppermost fiber in the top flange, was significantly better at matching the softening behaviour experienced at higher drifts for the *BeamwithHinges* elements using a modified Gauss-Radau integration scheme than for the other beam models.

2.6 Incremental Dynamic Analysis

Incremental Dynamic Analysis, IDA, is an analysis method that evaluates the response of a structure from yielding to failure under dynamic loading over a range of seismic loads. This method of analysis was first mentioned by (Bertero 1977) and latter developed by (Vamvatsikos and Cornell 2001).

IDA uses scaled Intensity Measures, IMs, such as first mode spectral acceleration and Damage Measure, DM, such as max interstorey drift by the use of nonlinear analysis to construct a complete picture of a structure's response. Using the first mode spectral acceleration as an IM is done by first transforming an unscaled accelerogram time-history from the time domain to the frequency domain, through a Fourier transformation, and then identifying the first mode spectral acceleration, $S(T_1)_{unscaled}$, for that accelerogram. The $S(T_1)_{unscaled}$ is then scaled to a target spectral acceleration, $IM = \lambda S(T_1)_{unscaled}$, to achieve a specific IM, and nonlinear dynamic analysis is performed by scaling the ground motion to the target IM. This process is repeated for multiple scale factors resulting in range of spectral acceleration values to provide a full picture for some DM as shown in Figure 2.6-1 (Vamvatsikos and Cornell 2001).

Ground motion-to-ground motion variation becomes apparent with IDA and some general behaviours can be observed. First observation is that a distinct linear elastic region is shown for all ground motions, this linear elastic region typically transitions to some variation of inelastic softening or hardening once inelastic behaviour in the structure is observed, such as brace buckling or MRF beam yielding as shown in Figure 2.6-2. Severe hardening and weaving behaviour can result in a higher IM having a lower or identical DM (Chopra 2012; Vamvatsikos and Cornell 2001). This behaviour is caused by timing variations in the structure's response at higher ground motion intensities, where for instance a lower storey yields earlier and then acts as a fuse for the above floors. In cases where two IMs have the same DM, it is typically assumed that the lower IM is assigned the DM. The ground motion randomness generally results in many ground motions having to be evaluated and then a specified percentile, such as 16th, 50th, or 84th percentiles are used to represent the overall behaviour of the structure.

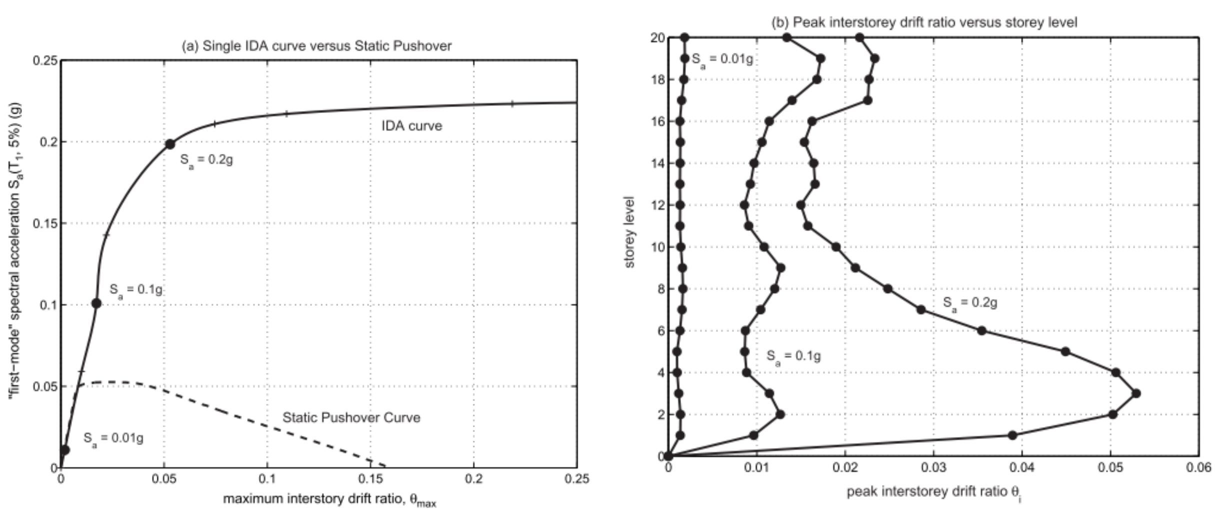

a) b)

Figure 2.6-1. Example of IDA curves for multiple IMs: a) static pushover IDA and b) peak interstorey drift along the building height under various intensities (Vamvatsikos and Cornell 2001)

Specific limit states can be identified using IDA for performance-based design criteria as discussed in the later Fragility Analysis section which gives specific DM limits for specific performance levels. However, limits, such as collapse, can also be set for IMs. Vamvatsikos and Cornell (Vamvatsikos and Cornell 2001) defines the collapse point to be when the tangent slope of the last point is equal to 20% of the elastic slope. In a less formulaic manner, collapse can simply be identified as the point where the subsequent points result in very large DMs for very small increases in IM. Most of these effectively result in identifying collapse to occur once the IDA curve flattens at high IMs.

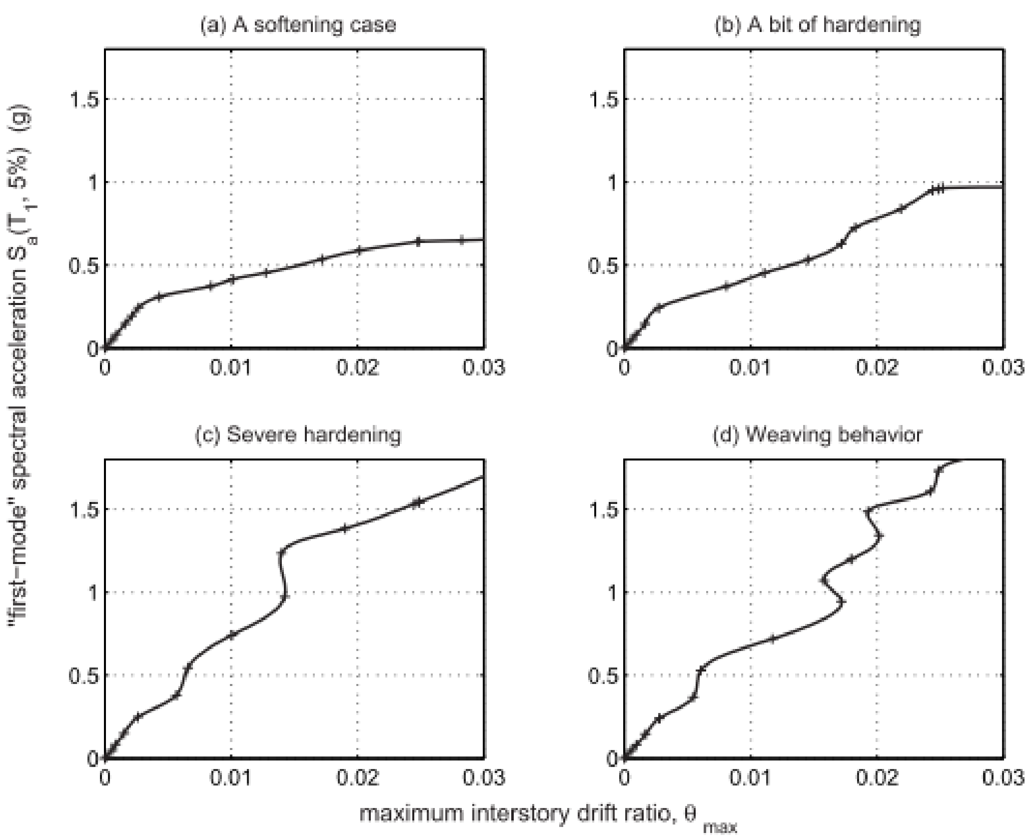

Figure 2.6-2. IDA curves for the same structure under 4 different ground motions: a) softening response, b) a bit of hardening response, c) severe hardening, d) weaving behaviour (Vamvatsikos and Cornell 2001)

2.7 Fragility Analysis

Fragility Analysis is a probabilistic methodology to assess the probability that a specific performance level is to be exceeded given a specific demand. Fragility Analysis attempts to quantify the uncertainties that result from the deterministic modes of evaluation implemented through typical means, such as Pushover Analysis or Incremental Dynamic Analysis. Fragility Analysis is typically quantified by the use of an Intensity Measure (IM), this intensity measure can be of a scalar or vector form (Baker and Cornell 2005; Zareian and Krawinkler 2007). A scalar form of the IM can take the form of spectral acceleration, deformation, peak ground acceleration, while the vector form consists of one of the previously mentioned scalar forms and epsilon, ε.

Epsilon is a parameter that measures difference between the observed logarithmic spectral acceleration of a ground motion with respect to the structure's first period, and the mean logarithmic spectral acceleration with respect to T_1, predicted by a ground motion attenuation equation, divided by the logarithmic standard deviation. Thus, epsilon is measured as a number of standard deviations that an observed response is from the mean of an attenuation equation as shown in Eq. (2.7.1). Attenuation prediction equations are used by seismologists to evaluate the energy loss, or attenuation of a ground motion given by different properties such as Moment Magnitude, the closest distance to the rupture plane, the type of fault, and the peak ground acceleration (Abrahamson and Silva 1997).

$$\varepsilon = \frac{\ln\big(S_a(T_1)\big)_{observed} - \mu_{\ln(S_a(T_1))_{Attenuation}}}{\sigma_{\ln(S_a(T_1))}} \tag{2.7.1}$$

Performance Levels, PL, are considered in fragility analysis as a goal post to evaluate the probability of said PL to be exceeded given a specific IM. These performance levels can be assigned by quantitative or qualitative means. Qualitatively, PLs regarding structural and non-structural systems are defined in 4 primary categories according to ASCE 41-13 (ASCE 2013)

1. Operational (O) – No structural damage and non-structural components can function as they were prior to the seismic event.

2. Immediate Occupancy (IO) – Building retains its structural strength and stiffness, and occupants can have immediate access to the structure where vital non-structural components remain functional.

3. Life Safety (LS) – Occupants of the building are protected from loss of life, and the structure remains to have a significant capacity against collapse and all non-structural damage is not life threating.

4. Collapse Prevention (CP) – Margin against collapse is limited, however, gravity loads still tend to be supported, and non-structural components have a risk of falling but high hazard materials are still secured.

Quantitative PLs are considered to correspond with qualitative PLs and can be judged to supersede the quantitative measures given by codes. For example, these PLs can be considered at the first yielding of a member or the initiation of a plastic storey mechanism (Wen et al. 2004). However, these mechanisms typically correspond to typical values assigned through qualitative means.

FEMA 356 (FEMA 2000) has assigned drift and residual drift limits for frames and braced frames that correspond to the qualitative PL descriptions. Braced frames PL limits are defined in Figure 2.7-1.

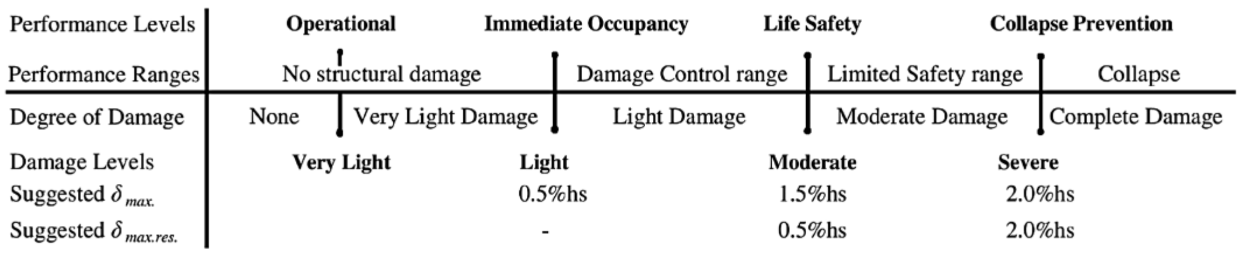

Figure 2.7-1. Mapping of Performance Levels for Braced Frames according to ASCE 41-13 (Tirca et al. 2016)

In fragility analysis, the fragility curve is developed in the scalar and vector forms by the Eqs. (2.7.2) and (2.7.3), respectively. Then, Eq. (2.7.2) shows the probability that the Performance Level (PL) is exceeded given the IM, where $\Phi[]$ is the lognormal cumulative distribution function (CDF), x is the IM under evaluation, m_R is the median of the fragility function where there is a 50% probability that the PL will be exceeded, and β_R is the logarithmic standard deviation. Considering the vector-form, in Eq. (2.7.3), β_2 and β_3 are determined for a fixed IM (scaled GM based on $S_a(T_1)$) and linear least-squares regression is done for the values of ε and the Engineering Design Parameter, EDP, (i.e. drift) as shown in Figure 2.6-2 and defined by Eq. (2.7.4). Herein, e is the prediction error also known as the residual and $\hat{\sigma}_e$ is the standard deviation of the residuals.

$$P(PL|IM = x) = \Phi\left[\frac{\ln\left(\frac{x}{m_R}\right)}{\beta_R}\right] \tag{2.7.2}$$

$$P(EDP = z | IM = x_1, \varepsilon = x_2) = \Phi\left[\frac{\ln\left(\frac{z}{\beta_2 + \beta_3 x_2}\right)}{\hat{\sigma}_e}\right] \tag{2.7.3}$$

$$\ln(EDP) = \beta_2 + \beta_3\varepsilon + e \tag{2.7.4}$$

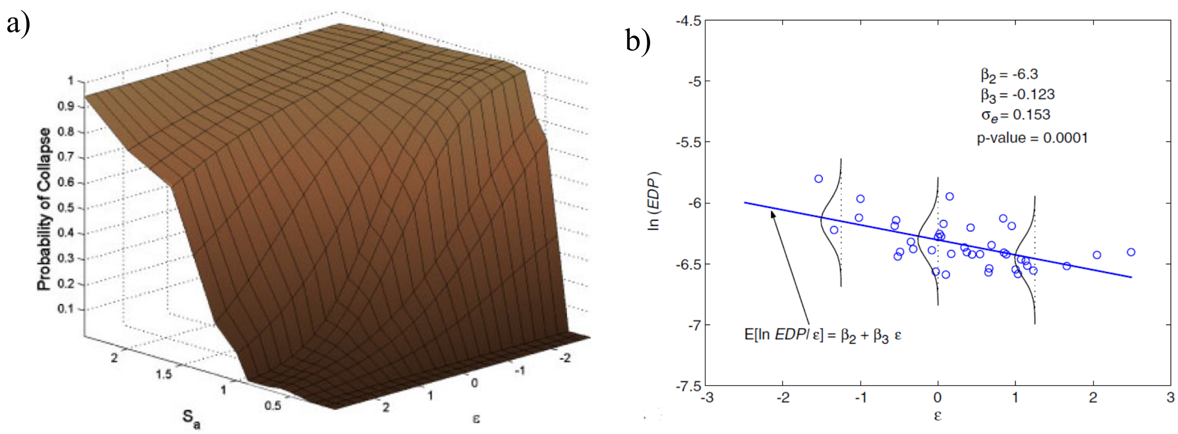

Figure 2.7-2. Vector form of fragility curve: a) Fragility curve for the probability of collapse given S_a and ε b) Linear regression of the response parameter vs ε for a fixed value of S_a (Baker and Cornell 2005)

The uncertainties that arise in the probability of collapse are aleatoric and epistemic. Aleatoric uncertainty represents the ground motion-to-ground motion variability. Epistemic uncertainty considers the lack of knowledge needed incorporate all of the elements within a model that could contribute to the model's response. In Eq. (2.7.2), aleatoric and epistemic uncertainty is not considered. To consider both aleatoric and epistemic uncertainty, β_R, can be defined by Eq. (2.7.5), where β_{RR} and β_{RU} are the uncertainty components that represent the aleatoric and epistemic uncertainties, respectively (Ellington et al. 2007). Aleatoric uncertainty is described by Eq. (2.7.6) where $\beta_{D|S_a}$ is the seismic demand uncertainty, and β_C is the capacity uncertainty.

$$\beta_R = \sqrt{\beta_{RR}^2 + \beta_{RU}^2} \tag{2.7.5}$$

$$\beta_{RR} = \sqrt{\beta_{D|S_a}^2 + \beta_C^2} \tag{2.7.6}$$

The seismic demand uncertainty, $\beta_{D|S_a}$, can be calculated through many modes of analysis for many types of intensity measures. Nonlinear Incremental Dynamic Analysis has been commonly used to determine the IM and EDP values required for the evaluation of the fragility curves (Baker and Cornell 2005; Tirca et al. 2016; Zareian and Krawinkler 2007). Considering IDA, each ground motion in each suite will have a corresponding data point $\{(IM_i, EDP_{max,i}), i = 1, \dots N\}$ where i is the ground motion under consideration of a suite with N ground motions for each performance level. To describe the relationship between the IM and the EDP, which will from now on be referred to as "first mode" spectral acceleration, S_a, and maximum drift, θ, respectively, methods of regression can be implemented to create a predictive equation. Due to the nonlinearity common in the relationship between spectral acceleration and drift, a power law form is used as shown in Eq. (2.7.7). By transforming the power law form into a logarithmic form as shown in Eq. (2.7.8), simple least squares regression can be utilized to determine the coefficients a and b. The standard error, s^2, is taken as the residual sum of squares divided by the total number of data point, n. The standard error provided in Eq. (2.7.9) is used in Eq. (2.7.10) to find the seismic demand uncertainty.

$$\theta_{predicted} = aS_a^b \tag{2.7.7}$$

$$\ln(\theta_{observed}) = \ln(a) + b\ln(S_a) \tag{2.7.8}$$

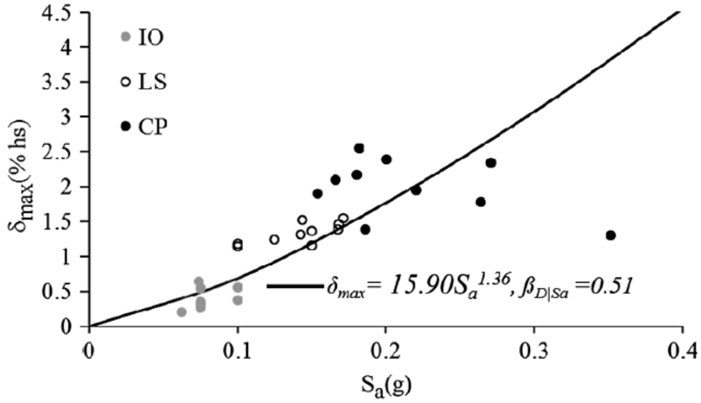

Figure 2.7-3. Linear regression results of the maximum drifts vs spectral acceleration for three Performance Levels: IO, LS and CP (Tirca et al. 2016)

$$s^2 = \frac{\sum\left[\ln(\theta_{observed}) - \ln\left(\theta_{predicted}\right)\right]^2}{n-2} \tag{2.7.9}$$

$$\beta_{D|S_a} = \sqrt{\ln\,(1+s^2)} \tag{2.7.10}$$

Chapter Three

Design Methodology and Analysis of Friction Sliding Braced Frames

Design of Friction Sliding Braced Frames (FSBF) provided herein are mainly based on the requirements presented for Concentrically Braced Frames (CBF) in the CSA S16-14 standard. However, some modifications to include the differences in nonlinear behaviour are presented. For this system, the inelastic behaviour is concentrated in the Pall Friction Dampers (PFD), while preserving the attached beams, columns, and connections in the elastic range. Capacity design method, as specified in the CSA S16-14, is implemented in the design of these surrounding members to include the probable capacity of seismic fusses (PFDs) along their load paths. The PFDs are designed to not slip under service loads including the code-wind force.

Little guidance in the NBCC 2015 is provided for selecting the ductility-related force modification factor (R_d) and overstrength-related force modification factor (R_o) for these systems with incorporated PFDs. However, since the PFD's brace support is not to experience in-plane nor out-of-plane buckling, it is assumed that the R_d factor for FSBF should be at least equal to that of Buckling Restrained Braced Frames (BRBF), where R_d = 4. PFDs do not exhibit overstrength behaviour and thus an overstrength-related force reduction factor of R_o = 1 is assigned. The majority of the differences between the design of FSBFs compared to CBFs are related to the behaviour of PFDs characterized by the slip force and slip length. However, from experimental testing conducted at Ecole Polytechnique Montreal, PFDs were able to sustain two times their slip force F_{slip}, without encountering damage. Thus, the question is: What PFD capacity should be used in capacity design? For this reason, it is proposed to control the axial force triggered from PFD to the frame by adding a second ductile fuse in the PFD-to-frame gusset plate connection that is designed to fail at a pre-determinate force. This permits a more economical design of columns, and a more reliable behaviour of the PFDs since limited information is available regarding their failure behaviour under loads greater than F_{slip}. The non-linear behaviour of PFDs has 4 stages: i) Elastic, ii) Slipping, iii) Bearing, and iv) Failure. The modelling of these stages, and their limits are specifically defined in the model to provide reliable results.

3.1 Design Methodology for Friction Sliding Braced Frames

The following guidelines were used for the design of the FSBF models herein, and basic design principles provided in the following provisions were incorporated (ASCE 2000, 2013; FEMA 2000, 2003; NBCC 2015):

- The minimum number of PFDs, to be displaced in the direction of an earthquake excitation, should be at least one in each quadrant of the building and two respectively such that one is displaced in *x*-direction and the other one in *y*-direction. Therefore, a minimum of eight PFDs should be installed in any given storey, where four are installed in the direction of the earthquake loading (e.g. *x*-direction) and another four are installed in the orthogonal direction.

- Irregular buildings controlled by torsion should not utilize PFDs to make the building regular.

- PFDs must not slide under factored wind loads.

- Design by the implementation of the equivalent static force procedure should use a ductility-related force modification factor selected among the proposed values of $R_d = 4$ or $R_d = 5$, where $R_0 = 1$. However, using $R_dR_o = 5$ may increase the system's instability.

- Distribution of the base shear, V, found by means of the equivalent static force procedure along the building height, should be used for the preliminary design of PFDs. Thus, distribute the storey shears into the braces to find their factored axial tensile and compressive forces, T_f and C_f respectively. Round the T_f and C_f, to the nearest 50 kN and consider this value as F_{slip}.

- For the selection of the HSS section for braces supporting the PFDs, select a section where their factored compressive resistance is greater than or equal to $1.3F_{slip}$. Use Class 1 or Class 2 sections for these HSS braces. In general, single diagonal braces are considered as supported braces for PFDs.

- For beams and columns of FSBF, capacity design principles are applied. The probable compressive resistance, C_u, of the brace supporting PFD should be projected into the beams and columns. By design, it is assumed that forces larger than C_u cannot be generated in braces as explained hereafter. In addition, the factored moment $M_f = 0.2ZF_y$, in combination with the probable axial compressive force from the brace projected into the columns should be considered in addition to the gravity load component for the design of columns. In general, W-shape sections are selected for columns and Class 1 section is recommended.

- The demand slip length, Δ_{slip}, in each PFD should be computed as the mean plus standard deviation of the interstorey drift resulted under a suite of minimum 7 ground motions, as determined by nonlinear dynamic analysis under design basis earthquake (2%/50 years). The slip length to be selected shall be $1.3\Delta_{slip}$. Furthermore, for steel braced frames, the peak interstorey drift for normal importance category buildings shall not exceed $2.5\%h_s$, where h_s is the storey height, according to NBCC 2015.

3.1.1 Gravity Load Calculations

Gravity loads are calculated according to the NBCC 2015, where loads are combined using different load combination cases as follows:

$$1.4D \tag{3.1.1}$$

$$1.25D + 1.5L + max(1.0S, 0.4W) \tag{3.1.2}$$

$$1.25D + 1.5S + max(1.0L, 0.4W) \tag{3.1.3}$$

$$1.25D + 1.4W + max(0.5L, 0.5S) \tag{3.1.4}$$

$$1.0D + 1.0E + 0.5L + 0.25S \tag{3.1.5}$$

Herein, D is the dead load, L is the live load, S is the snow load, W is the wind load, and E is the earthquake load as defined by the NBCC 2015.

3.1.1.1 Dead load, Live load, and Snow load calculations

According to the NBCC 2015, dead loads are calculated considering the self-weight of the members, composite slab, weight of partitions, where partition loads shall not be taken less than 1.0 kPa over the entire area of the floor, and the weight of permanent equipment.

Live loads are to be selected from the NBCC 2015 for occupancy types that are associated with the intended use of the building, tributary area, and assigned live load. The tributary areas are cumulative from the floors above to the floor under consideration. The cumulative areas are summed based on having the same use and occupancy type. Therefore, the roof tributary area does not contribute to the cumulative tributary areas below since their occupancies are not the same. This is true for assembly and non-assembly tributary areas as well.

Table 3.1.1-1: Live Load Reduction Factor Criteria

Occupancy	Live Load (kPa)	Cumulative Tributary Area, A or B (m^2)	LLRF
Assembly	< 4.8	-	1.0
Roof	-	-	1.0
Assembly	≥ 4.8	> 80	$0.5 + \sqrt{20/A}$
Non-Assembly	-	> 20	$0.3 + \sqrt{9.8/B}$

Snow loads vary depending on the geometry of the roof/exposed surface. The buildings studied herein, have flat roofs with urban exposure. For brevity, snow load calculations will not be shown in more detail. The snow load is calculated using the following equation:

$$S = I_s[S_s(C_b C_w C_s C_a) + S_r] \tag{3.1.6}$$

where I_s is the importance factor for snow, S_s is the 1-in-50-year ground snow load, C_b is the basic roof snow load factor, C_w is the wind exposure factor, C_s is the slope factor, C_a is the accumulation factor, and S_r is the 1-in-50-year rain load.

3.1.2 Seismic force and distribution along the building height

For the preliminary design of the structure, the equivalent static force procedure (ESFP) is used according to the NBCC 2015. The minimum lateral earthquake force, V, is calculated using the following formula:

$$V = \frac{S(T_a)M_v I_e W}{R_d R_o} \tag{3.1.7}$$

where $S(T_a)$ is the 5% damped spectral response acceleration, M_v is the factor to account for the higher mode effects on base shear, I_E is the importance factor of the structure, W is the seismic weight of the structure defined as 100% of the dead load plus 25% of the snow load, R_d is the ductility-related force modification factor and R_o is the overstrength-related force modification factor. Furthermore, V shall not be taken larger than the value prescribed in Eq. (3.1.8), nor shall it be less than the value given in Eq. (3.1.9) for any seismic force resisting systems (SFRS) with an R_d greater than or equal to 1.5:

$$V \leq max \begin{bmatrix} \frac{\frac{2}{3}S(0.2)I_E W}{R_d R_o} \\ \frac{S(0.5)I_E W}{R_d R_o} \end{bmatrix} \tag{3.1.8}$$

$$V \geq \frac{S(2.0)M_v I_E W}{R_d R_o} \tag{3.1.9}$$

Since the stiffness matrix used for eigenvalue analysis of the structure is derived by the stiffness of the columns (influenced by their connections), the beams, and the braces, the empirical formula used to estimate the fundamental period, T_a, for CBFs is used for FSBFs. It is also worth noting that since dynamic analysis will be performed, the value of T_a may be increased to a maximum of $2T_a$ for CBFs.

$$T_a = 0.025h_n \tag{3.1.10}$$

where h_n is the total height of the structure, in meters.

The ESFP estimates the forces considering a generalized single-degree-of-freedom system, where the first mode is emphasized as governing the building's response. As previously mentioned, the factor M_v is used to modify the base shear in order to consider the higher mode effects on the building. However, this factor does not affect how the higher modes influence storey shear distribution. As a building's height increases, higher modes have more influence on the top floor than they have influence on the base shear (Chopra 2012). To compensate for this, the NBCC 2015 requires a concentrated load at the top of the building, F_t. Since the period is proportional to the height, F_t is only included for buildings where the period is ≥ 0.7 s. The remainder of the base shear, $(V – F_t)$, is weight-height-proportionally distributed along the storey height as such:

$$F_x = (V - F_t)\left(\frac{W_x h_x}{\sum_{i=1}^{n} W_i h_i}\right) \tag{3.1.11}$$

where *x* is the storey under consideration, *n* is the number of storeys, *i* is the storeys under consideration and

$$F_t = \begin{cases} 0 & T_a \leq 0.7 \\ 0.07 T_a V \ \ for & 0.7 < T_a < 3.6 \\ 0.25V & T_a \geq 3.6 \end{cases} \tag{3.1.12}$$

The distribution of forces along the building height is shown in Figure 3.1-1.

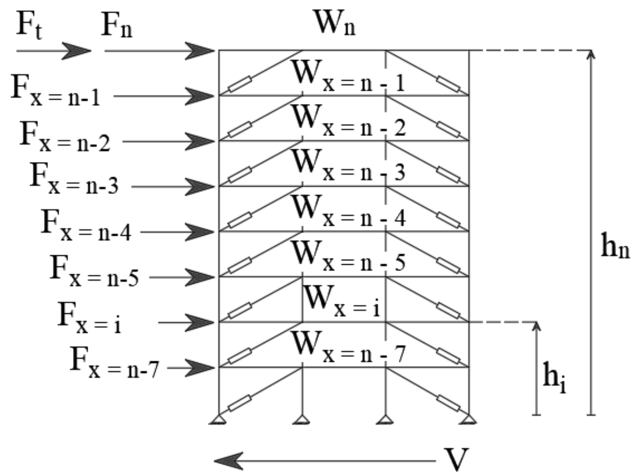

Figure 3.1-1. Distribution of Forces along the building height (ESFP)

3.1.3 P-delta and notional loads

System instability calculations are required according to CSA S16-14 by the application of notional loads, N, and by an amplifying translation load factor, U_2, at every storey height (P-delta effect). Notional loads are lateral forces added to all lateral load cases as a percentage of all factored gravity loads. Notional loads and the amplifying translational load factors used to amply the lateral force (P-delta) are defined as such:

$$N_i = 0.005 \ x \ \boldsymbol{\Sigma C_f} \tag{3.1.13}$$

$$U_2 = 1 + \left(\frac{\sum C_f}{\sum V_f} \frac{R_d \Delta_f}{h_s} \right) \leq 1.4 \tag{3.1.14}$$

Herein, C_f is the cumulative factored gravity loads component of the earthquake load case given in Eq. (3.1.5); V_f is the cumulative shear force, where the storey force is calculated according to Eq. (3.1.11); Δ_f is the interstorey drift at the floor under consideration; h_s is the height of the storey under consideration and R_d was defined above.

3.1.4 Wind load

It is necessary that the PFDs do not slip under extreme wind loads. Thus, wind loads distributed into the braces must not exceed the slip force of the device. This creates some limitations regarding the building geometries and locations where these devices may be installed. According to the NBCC 2015, for buildings that are not dynamically sensitive, wind load can be calculated using one of the three methods: i) Static Procedure, ii) Dynamic Procedure, iii) Wind Tunnel Procedure. For buildings that are defined as dynamically sensitive, wind loads must be calculated using one of the two methods: i) Dynamic Procedure, ii) Wind Tunnel Procedure. A dynamically sensitive building is defined below:

$$Dynamically\ Sensitive\ if \begin{cases} 0.25Hz \leq f_n \leq 1.0Hz; or \\ h_n > 60m; or \\ h_n > 4\dfrac{\sum h_i w_i}{\sum h_i} \end{cases} \tag{3.1.15}$$

where f_n is the lowest natural frequency of the building, h_n is the building height, h_i is the height from ground level to the floor under consideration, and w_i floor width normal to the height h_i.

Some buildings herein can be classified as not being dynamically sensitive. These structures were thus calculated using the appropriate static procedure. Below, the equation for wind pressure, p, according to the NBCC 2015 is given.

$$p = I_w q C_e C_t C_g C_p \tag{3.1.16}$$

Herein, I_w is the importance factor for wind, q is the reference velocity pressure for a probability of exceedance of 1-in-50-year, C_e is the exposure factor, C_t is the topographic factor, C_g is the gust factor, and C_p is the external pressure coefficient.

The exposure factor, C_e, is defined for different types of terrains to evaluate the variability of wind pressure associated with different types of wind exposure for the design of main structural elements. It is important to note that the exposure factor is not constant over the height of the building when calculating for the windward direction; it is a function of height from ground level to the floor under consideration, where h is the height of the floor under consideration from ground level. For the leeward direction, C_e is a constant value over the entire height of the building, taken at the height h = H/2, where H is the total height of the building,

$$Open\ Terrain: C_e = \left(\frac{h}{10}\right)^{0.28}; 1.0 \leq C_e \leq 2.5 \tag{3.1.17}$$

$$Rough\ Terrain: C_e = 0.5\left(\frac{h}{12.7}\right)^{0.50}; 0.5 \leq C_e \leq 2.5 \tag{3.1.18}$$

Dynamic Procedure for wind pressures varies largely from the Static Procedure in regard to the calculation of the gust factor, C_g. This factor considers the intensity of wind turbulence as a function of surface roughness. The gust factor also includes properties specific to the building's configuration such as, height, width, natural frequency of vibration, and damping.

$$C_g = 1 + g_p\left(\frac{\sigma}{\mu}\right) \tag{3.1.19}$$

$$g_p = \sqrt{2\,ln(\nu T)} + \frac{0.557}{\sqrt{2\,ln(\nu T)}} \tag{3.1.20}$$

$$\frac{\sigma}{\mu} = \sqrt{\frac{K}{C_{eH}}\left(B + \frac{sF}{\beta}\right)} \tag{3.1.21}$$

Regarding the Topographic Factor, C_t, the value shall be taken as 1.0 unless the building is located on a hill or an escarpment where the slope is greater than 0.1.

The External Pressure Coefficient, C_p, is calculated in the leeward direction and in the windward direction of the building and then combined at the end to determine the wind forces applied onto the structure. The sign convention for C_p is positive towards the face of the building, this sign convention must be taken into consideration when summing the resulting forces from the windward and leeward components. The following equations are used to evaluate C_p:

$$C_{p_{Windward}} = \begin{cases} 0.6, & \frac{H}{D} < 0.25 \\ 0.27\left(\frac{H}{D} + 2\right), & 0.25 \leq \frac{H}{D} < 0.1 \\ 0.8, & \frac{H}{D} \geq 1.0 \end{cases} \tag{3.1.22}$$

$$C_{p_{Leeward}} = \begin{cases} -0.3, & \frac{H}{D} < 0.25 \\ -0.27\left(\frac{H}{D} + 0.88\right), & 0.25 \leq \frac{H}{D} < 0.1 \\ -0.5, & \frac{H}{D} \geq 1.0 \end{cases} \tag{3.1.23}$$

3.1.5 Diagonal brace and Friction Damper design

The lateral force resisting systems studied herein are designed with single diagonal braces spanning across the entire bay width. Herein, the axial force transferred into the braces are storey shear forces including notional loads and P-delta effects as per Eqs. (3.1.11), (3.1.13), and (3.1.14), respectively. A ductile fuse by means of ductile gusset plate failure, as will be presented later, will be used to limit excessive axial forces that can be transferred from the PFD to the frame and could promote a predictable response of the structure. Hollow Structural Sections, HSS, are used for braces and are proportioned to respond elastically in tension and compression. All non-linear properties of the brace assembly come from the response of PFD. Figure 3.1-2 presents the typical components of PFDs; however, this cannot correspond to that produced by the manufacturer.

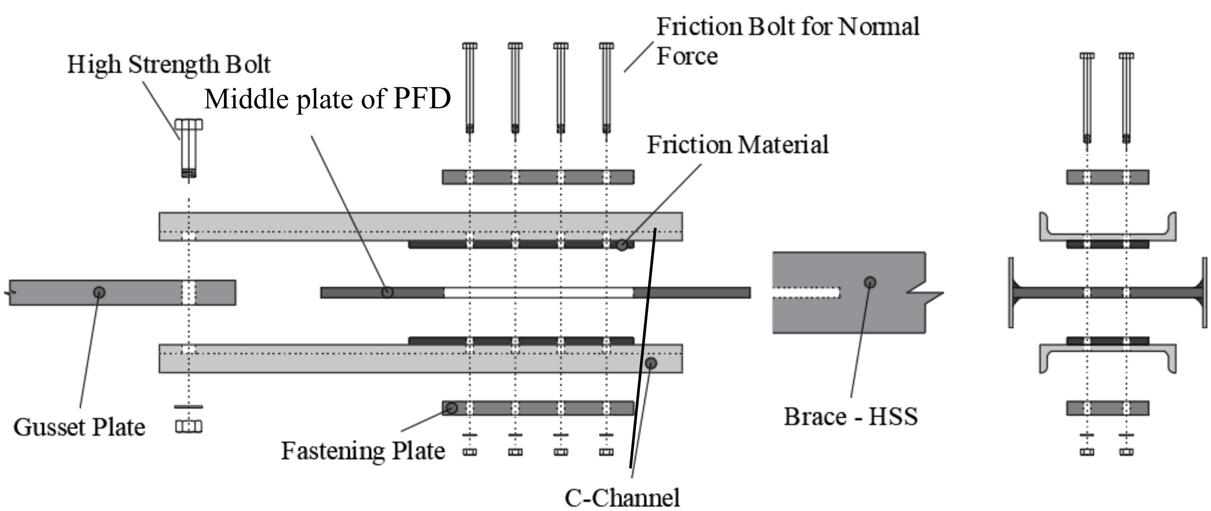

Figure 3.1-2. Pall Friction Damper Assembly (generic)

As shown in Figure 3.1-2, a PFD is fabricated using two C-Channel sections to which a friction material, something resembling a break lining pad, is attached, and clamped to a middle steel plate with smooth surface to which a perpendicular plate is welded to form a I-shaped section. The normal force, which will dictate the slipping force, is determined by the pretensioned force applied to the bolts of PFD. High strength bolts are used to connect the PFD to the gusset plate and an HSS brace is welded to the middle plate to form the entire brace assembly.

Once the factored loads are calculated, the slip force, F_{slip}, can be selected for the PFD. Ideally, the slip force should be as close to the compressive factored force, C_f, as possible to ensure slipping to occur under the proper demand. Slipping occurs once the external forces transferred from the supported HSS brace to PFD equates F_{slip}. For manufacturing reasons, the PFD is specified to have a slip force rounded up to the nearest 50 kN as described by Eq. (3.1.24) where, m is the nearest multiple (50 kN), and $\left\lceil \frac{C_f}{m} \right\rceil$ denotes rounding up to the nearest integer.

$$F_{slip} = m \left\lceil \frac{C_f}{m} \right\rceil \tag{3.1.24}$$

Once the slip force of PFD is selected, the compressive resistance, C_r, of the HSS brace is calculated according to Article 13.3.3.1 of the CSA S16-14. The brace is selected to have a compressive resistance computed with Eq. (3.1.25) that respects Eq. (3.1.26):

$$C_r \geq 1.3F_{slip} \tag{3.1.25}$$

where,

$$C_r = \frac{\varphi A F_y}{(1 + \lambda^{2n})^{\frac{1}{n}}} \tag{3.1.26}$$

Herein, n = 1.34, k = 1.0 (pinned-pinned), $\varphi = 0.9$ and the slenderness λ is provided in Eq. below.

$$\lambda = \sqrt{\frac{F_y}{F_e}} \tag{3.1.27}$$

$$F_e = \frac{\pi^2 E}{\frac{KL}{r}} \tag{3.1.28}$$

The factor of $1.3F_{slip}$ is comprised of a 1.1 factor of safety and a 1.15 factor related to the potential difference of slipping force at zero and maximum displacement found in the testing procedure for displacement-dependent devices in ASCE/SEI 7-10, Article 18.9 (ASCE 2010). For friction dampers, this difference of slip force is due to the dynamic and static coefficients of friction. The static coefficient of friction is larger than the dynamic coefficient of friction. For slipping to occur in the PFD, the static coefficient of friction needs to be exceeded. Then, the friction force during displacement decreases according to the dynamic coefficient of friction, where the entirety of the PFD's displacement occurs.

The last parameter to be specified by the designer is the slip length. Sufficient distance must be permitted by the PFD to avoid premature bearing. For preliminary design, the slip distance is selected as a value less than or equal to the maximum allowable interstorey drift projected into the brace. Final specifications of this slip length should be defined by the mean + standard deviation of the interstorey drift resulted from Non-Linear Dynamic Analysis (NLDA) under a minimum of 7 ground motion excitations, as specified by Article 4.1.8.20 3) of NBCC 2015. As was done for the slip force, a factor of 1.3 is applied to the slip length as well. This distance can be visualized in Figure 3.1-3 for the pivot extremes of a PFD under cyclic loading.

$$\Delta_{slip} = 1.3\Delta_{\mu+\sigma} cos\alpha \tag{3.1.29}$$

Herein, $\Delta_{\mu+\sigma}$ is the interstorey drift determined by summing the mean and standard deviation of all analyses completed by NLDA, and α is the brace angle relative to the bottom floor.

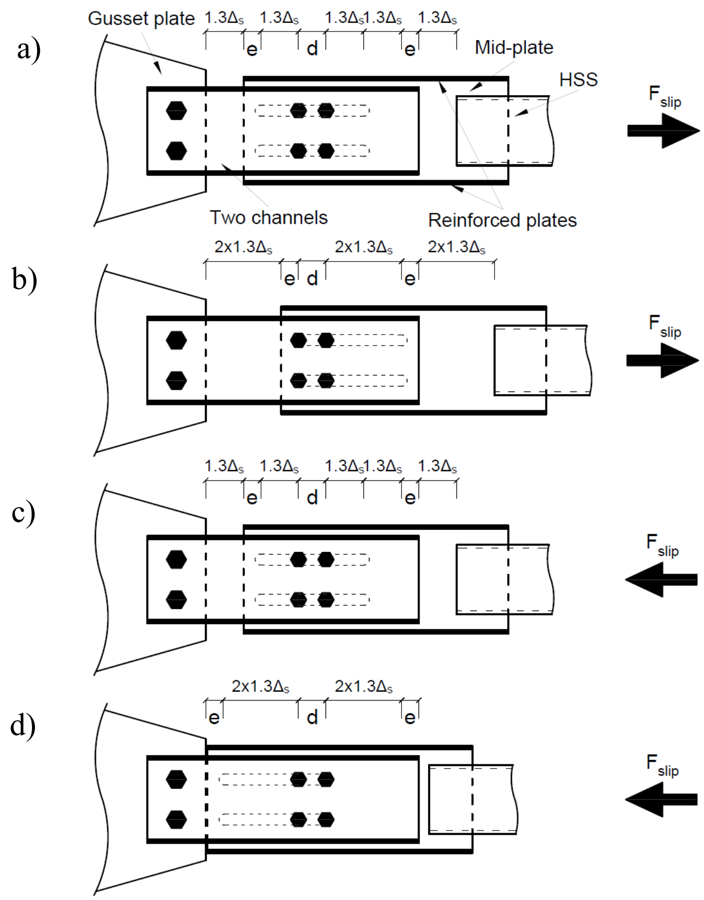

Figure 3.1-3. Pall Friction Damper design dimensions relative to all loading/displacement phases; a) initial position b) full slip length in tension c) reverse-initial position and d) full slip length in compression

3.1.6 Column design of Seismic Force Resisting System

Columns are to be designed using capacity design principles to prevent failure under excessive demand. Thus, for columns, the probable compressive resistance, C_u, of the HSS brace is projected into the columns using the load case defined by Eq. (3.1.5). No probable post-buckling compressive resistance, C_u', is required for this configuration since buckling of the HSS is not expected, as well as no probable tensile resistance, T_u, since tensile forces will be limited by the addition of a second ductile fuse located within the PFD to frame gusset plate connection. No inelastic behaviour is allowed to develop in columns of FSBF; members are to be design elastically. The probable compressive resistance of HSS brace projected into the column is evaluated by:

$$C_u = \frac{1.2C_r(R_yF_y)}{\varphi F_y} sin\alpha \tag{3.1.30}$$

where R_yF_y = 460 MPa for HSS braces and α is the brace angle relative to a horizontal line.

Columns will also be subjected to additional moments evaluated as:

$$M_f = 0.2ZF_y \tag{3.1.31}$$

where Z is the plastic section modulus of steel selected to be about the axis in bending in reference to the direction of seismic forces of the column.

Plastic moment resistance is calculated as:

$$M_r = \varphi ZF_y \tag{3.1.32}$$

where Z is the plastic section modulus of steel selected to be about the axis in bending in reference to the direction of seismic forces of the column, and $\varphi = 0.9$. A figure is showed below.

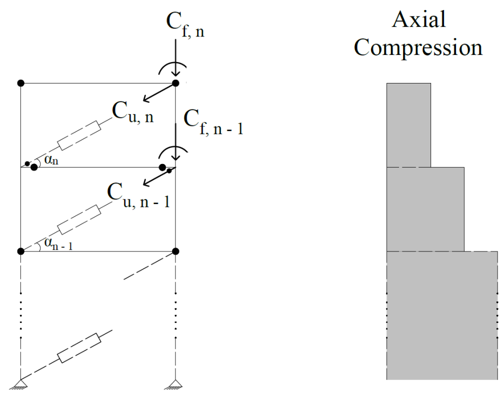

Figure 3.1-4. Force and Moment demands on columns of friction braced frame, loaded in compression, where column is continuous

According to Article 13.8.2, CSA S16-14, member strength and stability for Class 1 and 2 I-shaped members must resist an interaction between axial compression and bending moments as described by the limit below:

$$\frac{C_f}{C_r} + \frac{0.85U_{1x}M_{fx}}{M_{rx}} + \frac{\beta U_{1y}M_{fy}}{M_{ry}} \leq 1.0 \tag{3.1.33}$$

where $\beta = 0.6 + 0.4\lambda_y \leq 0.85$

Biaxial bending is not present in the models herein therefore the third term of Eq. (3.1.33) is equal to zero. The preceding interaction limit must be verified for three types of member strength: i) cross-sectional strength, ii) overall member strength, and iii) lateral torsional buckling strength.

i) Cross-Sectional Strength

$$C_r = \varphi A F_y \tag{3.1.34}$$

$$M_{rx} = \varphi Z_x F_y \tag{3.1.35}$$

$$U_{1x} = \left[\frac{\omega_1}{1 - \frac{C_f}{\frac{\pi^2 E I_x}{L^2}}} \right] \geq 1.0 \tag{3.1.36}$$

ii) Overall Member Strength

$$C_r = \frac{\varphi A F_y}{(1 + \lambda_x^{2n})^{\frac{1}{n}}}, where\; n = 1.34 \tag{3.1.37}$$

$$M_{rx} = \varphi Z_x F_y \tag{3.1.38}$$

$$U_{1x} = \left[\frac{\omega_1}{1 - \frac{C_f}{\frac{\pi^2 E I_x}{L^2}}} \right] \tag{3.1.39}$$

iii) Lateral Torsional Buckling Strength (λ is calculated on weak axis)

$$C_r = \frac{\varphi A F_y}{\left(1 + \lambda_y^{2n}\right)^{\frac{1}{n}}}, where\; n = 1.34 \tag{3.1.40}$$

$$M_{rx} = \varphi M_p = \varphi Z_x F_y \tag{3.1.41}$$

$$U_{1x} = \left[\frac{\omega_1}{1 - \frac{C_f}{\frac{\pi^2 E I_x}{L^2}}} \right] \geq 1.0 \tag{3.1.42}$$

For Eqs. (3.1.36), (3.1.39), and (3.1.42), $\omega_1 = 0.6 - 0.4\kappa \geq 0.4$, where $\kappa = \frac{M_{Min}}{M_{Max}}$ at opposite ends of the column. For columns pinned at one end and fixed at the other $\kappa = 0$ and $\omega_1 = 0.6$.

3.1.7 Beam design of Seismic Force Resisting System

Beams of FSBFs are loaded axially via storey shear and bending via gravity loads. Thus, Eq. (3.1.5) is used to describe the demands of the beams combining gravity loads and earthquake loads. Capacity design principles are used for the evaluation of demand on the beams. Figure 3.1-5 shows how axial forces are triggered from braces to the beams.

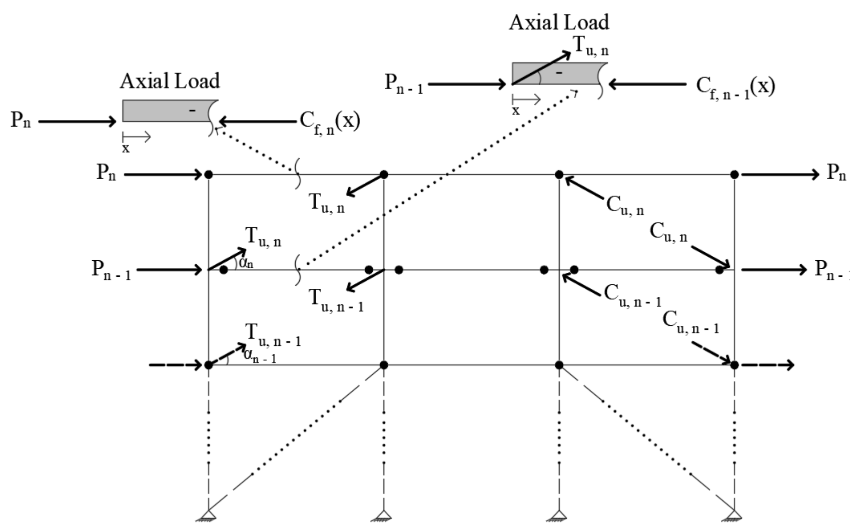

Figure 3.1-5. Projection of axial forces from PFDs to beams of FSBF

As previously mentioned, FSBFs beams and columns are to be designed to withstand the probable compressive strength of the braces, C_u, while the probable tensile force developed in HSS brace T_u is limited to C_u. The interaction considering axial tension force and bending moment demands as defined by Eq. (3.1.33) and Eq. (3.1.43) should be check.

$$\frac{T_f}{T_r} + \frac{M_f}{M_r} \leq 1.0 \tag{3.1.43}$$

3.1.8 FSBF - Building Description

The investigated buildings are the 4-storey and 8-storey buildings with the same floor plan and gravity loads that remain unchanged for all of the case studies, as shown in Figure 3.1-6. Three different SFRSs are considered such as: the bare FSBF, FSBF-CC (FSBF with continuous columns including gravity columns), and dual system, D-FSBF, as provided in Table *3.1.7-1*. For both 4-storey and 8-storey D-FSBF systems the design is conducted independently for R_d=4 and R_d=5. The FSBF system design is presented in this chapter. Later chapters will address the FSBF-CC and D-FSBFs. Many insights can be acquired by considering different aspects of these systems.

Table 3.1.7-1. Studied systems

System	**R_dR_o**	**Number of Storeys**
FSBF-I (4-St.)	4	4
FSBF-CC-I (4-St.)	4	4
D-FSBF-I (4-St.)	4	4
D-FSBF-II (4-St.)	5	4
FSBF-I (8-St.)	4	8
FSBF-CC-I (8-St.)	4	8
D-FSBF-I (8-St.)	4	8
D-FSBF-II (8-St.)	5	8

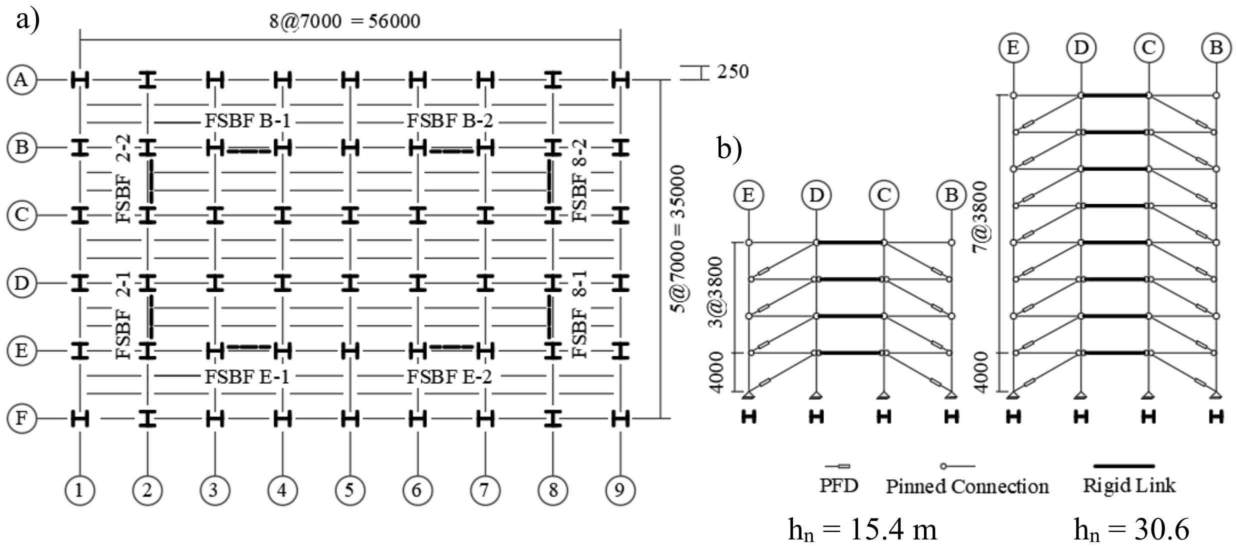

Figure 3.1-6. Building prototype: a) typical floor plan braced by bare FSBFs and b) elevations (N-S)

Figure 3.1-6 presents the floor plan and the elevation of FSBF located in grid line 2 (N-S direction). The bay spacing in the N-S direction and E-W direction is 7.0 m, where the number of bays is 5 and 8, respectively. The typical storey height of the building is 3.8 m and the first storey height is 4.0 m. PFDs are installed in braced frames displaced symmetrical in both orthogonal directions with respect to the center of mass, which is in the same location as the center of rigidity. Columns of FSBFs are oriented to have bending in the strong axis. The gravity loads considered on the building are in accordance with Section 3.1.1 and summarized in Table 3.1.7-2, where 1.0 kPa is considered for cladding walls. All columns of FSBFs, including gravity columns, are continuous over 2 storeys. The members selected for the FSBF-I (4-storey) and FSBF-I (8-storey) are shown in Table 3.1.7-4 and Table 3.1.7-5, respectively. The members selected for the gravity systems are given in Table 3.1.7-6 and Table 3.1.7-7.

Table 3.1.7-2. Gravity Loads

Loads	Roof (kPa)	Floor (kPa)
Dead	3.8	4.0
Live	1.0	2.4
Snow	1.64	-

3.1.9 Equivalent static force procedure and wind loads

According to ESFP, the period of the 4-storey building is T_a = 0.025 x 15.4 =0.385 s and $2T_a$ = 0.77s. In addition, the fundamental period of the 8-storey building is T_a = 0.025 x 30.6 =0.765 s and $2T_a$ = 1.53s. The seismic weight of the 4-storey and 8-storey buildings, as well as the base shear (ESFP) calculated for R_dR_0=4, are presented in Table *3.1.7-3*.

For Vancouver, the design spectral ordinates for 0.2, 0.5, 1.0, 2.0, and 5.0 s are 0.848, 0.751, 0.425, 0.257 and 0.080 g, respectively. The peak ground acceleration is 0.369 g.

Forces distributed into the braces are shown in Figure 3.1-8, Figure 3.1-9, Figure 3.1-10, and Figure 3.1-11 for FSBF-I (8-St.), FSBF-II (8-St), FSBF-I (4-St), and FSBF-II (4-St.), respectively. The supportive HSS brace was designed such as the brace compressive resistance, C_r, be greater than $1.3F_{slip}$.

Table 3.1.7-3. Dynamic Properties and Seismic Base Shear for 4-storey and 8-storey

System	Empirical Fundamental Period, $2T_a$	Fundamental Period (OpenSees) T_1	Seismic Weight, W	Base Shear (ESFP), V
	[s]	[s]	[kN]	[kN]
FSBF-I (4-st)	0.770	0.627	31970	4595
FSBF-I (8-st)	1.530	1.333	62847	5279

Applying the capacity design principle, it resulted that the HSS brace, designed as Class 1 or 2, is able to develop the probable compression force C_u and the probable tensile force T_u. According to the provisions developed for concentrically braced frames, the beams and column members are proportioned to carry the C_u and T_u forces developed in HSS braces. Ideally, the column is designed to carry a maximum axial compression force associated with C_u developed in HSS braces. Thus, to limit the axial force developed in PDFs behaving in bearing, a secondary ductile fuse is considered and designed for an axial force that should be less than C_u developed in HSS brace but greater than $1.3F_{Slip}$. If $1.3F_{Slip}$ was to be taken 30% larger, as a margin of safety to avoid premature gusset failure and allow for some marginal PFD bearing, $1.7F_{Slip}$ would be a value of interest. Interestingly, if $C_u/1.2$ is computed, values of axial force in the braces approximate $2F_{Slip}$.

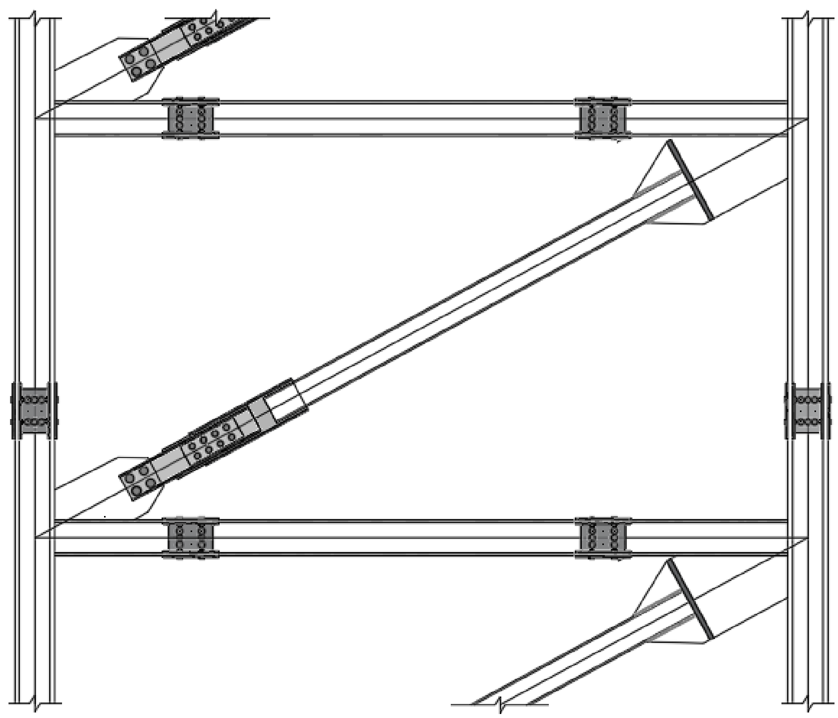

Figure 3.1-7. Brace-damper connection configuration in frame

Figure 3.1-8, shows the axial force of a single brace at each storey for the design of an 8-storey FSBF building. For this reason, the demand for gusset plate capacity design is selected to be $1.7F_{Slip}$. The brace-gusset connection, which is a welded HSS to gusset plate connection, as detailed in Chapter 4, is designed to respond elastically. The PFD is proposed to be installed at the bottom end of HSS brace and the brace-gusset connection will not fail before the damper-gusset connection.

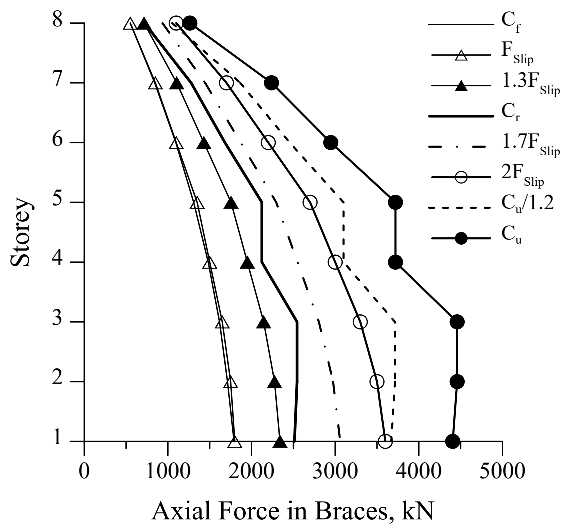

Figure 3.1-8. The 8-storey FSBF-I (R_dR_0=4) - Axial forces in braces along storey height

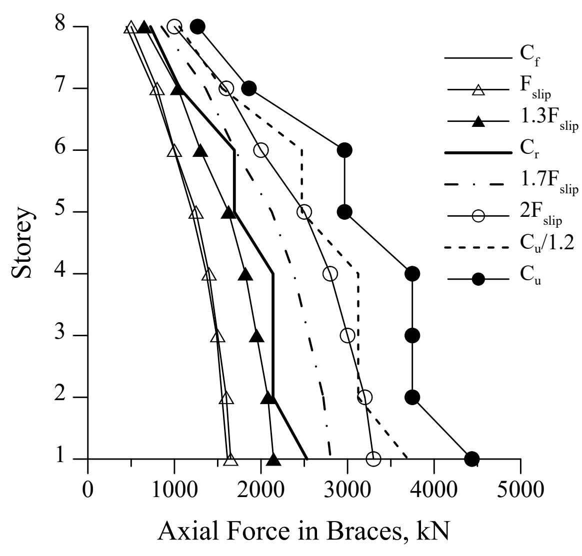

Figure 3.1-9. The 8-storey FSBF-II (R_dR_0=5) - Axial forces in braces along storey height

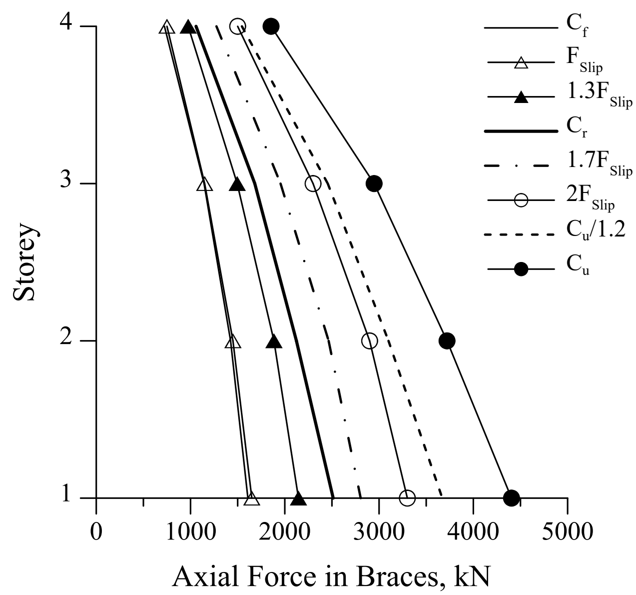

Figure 3.1-10. The 4-storey FSBF-I (R_dR_0=4) - Axial forces in braces along storey height

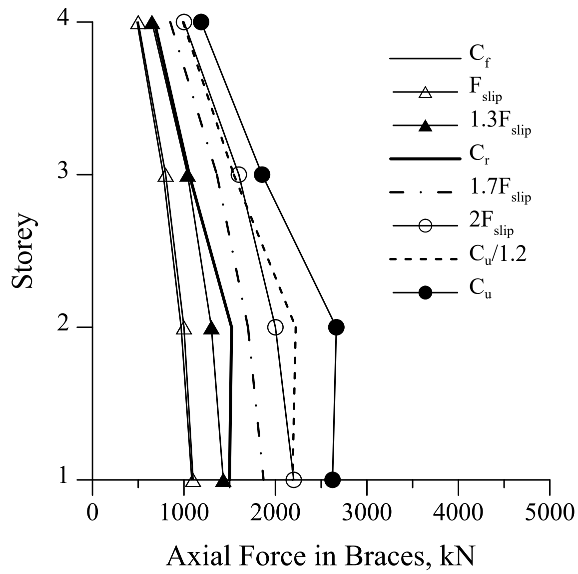

Figure 3.1-11. The 4-storey FSBF-II (R_dR_0=5) - Axial forces in braces along storey height

Table 3.1.7-4. FSBF-I (4-st.) and FSBF-CC-I (4-st.) - SFRS Member Sizes and Design Details

Storey	Braces	Columns	Beams	F_{slip} (kN)
4	HSS177.8X177.8X15.9	W310X117	W310X74	750
3	HSS228.6X228.6X12.7	W310X117	W310X129	1150
2	HSS254X254X12.7	W310X283	W310X129	1450
1	HSS254X254X15.9	W310X283	W310X143	1650

Table 3.1.7-5. FSBF-I (8-st.) and FSBF-CC-I (8-st.) - SFRS Member Sizes and Design Details

Storey	Braces	Columns	Beams	F_{slip} (kN)
8	HSS177.8X177.8X9.5	W310X86	W310X52	550
7	HSS203.2X203.2X12.7	W310X86	W310X74	850
6	HSS228.6X228.6X12.7	W310X202	W360X79	1100
5	HSS254X254X12.7	W310X202	W360X101	1350
4	HSS254X254X12.7	W310X342	W360X110	1500
3	HSS254x254x15.9	W310X342	W360X122	1650
2	HSS254x254x15.9	W310X500	W410X132	1750
1	HSS254X254X15.9	W310X500	W410X132	1800

Table 3.1.7-6. FSBF-I (4-st.) and FSBF-CC-I (4-st.) - Gravity System Members

Storey	Beams	Interior Columns	Exterior Columns
4	W360X32.9	W200X52	W200X31.3
3	W360X32.9	W200X52	W200X31.3
2	W360X32.9	W200X86	W200X52
1	W360X32.9	W200X86	W200X52

Table 3.1.7-7. FSBF-I (8-st.) and FSBF-CC-I (8-st.) - Gravity System Members

Storey	Beams	Interior Columns	Exterior Columns
8	W360X32.9	W200X41.7	W200X35.9
7	W360X32.9	W200X41.7	W200X35.9
6	W360X32.9	W250X67	W200X46.1
5	W360X32.9	W250X67	W200X46.1
4	W360X32.9	W250X80	W200X59
3	W360X32.9	W250X80	W200X59
2	W360X32.9	W250X115	W200X86
1	W360X32.9	W250X115	W200X86

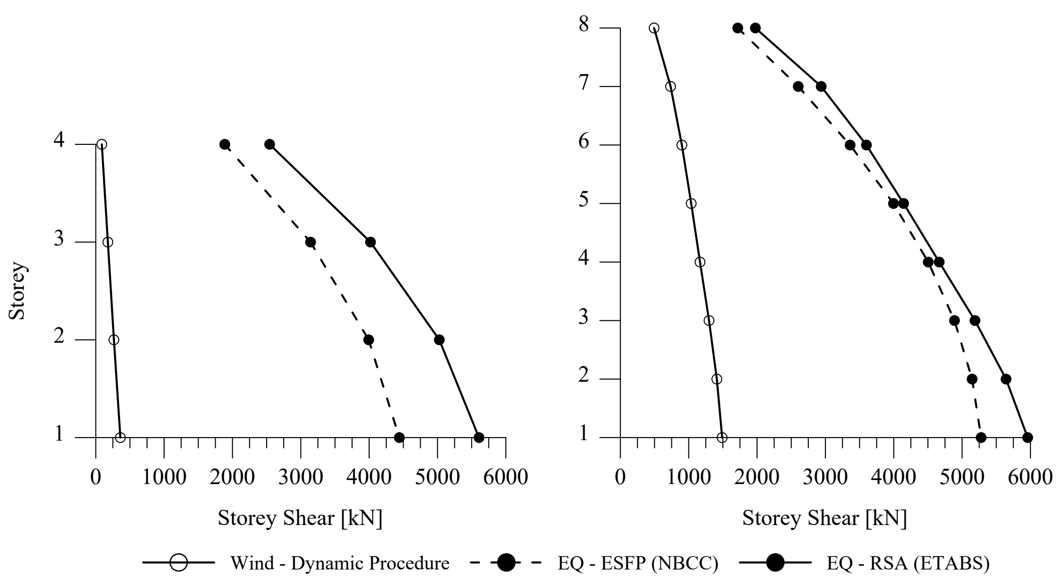

Figure 3.1-12. Storey Shear Distributions for FSBF-I (4-st.) (left) and FSBF-I (8-st.) (right)

Wind loads have been calculated for all the buildings according to Section 3.1.4 and are required to ensure that the building remains elastic under extreme wind loading. Inelastic behaviour of these systems only occurs once sliding of the PFD develops. Thus, if the factored base shear of the wind load is less than the earthquake base shear, sliding will not occur since sliding is designed to occur near the earthquake base shear demand.

The 4-storey building is low-rise ($h_n < 20m$) and the 8-storey building is high-rise according to NBCC 2015. Because the period of 8-storey building is greater than 1.0 s, Dynamic procedure should be employed for the calculation of wind loads. The calculation is presented in Table 3.1.7-8 and illustrated in Figure 3.1-12. It is worth noting that the 4-storey prototype is not dynamically sensitive according to the NBCC 2015, Clause 4.1.7.2 2), the base shear taken for low-rise buildings results in a factored base shear of 359 kN.

As shown in the preceding section, factored wind base shear does not exceed the seismic base shear for any of the building prototypes. Thus, the building remains elastic under wind loads, and no sliding is exhibited by PFDs.

Base shear comparison can be a simple method when the results are not close for seismic and wind base shear, however it is important to note that storey shear is not distributed similarly at each storey for wind loads as they are by means of modal analysis for seismic loads. The comparison of storey shear forces will ensure that slipping of the PFD does not occur at any storey. Storey shear for wind loads is distributed along the height of the building by considering the boundary layer preceding the windward and the leeward faces of the building. For the distribution of seismic loads, modal dynamic analysis is used herein.

Table 3.1.7-8. Wind Load Parameters and Base Shear (NBCC 2015)

Parameters	FSBF-I (8-St.) & FSBF-CC-I (8-St.)
f_{nD} [s^{-1}]	0.746
H [m]	30.6
Effective Width, w [m]	56
Terrain Type	Rough
Exposure at H, C_{eH}	0.776
$q_{1/50}$ [kPa]	0.45
Importance Factor, I_W	1.0
Wind Ref. Speed at 10m, $\bar{V}$ [m/s]	23.2
Damping Ratio, β	0.02
Mean Wind Speed at Roof, V_H [m/s]	20.5
K	0.1
w/H	1.83
Background Turbulence Factor, B	0.7
Gust Energy Ratio, F	0.081
Size Reduction Factor. s	0.012
Average Fluctuation Rate, v	0.19
Coefficient of Variance, σ/μ	0.31
Peak Gust Factor, g_p	3.78
Gust Coefficient, C_g	2.17
Windward Coefficient of Pressure, $C_{p\ windward}$	0.78
Leeward Coefficient of Pressure, $C_{p\ Leeward}$	0.47
Terrain Coefficient, C_t	1.0
Factored Base Shear, 1.4W [kN]	**1580**

3.1.8 Nonlinear Time History Analysis

3.1.8.1 Ground Motion Selection

According to Appendix J of the NBCC 2015, "the selection of ground motions should be done based on the tectonic regime, the magnitudes and distances that control the seismic hazard, and the local geotechnical condition at the site." The city of Vancouver, B.C., Canada is 50 to 100 km far from the Cascadia subduction fault which can subject the city to $M_w = 9$ mega-thrust subduction earthquakes. Crustal earthquakes in the region are expected to have moment magnitudes $M_w = 7$-7.5, and subduction earthquakes $M_w = 9$ (Atkinson and Goda 2011). Recorded ground motions are preferred over simulated ground motions as per NBCC 2015, thus crustal ground motions were selected from the NGA Peer Database (https://ngawest2.berkeley.edu), and the M_w = 9 Tohoku, Japan earthquake (March 11, 2011) was used for the simulation of subduction-zone ground motions. It is worth mentioning that Tohoku records are the proxy for Vancouver region. Building prototypes are designed for Site Class C which is defined to have an average shear wave velocity, $\bar{V}_{s30}$, between 360 and 760 m/s. Seven crustal and seven subduction-zone ground motions and their characteristics such as the Trifunac significant duration t_d, the main ground motion period T_m, the ground motion principal period, T_p, and the scale factor are presented in Table *3.1.8-1*. In addition, Table 3.1.8-1 also provides the values for the Joyner-Boore distance, R_{jb}, which is defined as the closest distance to the surface projection of the fault (Joyner and Boore 1981).

Table 3.1.8-1: Ground Motion Parameters

NGA	**Event**	M_w	**Comp (°)**	**PGA (g)**	**PGV (m/s)**	**R_{jb} (km)**	**t_d (s)**	**T_p (s)**	**T_m (s)**	**V_{s30} (m/s)**	**S.F.** *4-St.*	**S.F.** *8-St.*
Crustal Ground Motions												
802	1989, L. Prieta	6.9	090	0.321	0.434	7.58	8.02	0.22	0.57	381	1.80	1.50
15	1952, Kern County	7.36	021	0.159	0.152	38.4	30.3	0.36	0.54	385	2.00	3.55
787	1989, L. Prieta	6.9	360	0.277	0.313	30.6	11.6	0.30	0.69	425	1.20	1.90
1039	1994 Northrid.	6.7	180	0.272	0.221	16.9	14.2	0.26	0.47	352	2.20	2.50
736	1989, L. Prieta	6.9	227	0.105	0.206	40.8	21.4	0.30	0.95	450	3.10	3.20
838	1992, Landers	7.3	090	0.135	0.250	34.9	18.0	0.74	0.91	370	2.40	3.50
963	1994 Northrid.	6.7	090	0.568	0.516	20.1	9.1	0.26	0.54	450	0.80	1.10
Subduction Ground Motions												
FKS005	2011 Tohoku	9.0	EW	0.45	0.35	58.2	92	0.15	0.32	469	1.20	1.40
FKS009	2011 Tohoku	9.0	EW	0.86	0.56	70.8	66	0.18	0.27	409	1.40	2.60
FKS010	2011 Tohoku	9.0	EW	0.83	0.44	65.0	74	0.20	0.20	387	1.20	1.20
MYG001	2011 Tohoku	9.0	EW	0.43	0.23	52.1	83	0.26	0.27	441	1.80	2.80
MYG004	2011 Tohoku	9.0	EW	1.22	0.48	75.1	85	0.25	0.26	430	1.00	1.20
IBR004	2011 Tohoku	9.0	EW	1.03	0.38	71.4	33	0.15	0.21	382	1.10	1.90
IBR006	2011 Tohoku	9.0	EW	0.78	0.30	70.8	36	0.12	0.25	406	1.40	1.60

According to the NBCC 2015, the minimum number of ground motions in each suite is five if the total number of ground motions in all suites is not less than 11. All ground motions in each suite were then scaled to match the 2% probability of exceedance in 50 years design spectrum over the period of interest $0.15T_1$ and $2.0T_1$, where the mean, of all ground motions in the suite, does not fall more than 10% below the design spectrum.

The 2%/ 50 years design spectrum for Vancouver, the scaled ground motions and their mean are presented for both 4-storey and 8-storey buildings in Figure 3.1-13.

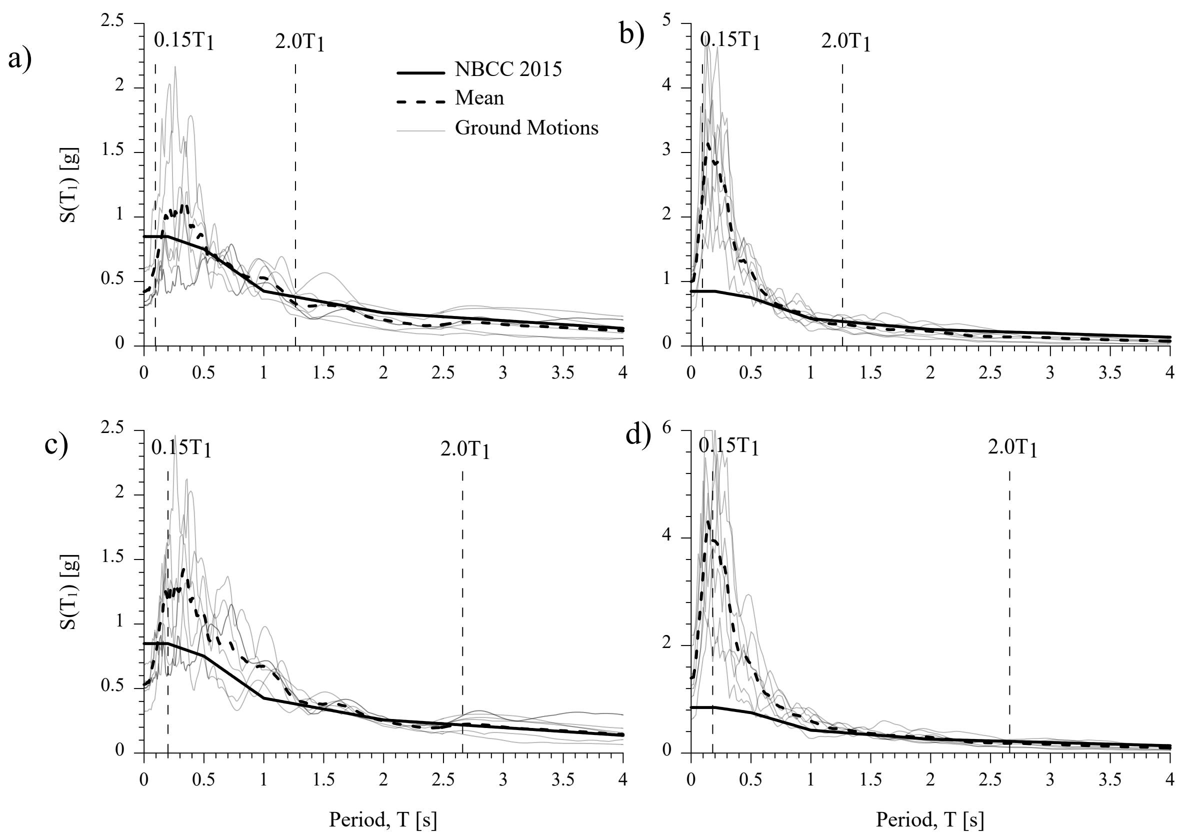

Figure 3.1-13. Scaled spectrums for ground motions according to NBCC 2015: a) Scaled crustal ground motion suite for FSBF-I (4-st.), b) Scaled subduction-zone ground motion suite for FSBF-I (4-st.), c) Scaled crustal ground motion suite for FSBF-I (8-st.), and d) Scaled subduction ground motion suite for FSBF-I (8-st.)

3.1.9.2 OpenSees Modeling

OpenSees (www.OpenSees.berkeley.edu) is an open-source finite element software developed by the University of California capable of efficiently running nonlinear time history analysis. The language used to model the systems can be written through Python (http://www.python.org) or Tcl (https://www.tcl.tk/about/language.html). The language used for the purposes of this research was a Tcl syntax structure.

Models in OpenSees can be defined as 2-D and 3-D models with up to six degrees-of-freedom. Herein, the models created are two-dimensional and have three degrees-of-freedom. The ability to define the structure as being two-dimensional is justified by the limited out-of-plane deformation found in these systems. Unlike Concentrically Braced Frames (CBFs), where out-of-plane buckling must be modelled to demonstrate the inelastic response of braces (Tirca et al., 2016), PFDs are more analogous with Buckling Restrained Braces (BRBs) and respond inelastically inline with the braces and thus no out-of-plane deformation is present.

To allow for OpenSees to have the ability to calculate eigenvalues and perform dynamic analysis, nodal mass must be assigned. Mass is defined as being lumped at a node with a defined direction. For the models developed herein, the mass of half of the building (Figure 3.1-14) was divided among the columns in the FSBFs and defined at each floor with only horizontal directionality. In order to mimic a rigid diaphragm, the top of each column, at each floor, of the FSBF is assigned to have equal degrees-of-freedom as the left most column shown in Figure 3.1-15. Thus, three of the four columns are slaved to the first column of the system. Column imperfections were defined to have a maximum out-of-straightness, at half the length of the member, of L/1000.

No predefined sections are present in OpenSees and therefore must be defined either as a simple function of the section's area, elastic modulus, and moment of inertia in the axis of bending, or as a fiber section. Fiber sections are defined by the command *Fiber* that allows a number of fibers over a geometric cross-section as shown in Figure 3.1-16. Fiber sections allow for stress to distribute and be measured throughout the section in order to accurately measure forces and deformation of members. For this reason, columns and beams part of the SFRS are modelled with fiber sections. Column and Beam elements are defined by the *element forceBeamColumn* function which is an iterative force-based algorithm that can handle distributed plasticity by means of Gauss-Lobatto Integration. Beams and columns of FSBF were assigned the material *Steel02,* which is based on the Giuffré-Menegotto-Pinto Model. This material choice was made to observe if any inelastic behaviour in the columns or beams occur at higher demand. Columns of FSBFs were discretized into eight continuous elements for proper deformation response and the number of integration points in each column element were defined as 4. Beams of FSBFs were defined as one element with 4 integration points. It is worth mentioning that braces are not attached to the beam, which response is expected to be elastically.

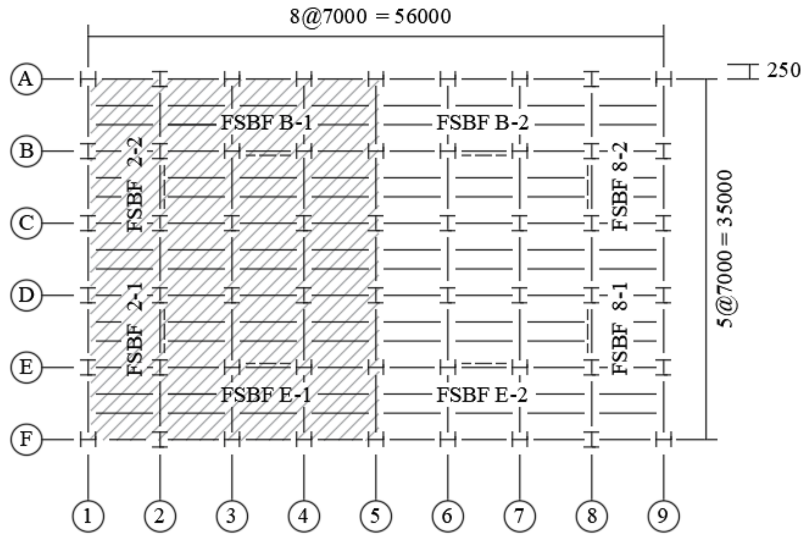

Figure 3.1-14. Half of Building Modelled in OpenSees (Shaded Area)

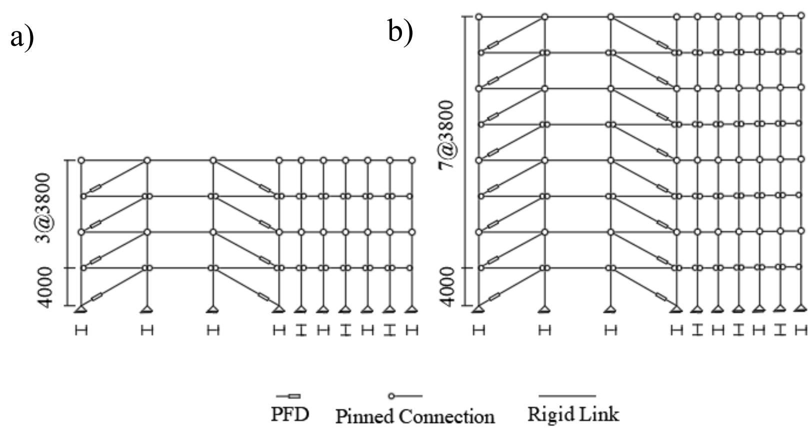

Figure 3.1-15. Two-Dimensional Frames Modelled in OpenSees for a) FSBF-I (4-st.) and b) FSBF-I (8-st.)

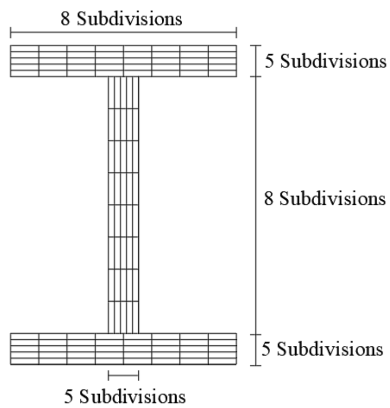

Figure 3.1-16. Fiber Sections for W-Shape

Gravity columns were defined to be one continuous element per storey over two storeys and defined by an elasticBeamColumn element since inelastic deformation is not expected to occur in these elements. Thus, only the area, modulus of elasticity, and the moment of inertia is required. Gravity columns are included in the system to account for P-Δ effects. In order to reduce the number of gravity columns in the model, columns with identical areas and axes of rotation are concentrated into a single column with N times the area and moment of inertia under bending, where N is the number of identical columns considered within the shaded area of Figure 3.1-14. The six gravity columns displayed in Figure 3.1-15 are described in Table 3.1.8-2. Each column located along gridline 5 in Figure 3.1-14 is taken to have 50% of the area and moment of inertia of each given column.

Table 3.1.8-2. Gravity Column Reduction Combinations

Gravity Column	**Number of columns, N**	**Column Location**	**Axis in Bending**
1	4	Interior (SFRS perpendicular to GM)	Weak
2	5	Interior	Strong
3	1	Interior	Weak
4	6	Edge	Strong
5	5	Edge	Weak
6	2	Corner	Strong

As previously mentioned, out-of-plane deformation is not expected to occur and therefore connections are restrained out-of-plane. To replicate the rigid diaphragm, the *equalDOF* functionality is assigned to all slaved joints. To account for the gusset plate length from the face of the column or beam, L_1, an *elasticBeamColumn* element is defined from the centerline-to-centerline intersection of the beam-column connection to the extreme point of L_1. This element is defined to have an area and moment of inertia 150% larger than the area of the HSS connected to that gusset. Gusset plate failure is not explicitly simulated by the model. All beam connections of FSBFs are located at the interface between the column flange and the beam, where shear tab connections would be located. These connections are assigned to be pinned, are elastic from the centerline of the column to the flange face of the column and have an area and moment of inertia equal to the beam. A 2% Rayleigh damping (mass and stiffness proportional damping) was computed for the first and third vibration mode and assigned to gravity columns designed to remain in the elastic range.

3.1.9.3 Modelling of Damper Material

OpenSees does not contain a model for friction damper, so the material construction was developed using three built-in *Uniaxial Materials:* i) three *Elastic-Perfectly Plastic Gap Materials, ii) Bouc-Wen Material,* and *iii) MinMax Material.* An idealized PFD model could be fully simulated by the *Bouc-Wen* material (Figure 3.1-19). However, it has been observed (Tirca et al. 2018) that these PFD devices can resist $2F_{slip}$ without failure. It is for this reason that a second seismic fuse, such as the gusset plate, should be designed to fail before or at $2F_{slip}$ since failure behaviour of PFDs are currently unknown. Therefore, the bearing phase of PFD must be included in the model to consider the behaviour once the entire slip length is exhausted and an idealized PFD material would be insufficient in modelling all behavioural phases of PFDs. Based on the research conducted by (Roik et al. 1988), the bearing phase can be modelled using multiple materials in parallel. Four distinct phases are defined in the PFD material: i) Bearing ii) First Yielding iii) Partial Plastification iv) Failure Threshold. These four phases are defined by the three *Elastic-Perfectly Plastic Gap Materials* and the *MinMax Material*, respectively. The back-bone curve, as shown in Figure 3.1-17, is built by summing the coordinates of all the materials in parallel. This can also be visualized by the free body diagram in Figure 3.1-18.

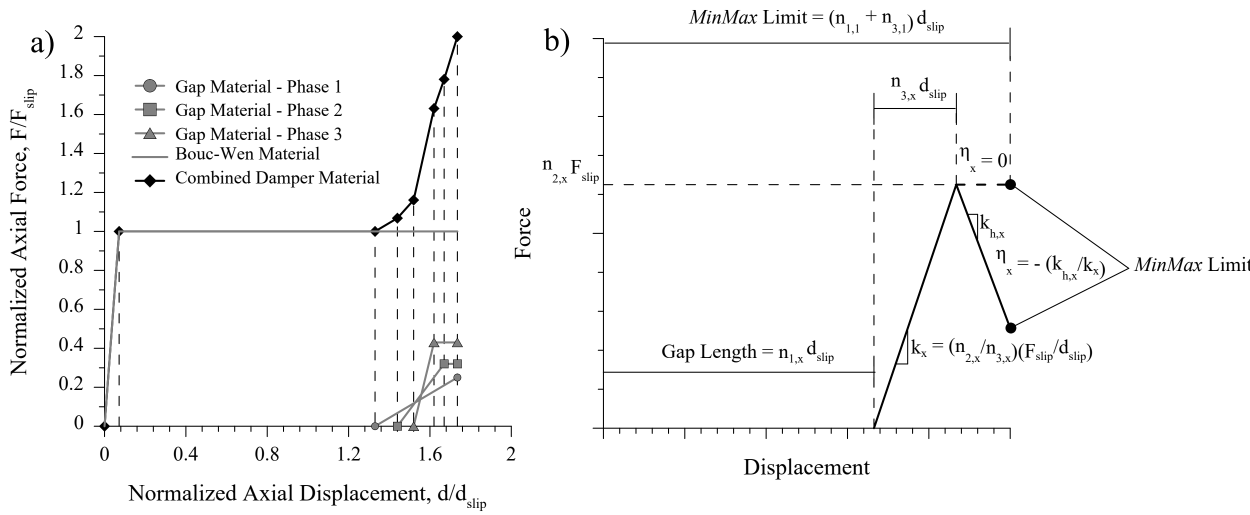

Figure 3.1-17: a) PFD Material Back-Bone Curve Decomposition Used in OpenSees b) *Elastic-Perfectly Plastic Gap Material* Parameters

The *Elastic-Perfectly Plastic Gap Material* (EPPGM) is defined by the gap length, stiffness, k, force at which the plastic state is reached, F_y, hardening ratio, η, and damage as shown in Figure 3.1-17 b). The gap length of each gap material is defined in OpenSees as a factor, $n_{1,x}$, of the slip length, d_{slip}. The yield force, F_y, is defined as a factor, $n_{2,x}$, of the slip force, F_{slip}. The bearing distance, which is a proportion of slip length, $n_{3,x}d_{slip}$, is defined as the distance from the gap length, where the material is initiated, to the yield force of that gap material. The coefficients used for the EPPGMs are labelled as $n_{i,x}$, where i is the i^{th} coefficient for the x^{th} EPPGM. The damper material contains $x = 3$ EPPGMs in tension and compression, and $i = 3$ coefficients per EPPGMs.

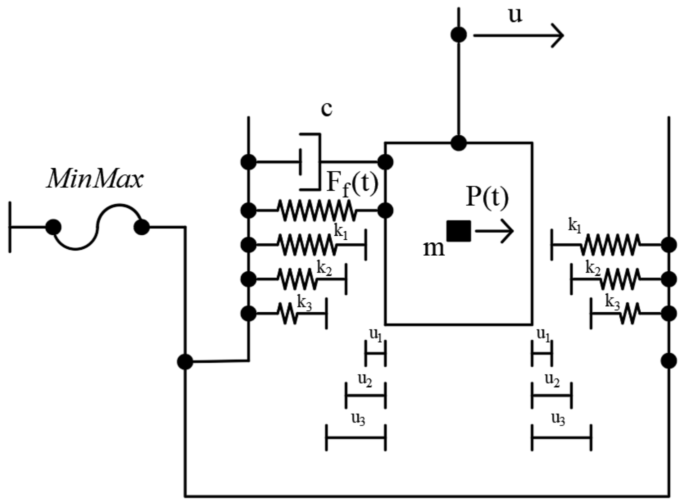

Figure 3.1-18. Freebody Diagram of PFD model using OpenSees

All models limit the maximum force of the combined material to 2F_{slip}, and by a *MinMax* Material, which is a function of strain/displacement, and is defined to be the distance at which the combined material is equal to 2F_{slip}, as shown in Figure 3.1-17. Thus, the summation of all the factors used to proportion the yielding force for each EPPGM, $\sum_{x=1}^{N=3} n_{2,x}$, is equal to unity, as shown in Table *3.1.8-3*. This results in the maximum force of the combined material to be equal to 2F_{slip}, since the *Bouc-Wen Material* is defined to yield at $F_{slip,}$ in combination with the maximum force produced by the summation of all the EPPGMs, gives a total force of 2F_{slip}, Eq. (3.1.44). The factors in Table *3.1.8-3* are indeterminant and thus initial values must be assumed. As previously mentioned, the usable slip length is 1.3d_{slip}, thus the factor $n_{1,1}$ should be approximately 1.3. The rest of the calibration of these values come from experimental testing and can be done with the aid of Eqs. (3.1.44) to (3.1.48).

Table 3.1.8-3. Factors Used for *Elastic-Perfectly Plastic Gap Material* Parameters

x (Gap Material)	**$n_{1,x}$ (Displacement)**	**$n_{2,x}$ (Force)**	**$n_{3,x}$ (Bearing Distance)**	**η**	**Damage**
1	1.30	0.25	0.405	0	0
2	1.40	0.32	0.230	0	0
3	1.50	0.43	0.100	0	0
Σ	**-**	**1.00**	**0.735**	**-**	**-**

$$F_{max}^{Combined} = F_{slip}^{Bouc-Wen} + \left(\sum_{x=1}^{N=3} n_{2,x}\right) F_{slip} = \left(1 + \left(\sum_{x=1}^{N=3} n_{2,x}\right)\right) F_{slip} = 2F_{slip} \quad (3.1.44)$$

$$n_{1,1} < n_{1,2} < n_{1,3} \quad (3.1.45)$$

$$n_{3,1} > n_{3,2} > n_{3,3} \quad (3.1.46)$$

$$n_{1,1} + n_{3,x} = 1 - \sum_{x=1}^{N=3} n_{3,x} \quad (3.1.47)$$

$$n_{1,1} + n_{3,1} < 2.0 \quad (3.1.48)$$

BoucWen Material in OpenSees (Song and Der Kiureghian 2006; Wen 1980, 1989), is used to describe the hysteretic shape as a function of stiffness of the brace. This material consists of nine parametric arguments: i) post-yielding stiffness to initial stiffness ratio, α; ii) initial stiffness, k_o; iii) linear to nonlinear transition parameter, n; iv) & v) hysteretic shape parameters, α, and β; vi) & vii) tangent stiffness parameters, A_o, and ΔA; viii) & ix) material degradation parameters, Δν, and Δη. The initial stiffness of the material is defined in Figure 3.1-19. Herein, the post-yielding stiffness to initial stiffness ratio is selected to be α = 0.001 to avoid convergence issues, the linear to nonlinear exponent is selected to be n = 10, tangent stiffness parameters are as follows, A_o = 1 and ΔA = 0, and the degradation parameters are Δν = Δη = 0. As observed in the test of a full-scale damper, (Tirca et al. 2018) PFDs do not exhibit visible deformation degradation and thus justifies the use of Δν = Δη = 0. The tangent stiffness is not variable and thus A_o equaling to unity controls that the tangent stiffness to be equal to the initial stiffness defined by k_o. In order to obtain proper tangent stiffness behaviours during loading and unloading stages, hysteretic shape parameters α and β are defined by Eqs. (3.1.49) and (3.1.50). These values result that during loading where α + β > 0 softening behaviour is exhibited and during unloading α - β = 0 a linear shape is achieved. The exponent *n* is used to control the sharpness of the transition from the initial stiffness to the post-yielding stiffness. Figure 3.1-19 shows a qualitative hysteretic diagram that represents the modelled shape of the response of the *BoucWen Material*. As shown, transitions from linear to nonlinear behaviour have a small, curved transition, as a function of *n*. These transitions avoid convergence issues that may arise when post-yielding stiffness is close to or equal to zero. The damper response shown in Figure 3.1-19 b) is simulated by including the following materials in parallel: 3 tension EPPG materials combined in parallel, 3 compression EPPG materials combined in parallel, and a *BoucWen material.* The later simulate the slipping response and the former the bearing stage in tension and compression. More information regarding the development of the OpenSees Material can be found in (Morales 2011).

$$\alpha + \beta = A_o \left[\frac{1}{u_y A_o} \right]^n \tag{3.1.49}$$

$$\alpha = \beta = \frac{\alpha + \beta}{2} \tag{3.1.50}$$

$$u_y = \frac{f_{sy}}{k_o} = \frac{F_{slip}}{k_{brace}} \tag{3.1.51}$$

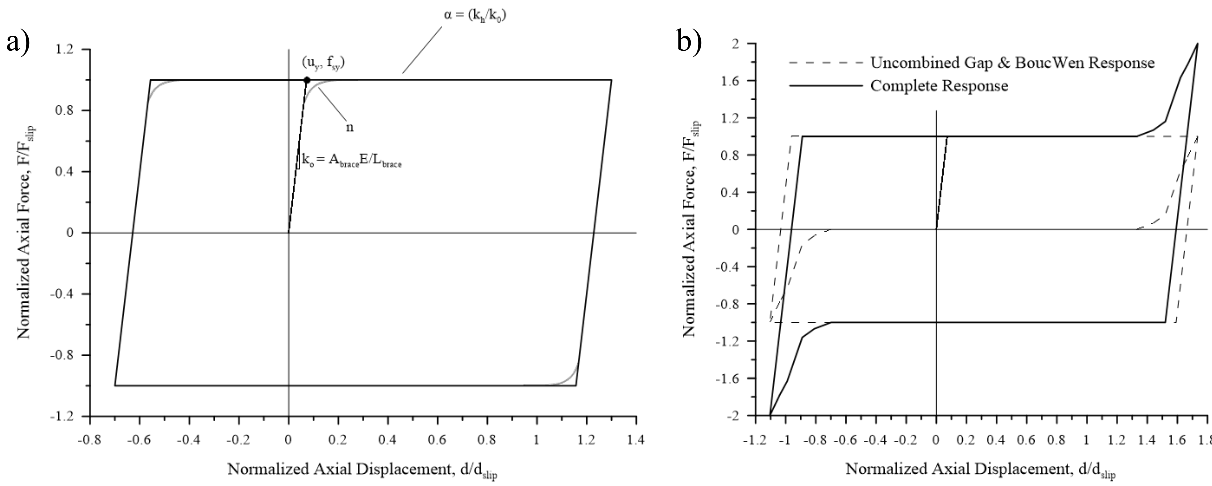

Figure 3.1-19. Modeling of PFD: a) *Bouc-Wen Material* and b) Response including bearing

Damping of the structure was applied according to the Rayleigh damping model to properly the relationship between the effects of mass and stiffness on the structure's damping coefficient. 2% critical damping was selected and applied to all gravity columns and HSS brace-to-frame connections by the use of a *region* object in OpenSees. Damping was not defined for the PFD link elements to avoid over damping of the system. Rayleigh damping, as present in the equation of motion, is defined by Eq. (3.1.52) where a_o and a_1 are the coefficients for mass and stiffness proportionality, respectively. Modal damping is defined by Eq. (3.1.54) and if all modes are assumed to have the same amount of damping, the mass and stiffness coefficients can be solved according to Eq. (3.1.55). The first and third mode were considered for the calculation of coefficients.

$$\boldsymbol{c} = a_0\boldsymbol{m} + a_1\boldsymbol{k} \tag{3.1.52}$$

$$\zeta_n = \frac{a_o}{2}\frac{1}{\omega_n} + \frac{a_1}{2}\omega_n \tag{3.1.53}$$

$$\frac{1}{2}\begin{bmatrix} 1/\omega_i & \omega_i \\ 1/\omega_j & \omega_j \end{bmatrix}\begin{Bmatrix} a_0 \\ a_1 \end{Bmatrix} = \begin{Bmatrix} \zeta_i \\ \zeta_j \end{Bmatrix} \tag{3.1.54}$$

$$\text{if } \zeta_i = \zeta_j \text{ then}$$

$$a_0 = \zeta \frac{2\omega_i\omega_j}{\omega_i + \omega_j} \quad and\ a_1 = \zeta \frac{2}{\omega_i + \omega_j} \tag{3.1.55}$$

3.1.9.4 Friction Sliding Braced Frame – Results at Design Level

Nonlinear Response History Analysis, NRH, in this section was completed considering both ground motion suites scaled at the design level. The scaling factor of each ground motion is shown in Table 3.1.8-4. As expected, the scale factor computed for the 4-storey building is higher than that for the 8-storey building due to its change in mass and stiffness, resulting in a lower period of vibration. It can also be observed that crustal ground motions, when scaled, have a lower demand than subduction ground motion. Another potentially important difference between subduction and crustal ground motions is the total number of cycles. From the subduction ground motions used herein, the maximum number of cycles observed was 1500, while the crustal ground motions show about 60 cycles. The subduction ground motions not only exhibit higher spectral demand but also larger Trifunac duration than crustal ground motions, which may contribute to cyclical fatigue accumulation. PFDs, however, have not been shown to exhibit fatigue or deterioration, over many cycles, since the yielding mechanism is the sliding of two friction interfaces. This is in contrast to CBFs which rely on the yielding of the steel brace material which yields strain accumulation. The combination of high hysteretic energy dissipation and low cyclic deterioration makes PFDs a good potential candidate even for subduction zone regions, as long as self-centering behaviour can be achieved at design level, which is the purpose of this research.

Table 3.1.8-4. Scaling ground motions for FSBF-I (4-st.) and FSBF-I (8-st.)

Design Level for all Ground Motions		FSBF-I (4-storey)		FSBF-I (8-storey)	
ID	**NGA**	**$S(T_1)$ [g]**	**SF**	**$S(T_1)$ [g]**	**SF**
C1	802	0.602	1.80	0.383	1.50
C2	15	0.714	2.00	0.481	3.55
C3	787	0.687	1.20	0.353	1.90
C4	1039	0.679	2.20	0.331	2.50
C5	736	0.555	3.10	0.415	3.20
C6	838	0.641	2.40	0.363	3.50
C7	963	0.576	0.80	0.439	1.10
S1	FKS005	0.741	1.00	0.425	1.40
S2	FKS009	0.720	1.20	0.388	2.60
S3	FKS010	0.592	1.00	0.443	1.20
S4	MYG001	0.695	1.80	0.434	2.80
S5	MYG004	0.719	1.00	0.414	1.20
S6	IBR004	0.731	1.00	0.327	1.90
S7	IBR006	0.779	1.20	0.503	1.60
Mean Crustal	**-**	**0.636**	**-**	**0.395**	**-**
Mean Subduction	**-**	**0.711**	**-**	**0.419**	**-**

3.1.9.4.1 4-Storey Friction Sliding Braced Frame

To observe the initial performance of the structures, the interstorey drift, residual interstorey drift, and floor acceleration which are shown in Figure 3.1-20 for FSBF-I (4-storey) are recorded. As per NBCC 2015, the mean plus standard deviation is used. For the FSBF-I (4-storey) model, where columns are only continuous over two storeys, the maximum interstorey drift is 1.20%h_s at the third storey and 3.37%h_s at the roof for crustal and subduction ground motion suites, respectively. Residual drift for FSBF-I (4-storey) is 0.88%h_s and 3.13%h_s, and floor acceleration is 0.81g and 1.25g for crustal and subduction suites, respectively. The structure is significantly below 2.5%h_s for interstorey drift, which is the serviceability requirement given by the NBCC for CBFs. Residual drift is important when considering the reparability of a structure in the aftermath of an earthquake event. Herein, a 0.5%h_s residual interstorey drift is considered to define the Reparability Limit State (RLS) (Erochko et al. 2011; McCormick et al. 2008). As observed, FSBF-I (4-storey) exceeds the RLS and a potential solution to reduce this level of damage should be explored.

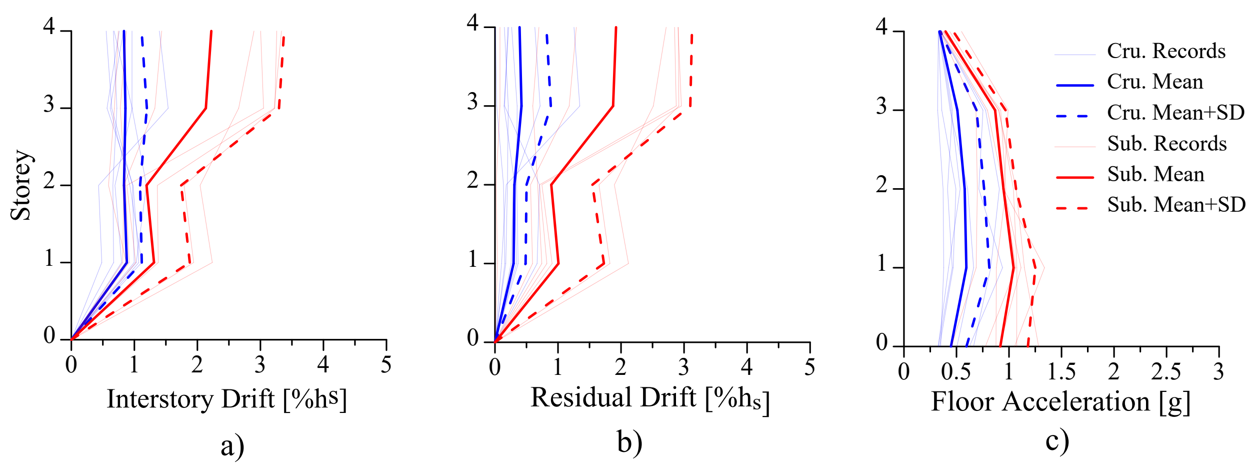

Figure 3.1-20: Response of FSBF-I (4-storey) at Design Level under srustal and subduction ground motions in terms of: a) ISD, b) RISD, and c) FA

To demonstrate the behaviour under crustal GM Landers, 1992, #838-90 and subduction GM Tohoku, 2011, #MYG001, Figure 3.1-21 shows the interstorey drift as a time-series for crustal and subduction, respectively. Maximum interstorey drift of each floor occurs within the Trifunac duration, or the most significant portion of the ground motion, as expected, and distinct floor separation occurs under crustal and subduction ground motions.

Figure 3.1-22 shows the hysteretic shape of PFD installed in the left brace of first storey under ground motions #838-90 and #MYG001 for FSBF-I (4-St.) at Design Level. It is observed that the structure does not exhibit any bearing behaviour under design demand. Thus, the slip length is sufficient for the structure and excess forces are not created by PFDs. For clarity, a proper slip distance should be designed to avoid bearing and promote proper function of the damper. Slip distance and bearing should not be designed as a means to limit interstorey drift to the desired displacement. This should be done through proper SFRS design.

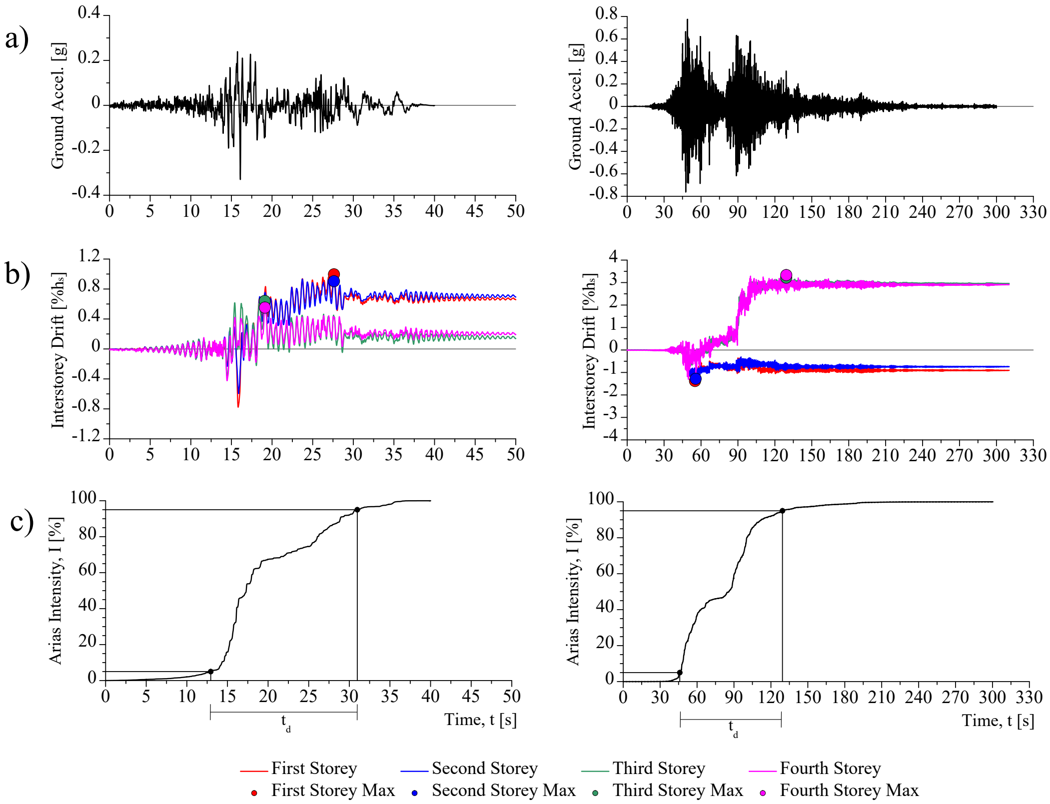

Figure 3.1-21. Response of FSBF-I (4-storey) under crustal GM Landers, 1992, #838-90 (left) and Subduction GM Tohoku, 2011, #MYG001 (right): a) Scaled Ground Acceleration, b) ISD time-history of all floors and c) Arias Intensity for GMs

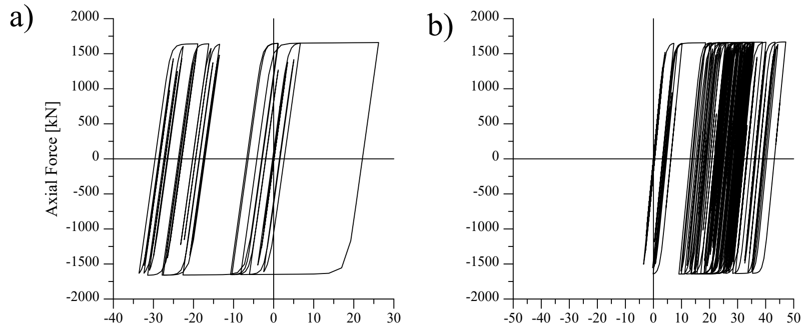

Figure 3.1-22. Hysteresis response of PFD installed in the left brace of first storey of FSBF-I (4-storey) under: a) crustal GM #838-90 and b) subduction GM #MYG001 scaled at Design Level

3.1.9.4.2 8-Storey - Friction Sliding Braced Frame

The FSBF-I (8-storey) building was subjected to Nonlinear Response History analysis (NRH) under both crustal and subduction ground motion suites scaled at Design Level. The building's seismic response was analysed in terms of interstorey drift, residual interstorey drift and floor acceleration as depicted in Figure 3.1-23. As plotted, the building collapsed under all subduction ground motions and 5 out of 7 crustal ground motions, but #963-90 and #802-90. All of the collapsed models have been excluded from Figure 3.1-23, and thus the mean and mean plus standard deviation does not contain this information. However, even excluding the collapsed models, the response of the remaining structures is well above the 2.5%h_s code limit.

Figure 3.1-24 shows the time-history of FSBF-I (8-storey) under GM #963-90. It is observed that the floors diverge into groups of two. These groups are due to the continuity of columns over two floors adding flexural stiffness and having the ability to distribute loads appropriately. Considering the following, increased seismic performance of this type of structure is required.

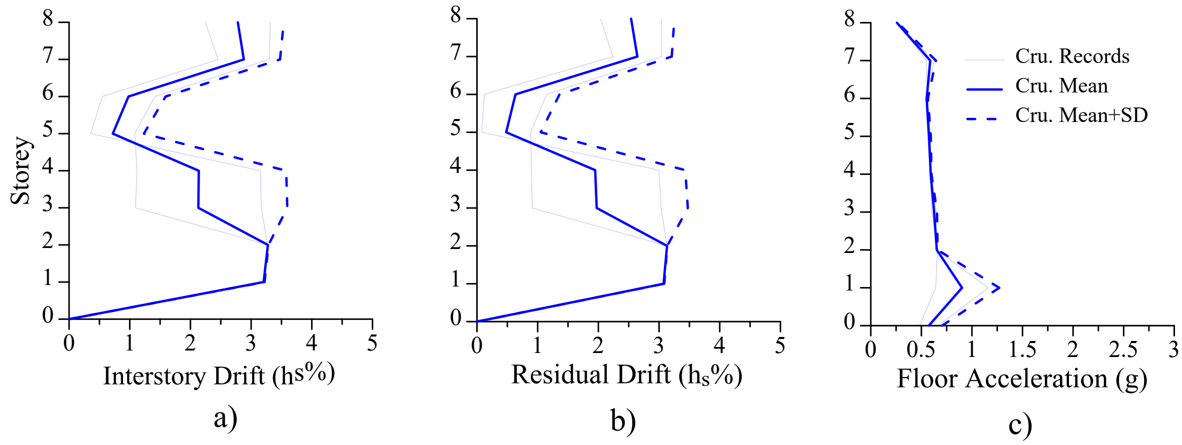

Figure 3.1-23. Response of FSBF-I (8-storey) under crustal records scaled at Design level expressed in terms of: a) ISD b) RISD and c) FA

Unlike the 4-storey FSBF–I building, the 8-storey FSBF-I experienced bearing of the PFDs at the first storey. These observations are shown in Figure 3.1-24, where it can be found that bearing of the first floor for FSBF-I (8-storey) has exceeded $1.7F_{slip}$ which would be the desired connection failure point. These structures are instable and the design of bare FSBFs should be avoided based on these observations.

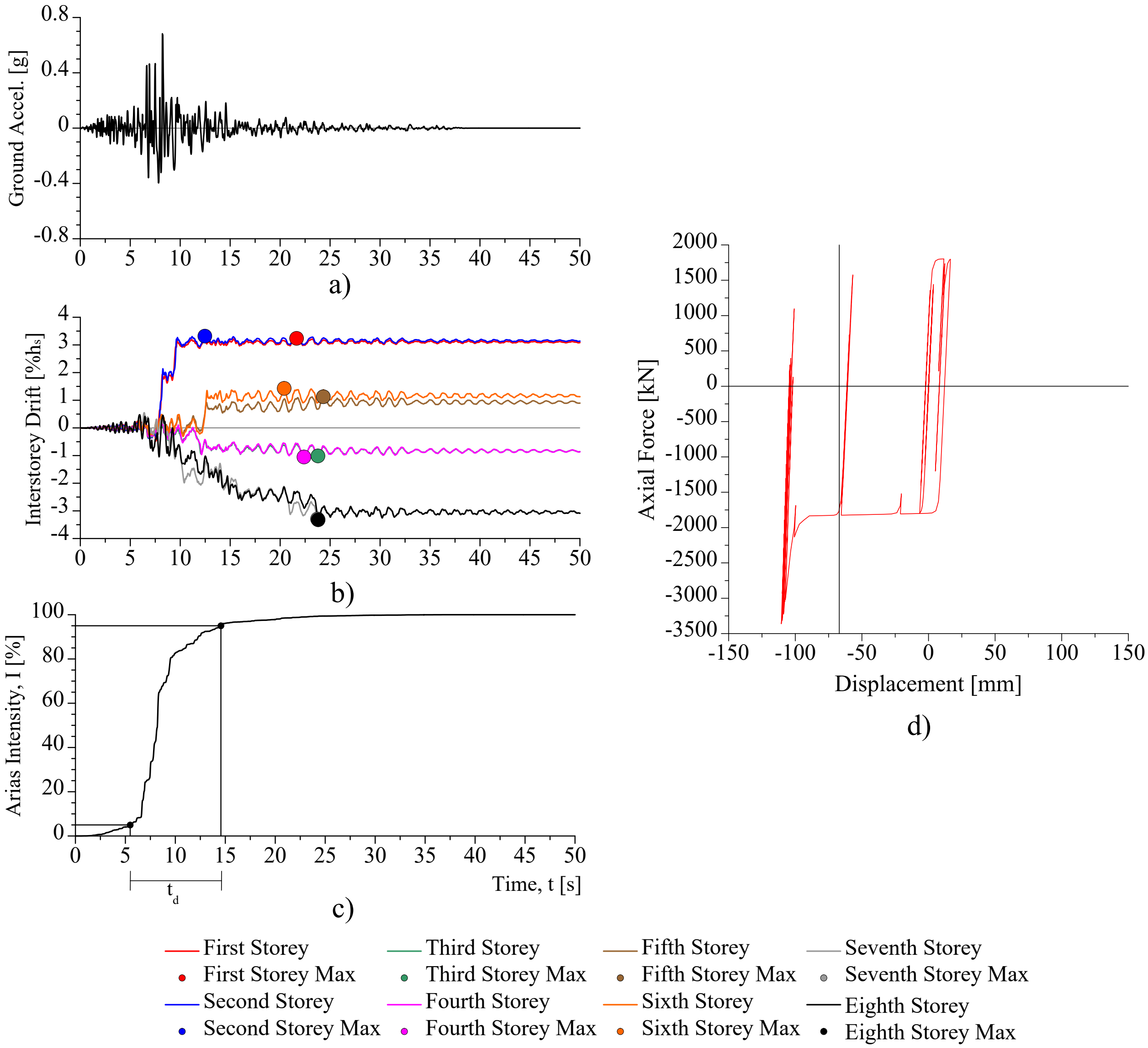

Figure 3.1-24. Response of FSBF-I (8-storey) under scaled crustal GM Northridge, 1994, #963-90 to design level: a) scaled ground acceleration, b) Interstorey drift Time-History of all floors, c) Arias Intensity of GM and d) hysteresis of PFD installed in the left brace of 1st floor

3.2 Incremental Dynamic Analysis - Friction Sliding Braced Frame

To further investigate the seismic performance of these systems, including their collapse, incremental dynamic analysis was completed for all bare FSBFs. Incremental Dynamic Analysis, IDA, (Vamvatsikos and Cornell 2001), is a method used to measure the performance of a structure at multiple intensity levels. Herein, the intensity level considered is pseudo-acceleration and the response is interstorey drift. Collapse of the structure is determined as a function of interstorey drift, where very large maximum displacement is achieved with a small increase in pseudo-acceleration demand; thus, resulting in a complete flattening of the IDA curve. This type a collapse assessment can also be used to judge appropriate R ductility reduction factors, as will be discussed later.

The IDA curves for 4-storey bare FSBF system is presented in Figure 3.2-1 under crustal and subduction ground motions suites. The 50th percentile of the seven ground motions contained in each suite is identified by the red line. The 50th percentile is used to identify the collapse point of the structure and other phenomena. Collapse, as measured by the 50th percentile, occurs when the maximum interstorey drift of any one floor is approximately 3.5%h_s. All IDAs contain a distinct and tight linear region up to the code demand for crustal suites.

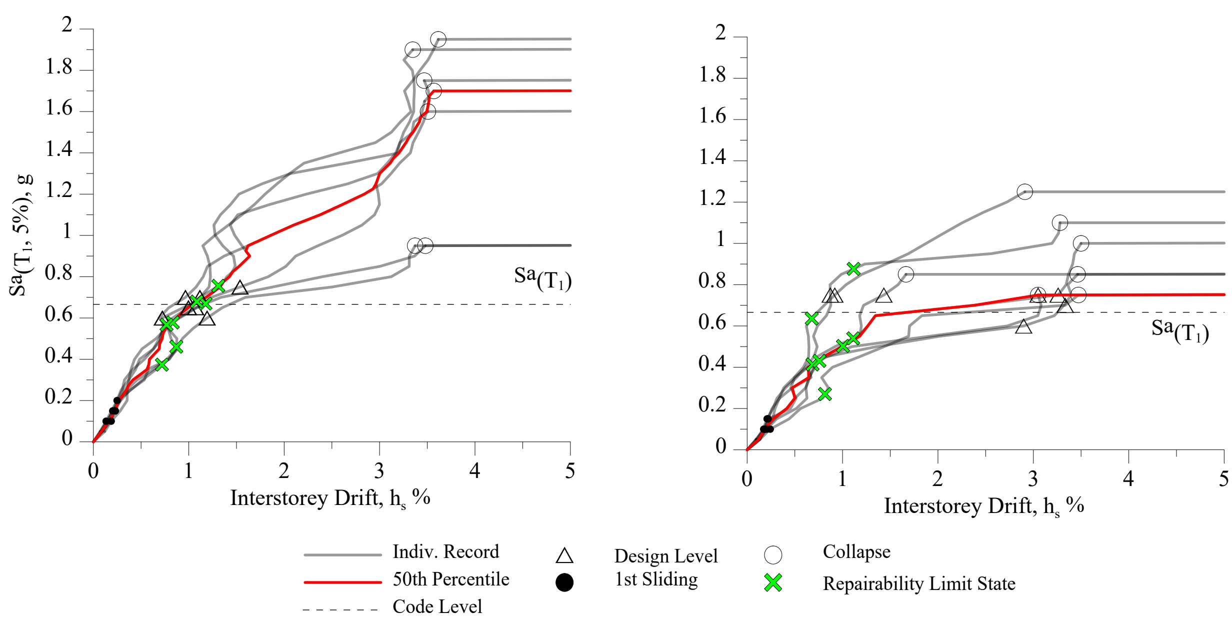

Figure 3.2-1. IDA curves of FSBF-I (4-storey) under: a) crustal GMs and b) subduction GMs

The IDA curves of 8-storey bare FSBF-I system are shown in Figure 3.2-2, where the median response fails below the code demand level for both crustal and subduction ground motion suites. Collapse, as is the case for FSBF-I (4-storey), occurs at 3.5%h_s. These responses do not justify the design of any other structure at or above 8-storeys with a bare FSBF and demonstrates the necessity for an ameliorated seismic force resisting system.

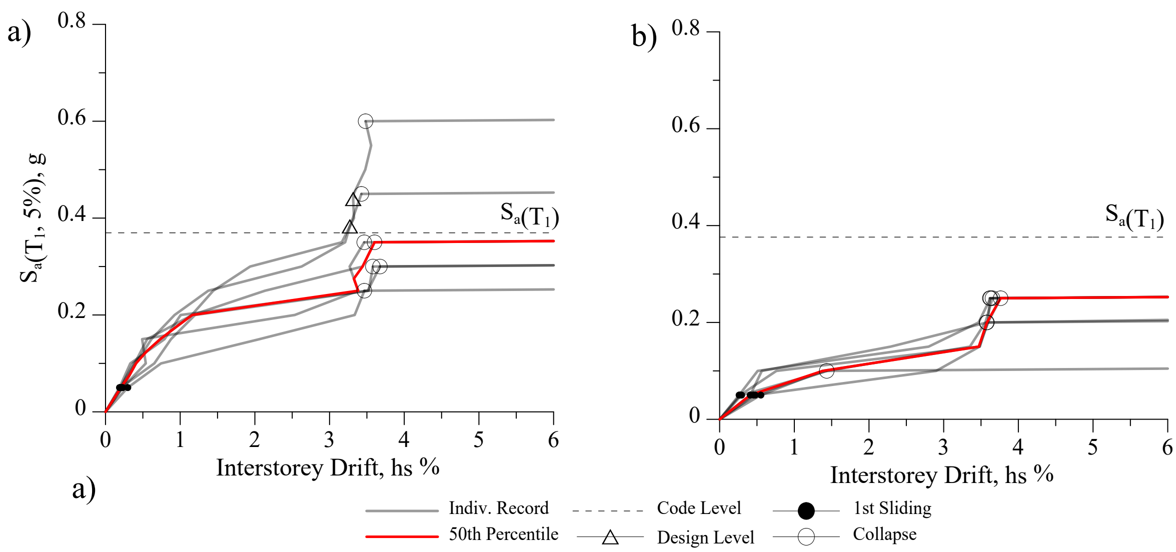

Figure 3.2-2. IDA curves of FSBF-I (8-storey) under: a) crustal GMs and b) subduction GMs

Chapter Four

Friction Sliding Braced Frames with Continuous Columns

As seen in the last chapter, bare Friction Sliding Braced Frames do not meet minimum requirements under design level. These issues are mostly due to the structure's inability to return to its initial position, due to the lack of frame-action needed to redistribute loads during large ground excitation. Meanwhile, PFDs do not show a ductile failure mode. The work presented in this chapter is the first attempt at achieving sufficient frame-action in order to lower the residual interstorey drift and achieve adequate performance. Furthermore, assuring a ductile failure mode by developing a secondary ductile fuse through appropriate gusset plate failure mechanisms is proposed.

4.1 Secondary Ductile Fuse Design – Gusset Plates

In general, the upper end of the PFD is attached to the bottom end of a HSS supportive brace, and the bottom end of PFD is attached, by bolts, to the gusset plate that is connected to the frame. However, little information is available on the failure mode of PFDs and from one experimental test, it resulted that PFDs could sustain larger force than the design slip force F_{slip}. From full-scale physical tests done at École Polytechnique, Montréal (Tirca et al. 2018), it resulted that a PFD attached to a short supportive brace did not reach failure when loaded in bearing up to $2F_{slip.}$ Thus, on one hand, the gusset plate should be designed to provide sufficient strength to avoid premature failure of PFD and on the other hand it should control the magnitude of force triggered from the PFD to the frame. Typically, the PFDs are connected to the gusset plate via two high-strength bolts of grade ASTM A490 (F_u = 1035MPa), however, more bolts are required if the demand is greater. It is recommended to install PFDs at the lower end of the support HSS brace and to consider the secondary ductile fuse in the gusset plate-damper connection. The connection should be designed to show a ductile failure mode, while shearing of bolts and gusset plate fracture should be avoided.

Thus, as explained in Chapter 3, the supportive HSS brace was designed so that the brace compression resistance, C_r is greater than $1.3F_{slip}$. Applying the capacity design principle, it resulted that the HSS brace designed as Class 1 or 2, is able to develop the probable compression force C_u and the probable tensile force T_u. According to the provisions developed for CBFs, the beam and column members are proportioned to carry the C_u and T_u forces developed in the HSS braces. As depicted in Figure 3.1-8 to Figure 3.1-11, it resulted that C_u, equaling $1.2C_r$, is much greater than the $2F_{slip}$. Herein, C_r is calculated with Φ =1 and R_yF_y =460 MPa. In order to provide a safe design for column and beam members, a secondary ductile fuse is proposed to yield before an axial force of $2F_{slip}$ is developed in PFD. As depicted in the aforementioned figures, $2F_{slip}$ corresponds to $C_u/1.2$ which is in fact C_r computed with Φ=1 and R_yF_y =460 MPa. In this work, the secondary ductile fuses are activated when $1.7F_{slip}$ is reached in the PFDs; hence, the gusset plates are designed to fail in a ductile manner under $1.7F_{slip}$. As depicted in Figure *3.1-7*, the top end HSS brace is welded to the gusset plate and the connection is designed to resist the probable compression resistance C_u of HSS brace. This assures that the brace-gusset connection will not fail before the PFD-gusset connection, presented hereafter.

4.1.1 Gusset Plate-PFD Connection

Herein, the design of gusset plate to PFD connections consists of the design of high-strength bolts in a shear bearing-type connection. In general, there are two broad categories of failure in bolted PFD-gusset plate connections subjected to tensile force:

a) failure of the bolts in double shear (Figure 4.1-1) and

b) failure of the parts being connected (Figure 4.1-3)

The bolt spacing and edge distance will affect the bearing strength of a connection. It is worth mentioning that oversized holes are not allowed in bearing-type connections. As per clause 22.3 of CSA-S16-14, the minimum distance between centres of bolt holes shall be 2.7 times the bolt diameter; the minimum distance from the centre of a bolt hole to an edge shall be bigger than 1.75 x bolt diameter (d_b) for bolt diameter over 1 ¼ inch (31.75 mm). However, the maximum distance from the centre of a bolt hole to an edge shall be not greater than 150 mm.

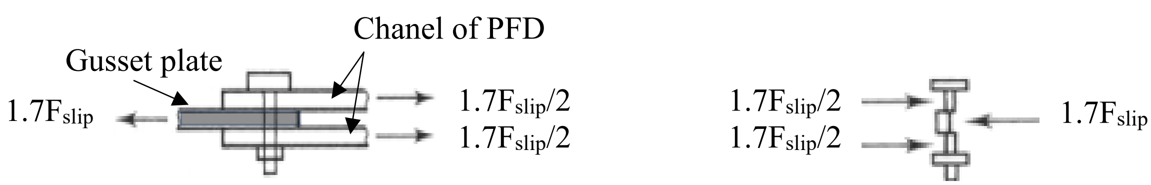

Figure 4.1-1: Force transferred from the PFD to the gusset plate and bolts

According to (Astaneh-Asl 1998), the failure mode hierarchy of a typical brace to gusset bolted connection is:

a) Slippage of bolts in bolted connections,

b) Yielding of gross area of plates used in the connection,

c) Bearing failure of bolt holes,

d) Local buckling of plates used in the connection

e) Edge distance fracture and bolt spacing failure in bolted connections,

f) Fracture of effective net area of plate in the connection,

g) Block shear failure, tear-out

h) Shearing of bolts.

The above desirable hierarchy of failure modes are shown in Figure 4.1-3. All failure modes should be verified to ensure that they will not occur before axial force in the PFD-brace reaches $1.7F_{slip}$.

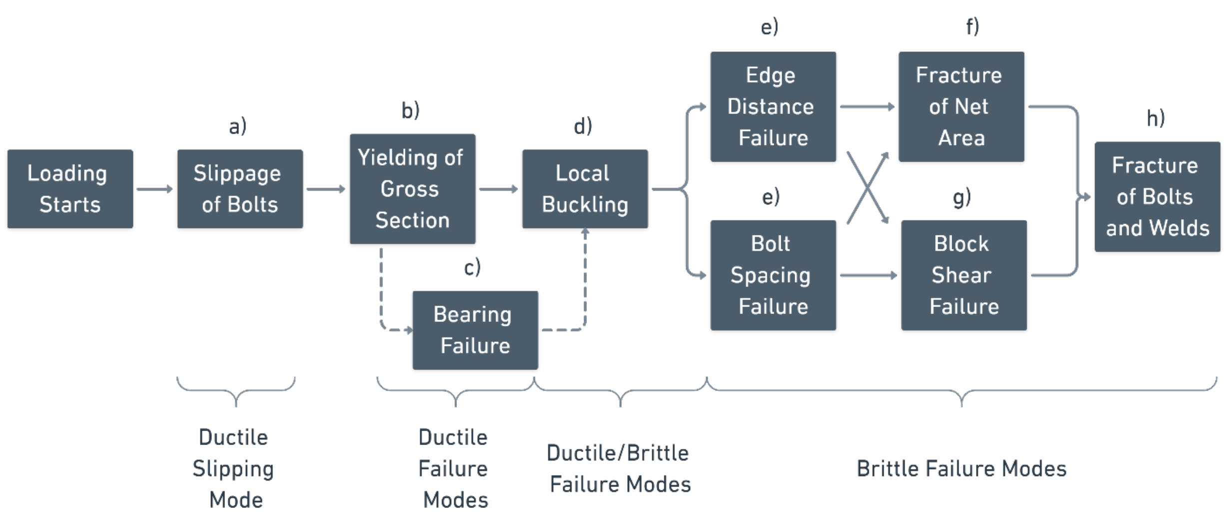

Figure 4.1-2: Failure modes of bolted connection of PFD-gusset plate in a hierarchical order considering ductile failure modes after (Astaneh-Asl 1998).

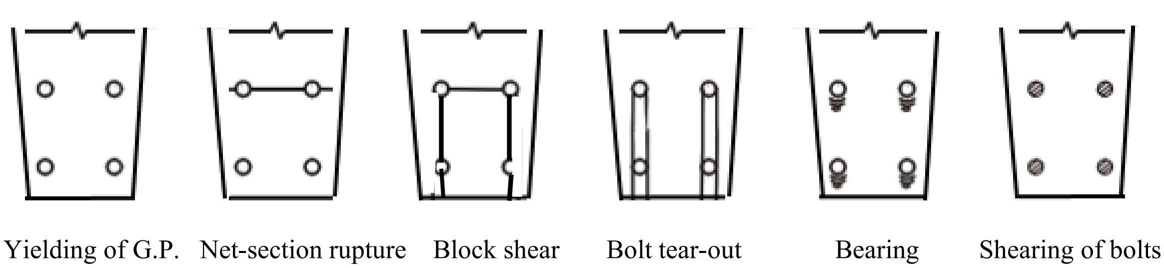

Figure 4.1-3: Typical failure modes of bolted connection (Qing and Driver 2008)

Considering a 4 bolt connection, these failure modes can be represented schematically as per Figure 4.1-3. Several tests were carried out by Qing and Driver (2008) in order to characterised the above failure modes (Qing and Driver 2008). From testing of specimens in Series C (thicker web), the tear-out failure mode is presented below (Figure 4.1-4)

a) b)

Figure 4.1-4. Tier-out failure mode for specimen in Series C: a) specimen loaded to failure (monotonic loading) and b) specimen unloaded right after the peak (as per Qing and Driver, 2008)

Thus, as per Figure 4.1-2, yielding of gusset and bearing of gusset are ductile failure modes that are targeted to occur first, followed by bolt tearing-out. It is worth mentioning that bolt-tear out can govern the failure mode for connections with small end distances.

The equations provided in CSA-S16-14 standard are employed to check the failure modes of bolted connections consisting of a gusset plate inserted between the 2 C-channel sections of the PFD. Considering 4 high-strength bolts of grade ASTM A490 (F_u=1035 MPa) and d_b=38 mm diameter, the end distance should be > 1.75xd_b which yields 66.5 mm. The pitch should be ≥ 2.7d_b = 102,6 mm.

i) Bearing of Bolt Holes of Gusset Plate

In accordance with CSA S16-14, tearing of gusset plate due to bolt bearing is calculated by the following equation:

$$B_r = 3\varphi_{br} n_{bolts} t_g d_{hole} F_u \tag{4.1-1}$$

where, $\varphi_{br} = 0.8$, *n* is the number of bolts, t_g is the thickness of the gusset plate, *d* is the diameter of the hole, and F_u is the ultimate strength of the gusset. Herein, φ_{br} is the bearing resistance factor. A representation is shown in Figure 4.1-5, where, for example, considering $n_{bolts} = 2$, $d_{hole} = 40mm$, $t_g = 25mm$ it results $B_r = (3)(0.8)(2)(25mm)(40mm)(1035MPa)(10^{-3}) = 4968\ kN$

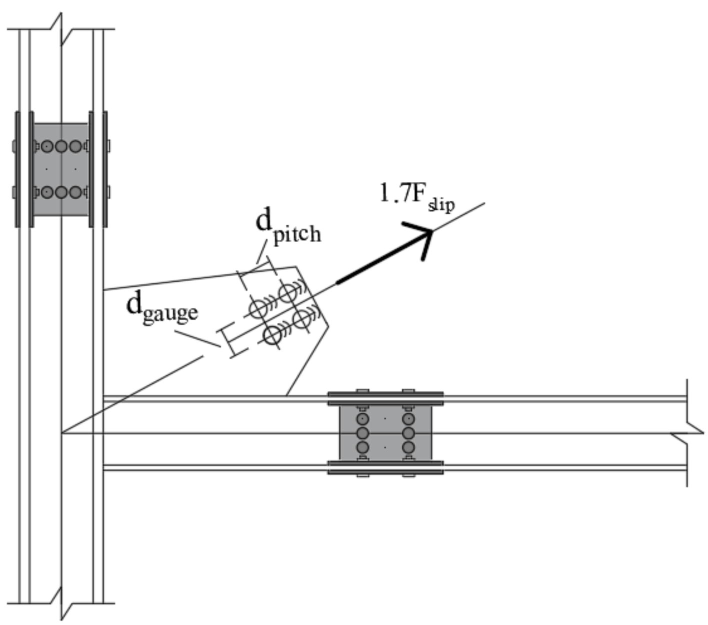

Figure 4.1-5. Gusset failure due to bolt bearing

ii) Shearing of Bolts

Shearing of bolts is calculated according to the following equation where bolts should not be threaded in the plane of shearing:

$$V_r = 0.6\varphi_b nmA_bF_u \tag{4.1-2}$$

where, $\varphi_b = 0.8$, n is the number of bolts, m is the number of shear planes, A_b is the area of the bolt and F_u is the ultimate strength of the bolt. As shown in Figure 4.1-1, $m = 2$.

Shearing of bolts should be avoided because of its brittle failure mechanism. The maximum capacity of a two-bolted connection using a 38mm ASTM A490 High Strength Bolts with F_u = 1035 MPa, and 2 shear planes, where the bolt threads do not intercept the shear planes, is: $V_r = (0.6)(0.8)(2)(2)(1133.54mm^2)(1035MPa) = 2253\ kN$. Thus, more than two bolts must be used in instances where $1.7F_{slip} > V_{rmax} = 2253\ kN$. This demand is easily exceeded at the lower floors of the buildings studied herein. As resulted, the bearing failure of bolt holes is about 2 times bigger than the shearing of bolts; hence, failure in bearing will not occur.

iii) Yielding/Fracture of Gusset Plate in Tension

Failure of the gusset plate may occur by the yielding of the gross area of the gusset plate or by the fracture along the net area as described in the equations below, as well as in Figure 4.1-6 and Figure 4.1-7.

$$T_r = min\begin{cases} \varphi_s A_g F_y \\ \varphi_u A_{ne} F_u \end{cases} \tag{4.1-3}$$

$$A_g = t_g W_w \tag{4.1-4}$$

$$A_{ne} = 0.75 t_g W_{w\,net} \tag{4.1-5}$$

Herein, for the case of PFD to gusset plate bolted connection, $W_{w\ net}$ is the net Whitmore width, and W_w is the gross Whitmore width.

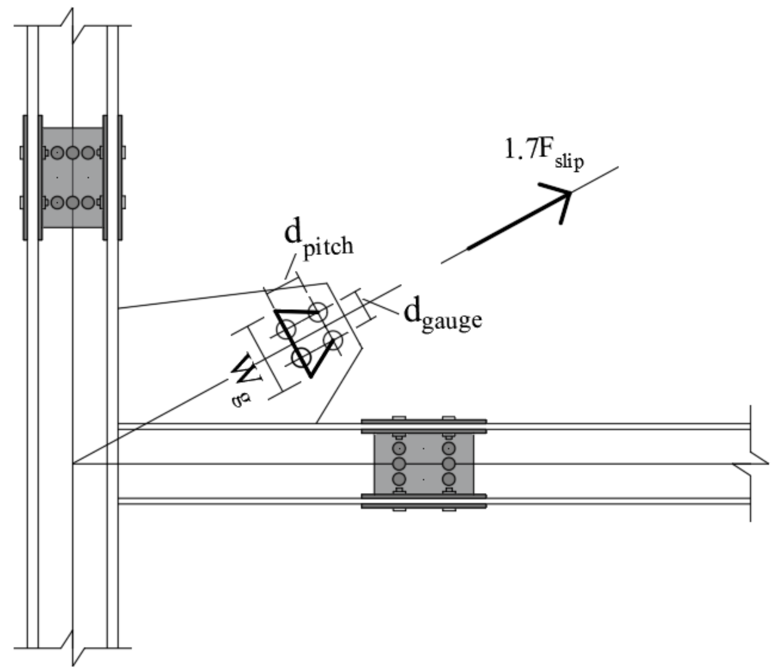

Figure 4.1-6. Gross section yielding of gusset

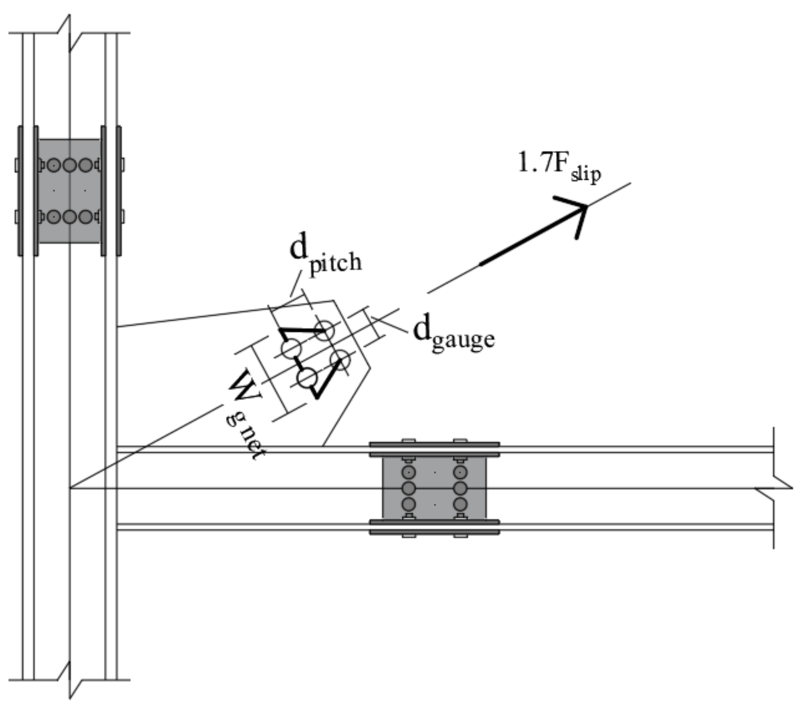

Figure 4.1-7. Net section fracture of gusset plate

iv) Block Shear and Bolt Tear-out of Gusset Plate

Block shear of the gusset plate combines the gross area in shear and the net area of a connection in tension (Fig. 4.1-8). The following equation is used to find the tensile resistance in block shear:

$$T_r = \varphi_u \left[U_t A_n F_u + 0.6 A_{gv} \frac{F_y + F_u}{2} \right] \tag{4.1-6}$$

where $U_t = 1.0$ and $\varphi_u = 0.75$.

Depending on the channels of PFD and the thickness of the gusset plate, it is possible that the channel of the PFD needs to be checked for block shear as well. Block shear failure is most likely the desired mode of failure. This mode of failure can be triggered by varying the end distance between the line of bolts, perpendicular to the load's line of action, and the end of the gusset plate. To check the bolt tear-out resistance, only the second term of Eq. (4.1-6) should be considered.

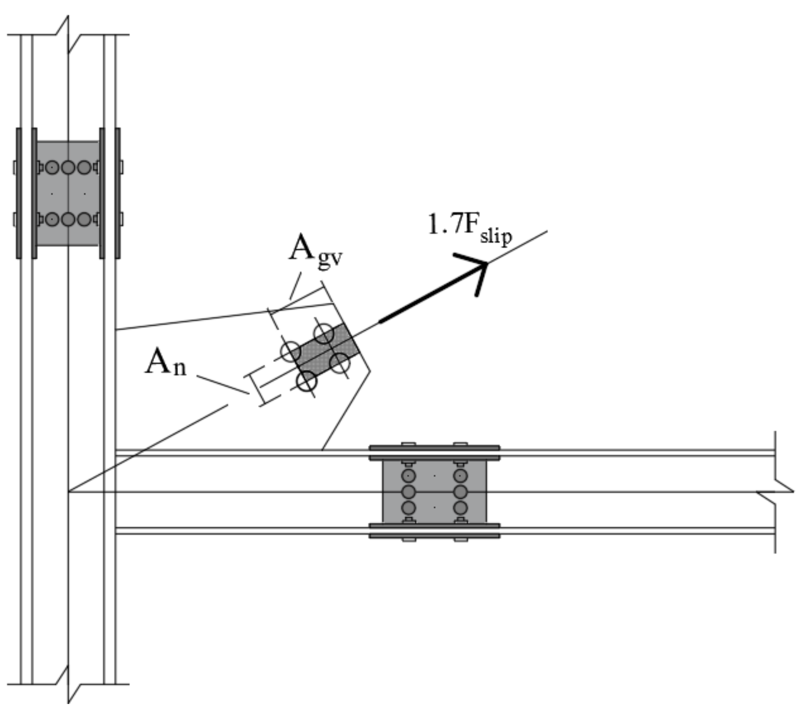

Figure 4.1-8. Block shear of gusset plate for bolted connection

For studied 4-storey FSBF building (FSBF with continuous gravity columns,) the data concerning connections of PFD to gusset plate are given in Table 4.1-1 and Table 4.1-2. Similarly, for the 8-storey FSBF building the data concerning connections of PFD to gusset plate are given in Table 4.1-3 and Table 4.1-4. These gusset plates however are not simulated in the numerical model.

Table 4.1-1. Gusset plate design as component of bolted connection: PFD-frame of FSBF (4-st.)

Storey	$1.7F_{Slip}$ (kN)	Num. Bolts	Bolt Size (mm)	t_g (mm)	Gauge (mm)	Pitch (mm)	End Distance (mm)	W_w (mm)	Failure Mode
4	1275	4	38	22	100	150	80	273	Block Shear
3	1955	4	38	32	100	150	80	273	Block Shear
2	2465	4	38	38	100	170	80	296	Block Shear
1	2805	4	38	38	100	180	90	308	Block Shear

Table 4.1-2. Bolted connection of PFD to frame of FSBF (4-st.) and its potential failure modes

Storey	Design Load	Bolt Bearing	Bolt Shearing	Tensile Yield./Frac.	Block Shear
	$1.7F_{slip}$ (kN)	B_r (kN)	V_r (kN)	T_r (kN)	T_r (kN)
4	1275	3802	4529	1367	1317
3	1955	5530	4529	1988	1973
2	2465	6566	4529	2637	2480
1	2805	7084	4529	2994	2823

Table 4.1-3. Gusset plate design as component of bolted connection: PFD-frame of FSBF (8-st.)

Storey	$1.7F_{Slip}$ (kN)	Num. Bolts	Bolt Size (mm)	t_g (mm)	Gauge (mm)	Pitch (mm)	End Distance (mm)	W_w (mm)	Failure Mode
8	935	4	38	16	100	150	70	273	Block Shear
7	1445	4	38	25	100	140	70	262	Block Shear
6	1870	4	38	32	100	150	70	273	Block Shear
5	2295	4	38	38	100	150	80	273	Block Shear
4	2550	4	38	41	100	160	80	285	Block Shear
3	2805	4	38	44	100	170	80	296	Block Shear
2	2975	4	38	44	100	180	100	308	Block Shear
1	3060	4	38	44	100	180	100	308	Block Shear

Table 4.1-4. Bolted connection of PFD to frame of FSBF (8-st.) and its potential failure modes

Storey	Design Load	Bolt Bearing	Bolt Shearing	Tensile Yield./Frac.	Block Shear
	$1.7F_{slip}$ (kN)	**B_r (kN)**	**V_r (kN)**	**T_r (kN)**	**T_r (kN)**
8	1262	2764	4529	994	958
7	2238	4320	4529	1462	1451
6	2947	5529	4529	1988	1915
5	3720	6566	4529	2361	2343
4	3720	7084	4529	2696	2601
3	4458	7603	4529	3053	2871
2	4458	7603	4529	3213	3109
1	4405	7603	4529	3213	3109

4.1.2 Gusset Plate-Brace Connection

Connections between the top-end of HSS braces and gusset plates should be checked for the following failure modes: i) Shear Resistance of Brace Welds, ii) Tensile Resistance of the Base Metal of the Welds (gusset plate or brace tearing), iii) Yielding of Gusset Plate, iv) Buckling of Gusset Plate, v) Net Fracture of Brace, and vi) Block Shear Failure. HSS members are slotted and inserted into the gusset plate where the HSS brace member is then welded by four filet welds. Shearing of welds should be avoided. The HSS brace to frame welded connections are designed not to fail before the yielding of secondary ductile fuse.

4.2 Friction Sliding Braced Frame with Continuous Columns – Results

Regarding the design of the continuous columns of FSBF-CC-I, no member sizes were altered from the bare FSBF design. The only difference is that all columns including gravity columns are continuous from the ground floor to the roof. Beam-column connections are still pinned. The design for bare FSBF is shown in Chapter 3.

4.2.1.1.1 4-Storey - Friction Sliding Braced Frame with Continuous Columns (FSBF-CC-I) at Design Level

Interstorey drift (ISD), residual interstorey drift (RISD), and floor acceleration (FA) at design level are shown in Figure 4.2-1 for 4-storey FSBF-CC-I (R_dR_0=4). At design level demand, the maximum ISD resulted at roof is 1.19%h_s and 1.47%h_s under crustal and subduction ground motion suites, respectively. For the 4-storey bare FSBF-I (columns are only continuous over two storeys) presented in Chapter 3, the maximum ISD was 1.20%h_s at the third storey under crustal GMs and 3.37%h_s at the roof under subduction GMs, respectively. This results in about 1% and 56% reduction in ISD under crustal and subduction GM suite, respectively. Subsequently, at design level, RISD is 0.88%h_s and 3.13%h_s for bare FSBF-I. When FSBF-CC-I was employed, RISD reduced to 0.62%h_s and 1.02%h_s under crustal and subduction GMs, respectively. Hence, the reduction in RISD is 29% and 67% under crustal and subduction GMs, respectively. Floor acceleration for FSBF-I is 0.81g and 1.25g and for FSBF-CC-I slightly decreases to 0.76g and 1.22g under crustal and subduction GMs, respectively. Hence, a 6% and 2% reduction is observed. As shown from the above, employing FSBF-CC-I instead of FSBF-I leads to substantial ISD and RISD reduction due to the marginal improvement of the frame-action provided by the continuous columns. Employing the FSBF-CC-I, the ISD is within the 2.5%h_s code limit for buildings of normal importance category. Subsequently, the residual drift saw an improvement for both crustal and subduction suites. These results are consistent with research (Ji et al. 2009, and MacRae et al. 2004) where evidence for a reduction in residual drift was observed by increasing column stiffness under crustal ground motions. To date, similar research under subduction ground motions is limited. As specified in the previous chapter, a Reparability Limit State (RLS) is achieved when the RISD of 0.5%h_s is reached. This is consistent with other researchers' findings (McCormick et al. 2008). As observed, both systems, FSBF-I and FSBF-CC-I, exceeded the targeted RLS and thus additional frame-action provided by a backup MRF added in parallel with the bare FSBF system could be the solution.

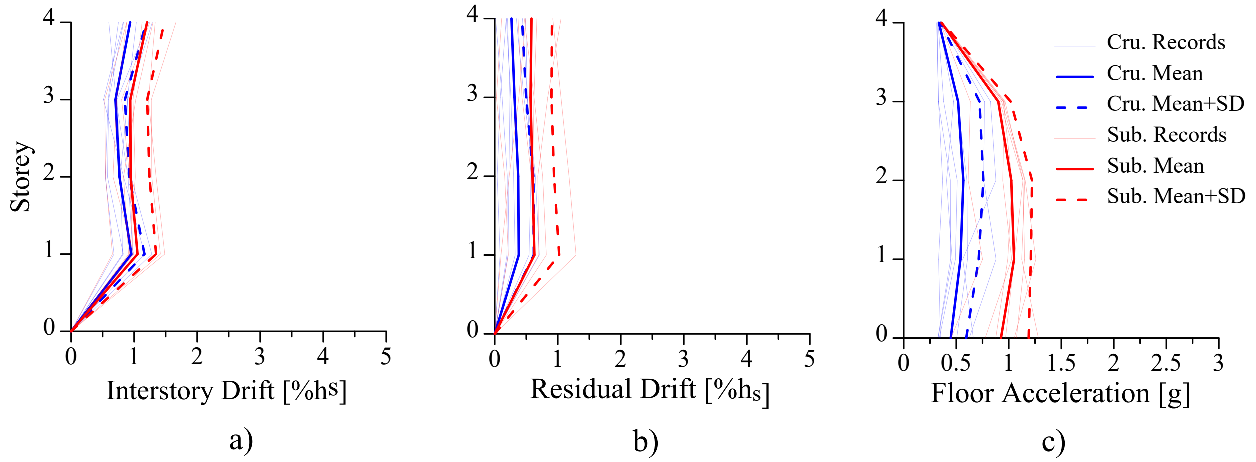

Figure 4.2-1. Response of FSBF-CC-I (4-st.) building under crustal and subduction GMs (design level): a) ISD, b) RISD, and c) FA

To demonstrate the FSBF-CC-I building's response under #838-90 Landers (1992) crustal GM and #MYG001 Tohoku (2011) subduction GM, the ISD time series recorded at all floors are provided in Figure 4.2-2 together with the accelerogram and Arias intensity of selected records. Figure 4.2-2 shows that maximum ISD of each floor occurs within the Trifunac duration (significant duration), as expected, and maximum RISD is observed to be larger for FSBF-I (see Figure 3.1-21) than for the FSBF-CC-I. Herein, the peak RISD occurs at 1st and 2nd floors.

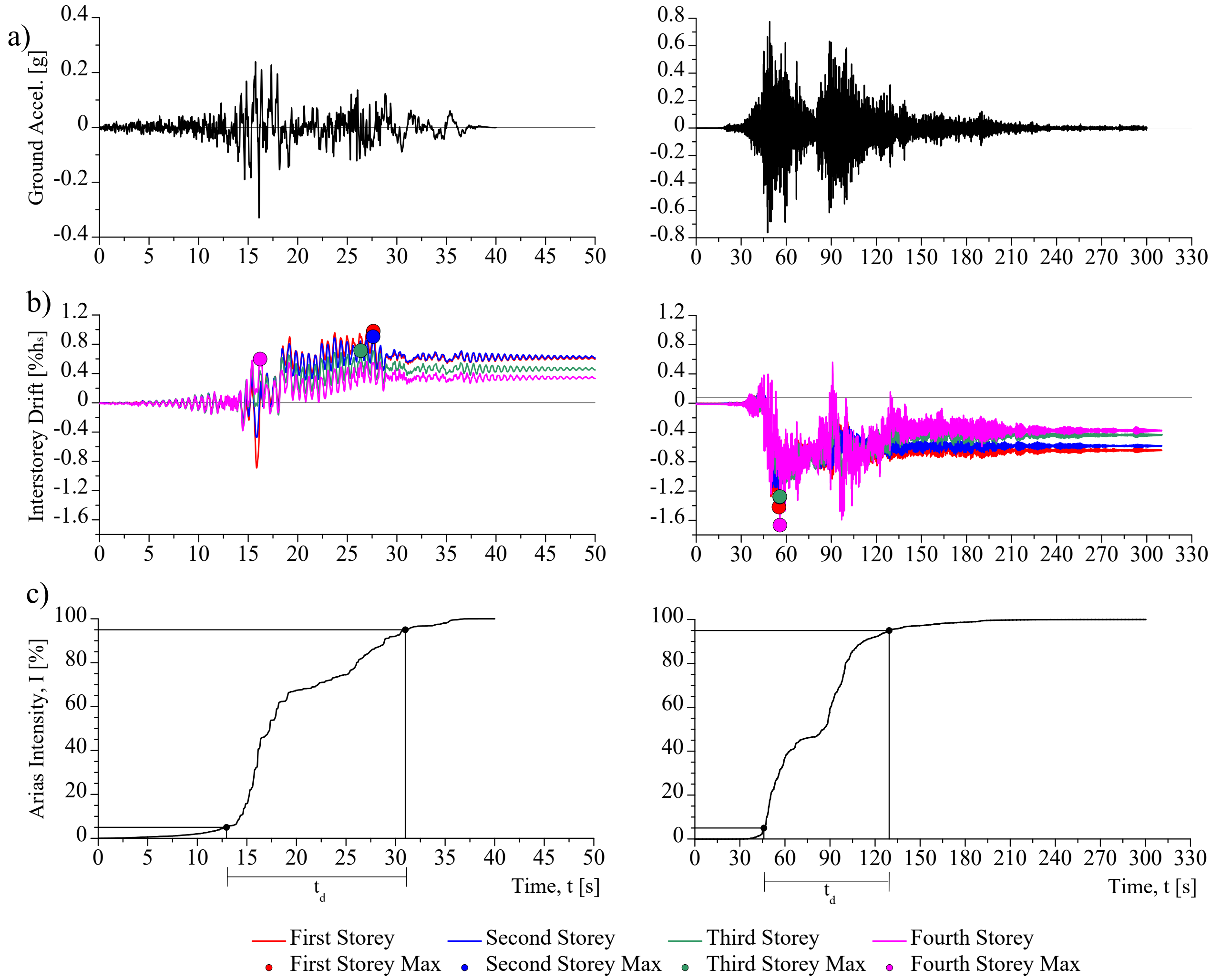

Figure 4.2-2. Response of 4-storey FSBF-CC-I under crustal GM Landers, 1992, #838-90 (Left) and subduction GM Tohoku, 2011, #MYG001 (Right): a) scaled ground acceleration, b) ISD time-history of all floors, c) Arias intensity for GMs

Figure 4.2-3 shows the hysteretic shape of PFD installed in the left brace located in the first storey of FSBF-CC-I (4-st.) under ground motions #838-90 and #MYG001 scaled at Design Level. It is observed that the PFD does not exhibit any bearing behaviour under the Design Level demand. Thus, the slip length selected is sufficient and excess forces greater than F_{slip} are not generated by PFDs. It is also worth noting that, comparing the responses of FSBF-I and FSBF-CC-I, variation in terms of total displacement at the first floor is similar even though the overall building behaviour has improved. This observation can be attributed to the difference in force distribution across the storey heights due to continuous columns of FSBF-CC-I and an unchanged stiffness at the bottom floor between FSBF-I and FSBF-CC-I.

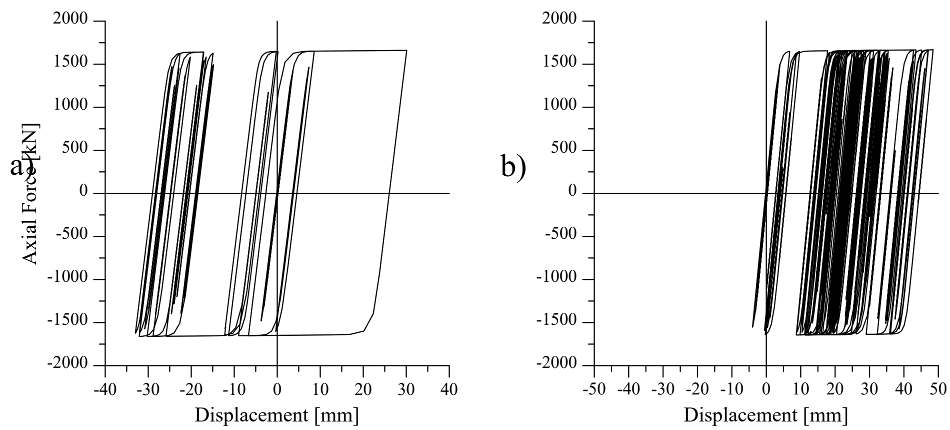

Figure 4.2-3. FSBF-CC-I (4-st.) building response in terms of PFD hysteresis of left brace for first storey under: a) GM #838-90 and b) #MYG001 at Design Level

4.2.1.1.2 8-Storey - Friction Sliding Braced Frame with Continuous Columns (FSBF-CC-I) at Design Level

The FSBF-CC-I was modelled with the idea to improve the seismic response of the 8-storey bare FSBF-I. All member and PFD design remains unchanged when comparing with the bare FSBF; however, only the braced frame and gravity columns are continuous from the ground floor to the roof. However, this improvement was to sufficient to sustain the input resulted under the scaled subduction ground motions at Design Level and the FSBF-CC-I experienced early collapse. Nevertheless, the 8-storey FSBF-CC-I building withstands the shaking under all crustal GMs but one #15-021. All of the collapsed responses have been excluded from Figure 4.2-4, and thus the mean and mean plus standard deviation does not contain this information. However, even excluding the collapsed responses, the peak ISD is well above 2.5%h_s and the RISD is very large and the response is not acceptable.

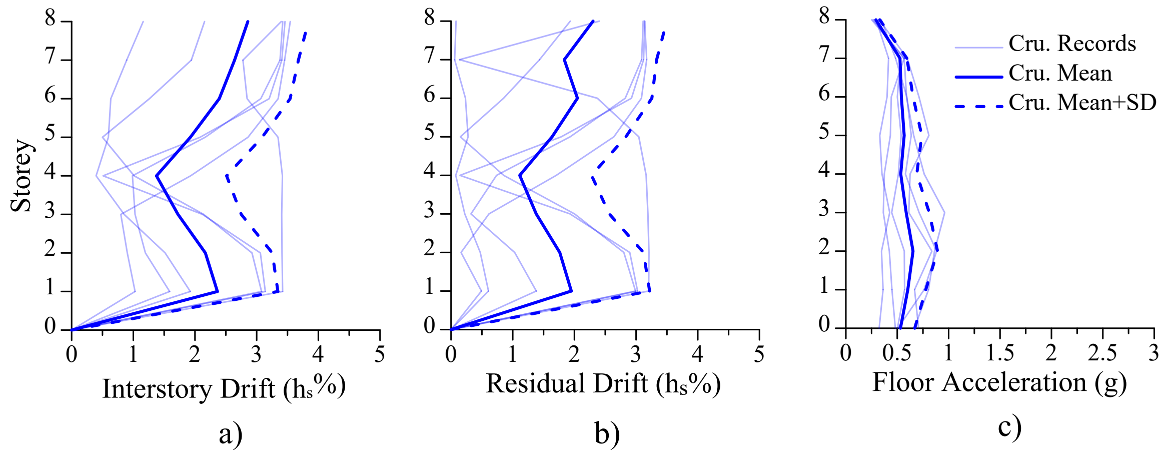

Figure 4.2-4. Response of 8-storey FSBF-CC-I under crustal ground motions (Design Level): a) ISD, b) RISD, c) FA

Figure 4.2-5 shows the time-history ISD series at each floor of the FSBF-CC-I (8-st.) under GM #963-90. The response shows large RISD and the deformed shape show the effect of higher modes. As resulted, the FSBF-CC-I is not permitted to be used for 8-storey buildings, without the addition of backup MRF that will be presented as a component of Dual system in Chapter 5.

Unlike the 4-storey building, the PFDs located at the first floor of 8-storey FSBF-CC-I building experienced bearing. These observations are shown in Figure 4.2-5, where approximately 1.5F_{slip} is observed as a peak force in the brace-damper assembly.

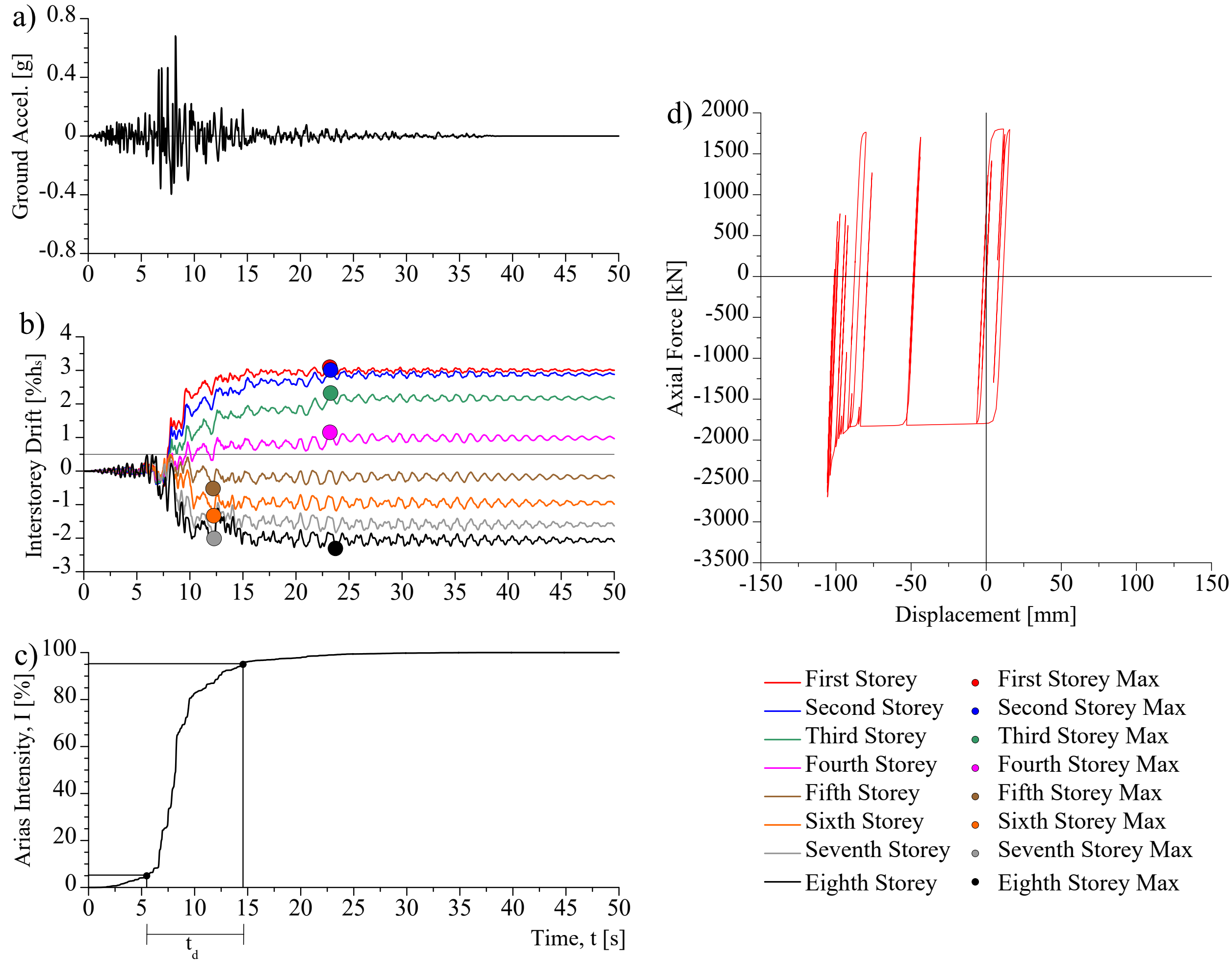

Figure 4.2-5: Response of 8-storey FSBF-CC-I under crustal GM Northridge, 1994, #963-90 (Design Level): a) scaled record b) ISD time-history series plotted at all floors c) Arias intensity of GM d) first floor – left brace – PFD hysteresis

4.3 Incremental Dynamic Analysis of 4 and 8-storey Friction Sliding Braced Frame with Continuous Columns Buildings

To further investigate the seismic performance of these systems, including their collapse, incremental dynamic analysis (IDA) was completed for studied 4-storey and 8-storey FSBF-CC-I buildings. The IDA, (Vamvatsikos and Cornell 2001), is a method used to measure the performance of a structure at multiple intensity levels. Herein the intensity measure considered is the spectral acceleration $S_a(T_1)$ and the selected engineering demand parameter is ISD. Collapse of the structure is determined as a function of interstorey drift where very large maximum displacement is achieved under a small increase in spectral acceleration demand; thus, resulting in a complete flattening of the IDA curve. This type a collapse assessment can also be used to judge appropriate R_d factor, as will be discussed later in Chapter 6.

The IDAs for 4-storey FSBF-CC-I building under crustal and subduction GMs, are provided in Figure 4.3-1 a) and b), respectively. The 50th percentile of the seven ground motions contained in each suite is identified by the red line. The 50th percentile is used to identify the collapse point of the structure and other phenomena. As depicted, collapse, as measured by the 50th percentile, occurs when the peak ISD among floors is approximately 3.5%h_s.

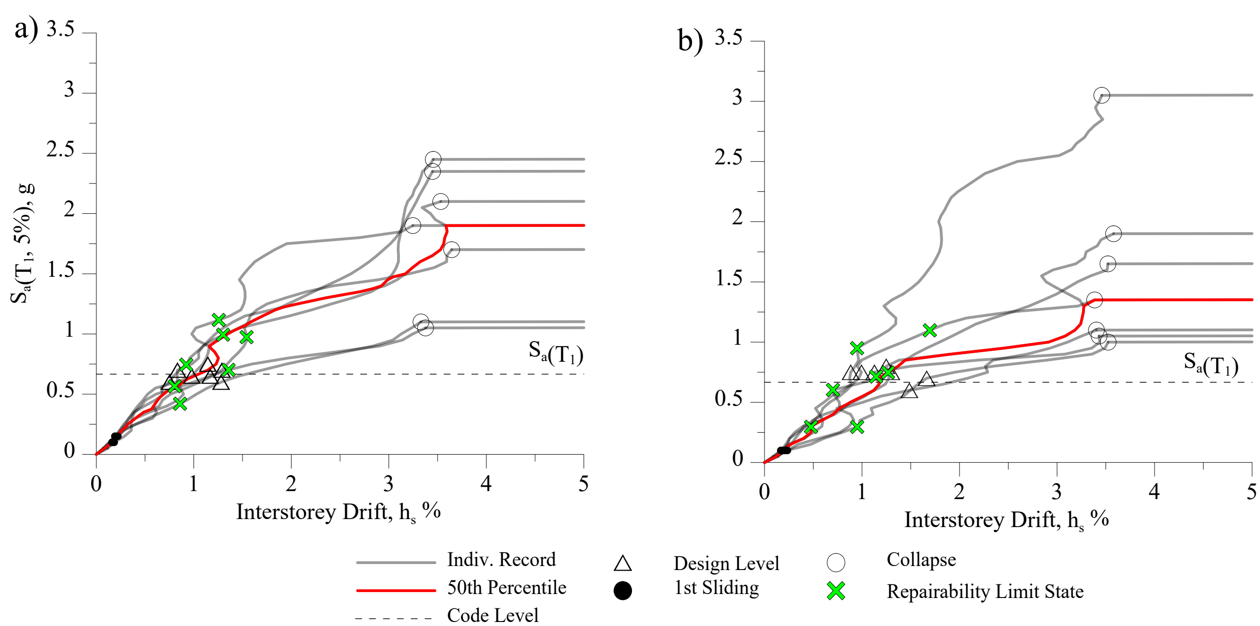

Figure 4.3-1. IDA curves for 4-storey FSBF-CC-I building under: a) crustal GMs and b) subduction GMs

In all IDAs, the linear segment (elastic response) is followed by weaving or softening behaviour under crustal GMs and mostly softening response under subduction GMs. However, all ground motions contain alternative hardening and softening segments, but hardening is observed above the code level demand for most ground motions in the crustal suite and more softening characteristics are found under the subduction suite. Sliding of the first PFD occurs as early as $S_a(T_1) = 0.1g$ which is signified by the attainment of F_{slip} in the device.

IDA curves for 8-storey FSBF-CC-I building resulted under crustal and subduction GMs are plotted in Figure 4.3-2. As depicted, the building cannot withstand design level demand under subduction GMs. Furthermore, 50th percentile collapse occurs slightly above Design Level under crustal GMs. As depicted, under subduction IDAs, the system experienced softening almost immediately after sliding of the first PFD.

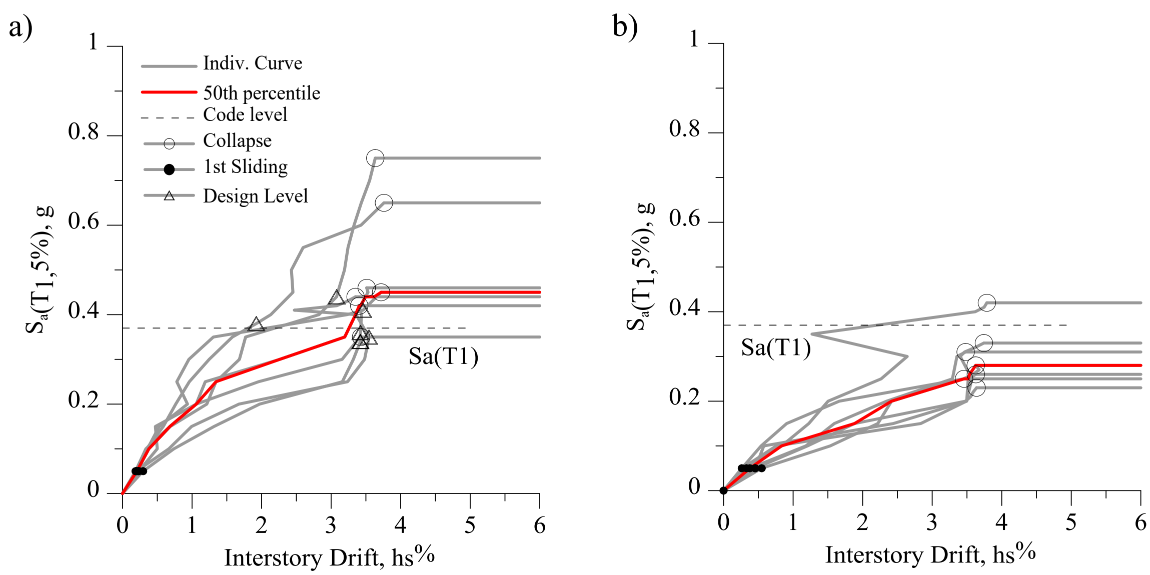

Figure 4.3-2. IDA curves for 8-storey FSBF-CC-I building under: a) crustal GMs and b) subduction GMs

To summarize, the 4-storey FSBF-CC-I building shows promise response under crustal ground motions. However, under subduction ground motions, the FSBF-CC-I system showed lack stability early in their response and near code demand level. For the 8-storey FSBF-CC-I building, the responses under both crustal and subduction GMs, show unsatisfactory behaviour. Thus, designing the system as a Dual FSBF system is recommended. The design of Dual Friction Sliding Braced Frame system is provided in Chapter 5.

Chapter Five

Design Methodology for Dual Friction Sliding Braced Frames

The performance limitations of the previous seismic force resisting systems: bare FSBF and FSBF with continuous columns (FSBF-CC) were presented in the previous chapters. To overcome their drawbacks, the FSBF will be analysed as a Dual system that contains a parallel backup moment resisting frame (MRF). Recent research on Dual system composed of Buckling-Restrained Braced Frames and backup MRF (Sahoo and Chao 2015) has shown promise in substantially reducing RISD by the addition of a backup moment frame. The similarities between these two systems provides us with reason to explore the effectiveness of a dual system configuration for FSBF structures. Design of the backup MRF is done with respect to the NBCC 2015 and CSA S16-14 standard. Design methodology used for Dual FSBF is presented, nonlinear time-history analysis is carried out for low-rise and middle-rise buildings under crustal and subduction suites, and investigation into the effects of design ductility is presented.

5.1 Design of Backup Moment Resisting Frames for Dual Friction Sliding Braced Frame System

The results for the bare FSBFs designed in high-risk seismic zones are unsatisfactory for both low-rise and middle-rise buildings. The importance of the backup MRF, additional to the FSBF system, is to reduce the ISDs and RISDs to an acceptable level. An advantage of ductile fuses, such as Pall

Friction Dampers, is the ability to be easily inspected and replaced after a damaging seismic event. Furthermore, the lack of degradation of PFD's components under dynamic cyclical loading permits the device to maintain a consistence hysteretic shape under many cycles, as was observed during the tested specimen under the 2011 Tohoku earthquake (Tirca et al. 2018). However, the time-degradation of friction shim material is unknown.

The design of Dual Friction Sliding Braced Frames, D-FSBF, are first done by designing a bare FSBF system as defined in Chapter 3. The backup MRF is then designed in parallel to FSBF by considering an additional 25% of the design base shear, V. The main purpose of adding the backup MRF is to provide elastic frame-action, however inelastic behaviour of the MRF is possible. Schematically, this behaviour is shown in Figure 5.1-1. The trilinear response of the combined system can be defined for a SDOF system by Eqs. (5.1.1) and (5.1.2) where Δ_b is the elastic displacement given by the braces, Δ_f is the elastic displacement given by the backup MRF, V_b is the base shear provided by the braces, V_f is the base shear provided by the backup MRF, k_b is the stiffness of the brace, k_f is the stiffness provided by the backup MRF, and V_1, V_2, V_3 are the pivotal base shears for each line of the trilinear response. Since the backup MRF is design to resist an additional 25% of base shear, V, and due the nature of ductile MRFs, the stiffness of the MRF will be inherently insignificant when compared to that of the FSBF system.

$$\begin{bmatrix} \Delta_b \\ \Delta_f \end{bmatrix} = \begin{bmatrix} \dfrac{V_b}{k_b} \\ \dfrac{V_f}{k_f} \end{bmatrix} \tag{5.1.1}$$

$$\begin{bmatrix} V_1 \\ V_2 \\ V_3 \end{bmatrix} = \begin{bmatrix} k_b\Delta + k_f\Delta, & 0 < \Delta \leq \Delta_b \\ k_b\Delta_b + k_f\Delta, & \Delta_b < \Delta \leq \Delta_f \\ k_b\Delta_b + k_f\Delta_f, & \Delta_f < \Delta \leq \Delta_{rup} \end{bmatrix} \tag{5.1.2}$$

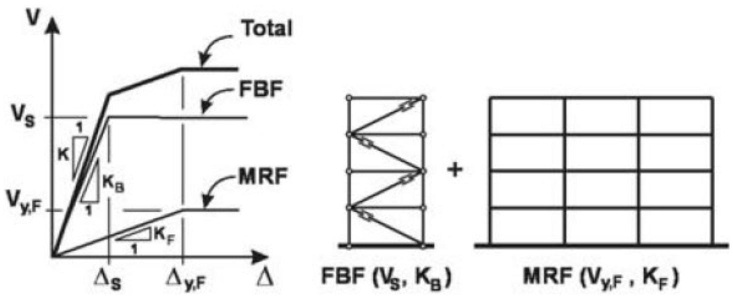

Figure 5.1-1. Decomposition of the trilinear force-displacement response of D-FSBF (Tirca et al. 2018)

Moment resisting frames, according to CSA S16-14, follow a capacity design principle where plastic hinges are located at beam ends. Herein, the plastic zone region of the beams do not contain reduced beam-sections. Beam sections are first selected considering the storey shear force given by the earthquake load combination shown qualitatively in Figure 5.1-2. Once beam sections are selected, capacity design method is used to size the MRF columns by considering the “strong column weak-beam” principle.

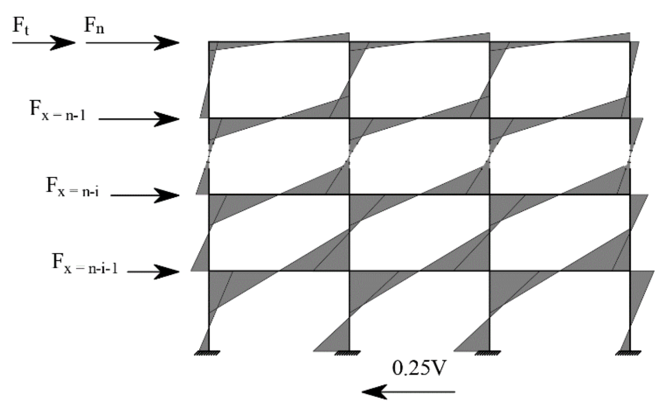

Figure 5.1-2. Qualitative bending moment diagram of MRF under lateral loads

$$M_{pr} = 1.1R_yF_yZ_x \tag{5.1.3}$$

$$V_h = V_{hE} + V_{hG} = \frac{2M_{pr}}{L_h} + \left(\frac{\sum e_iP_i}{L_h} + \frac{wL_h}{2}\right) \tag{5.1.4}$$

The maximum probable bending moment located at the hinge developed in beams, M_{pr}, is given by Eq. (5.1.3), where R_y is taken to be 1.1 for I-shaped beam (CSA S16-14), and Z_x is the plastic section modulus for strong axis bending. The MRF's beam and column sections should be Class 1. The shear force located at the plastic hinge is defined by Eq. (5.1.4) where L_h is the distance between both hinges of the beam, P_i is a point load located on the beam, e_i is the distance of the point load from the hinge, and w is the distributed load on the beam as defined in Figure 5.1-3. For the purposes of column design, the shear force and moment at the column's face is defined by Eqs. (5.1.5) and (5.1.6), respectively. The moment at the centerline of column, M_c, must satisfy Eq. (5.1.7). To satisfy the principle strong column-weak beam, Eq. (5.1.8) should be satisfied. Thus, the summation of the factored flexural resistance of the columns above and below the beam under consideration must be larger than the moment at the centerline of the column caused by the maximum probable bending moment due to hinging of the beams. The factored flexural resistance, M'_{rc} (Eq. (5.1.8)) is calculated at the intersection of the beam and column centerlines, where M_{pc} is the nominal plastic moment resistance of the column and C_y is the axial compression at yield.

$$V_{cf} = V_h + wx \tag{5.1.5}$$

$$M_{cf} = M_{pr} + V_hx + \frac{wx^2}{2} \tag{5.1.6}$$

$$M_c = \sum \left[M_{pr,i} + V_{h,i}\left(x_i + \frac{d_c}{2}\right) + w_ix_i\left(\frac{x_i}{2} + \frac{d_c}{2}\right)\right] \tag{5.1.7}$$

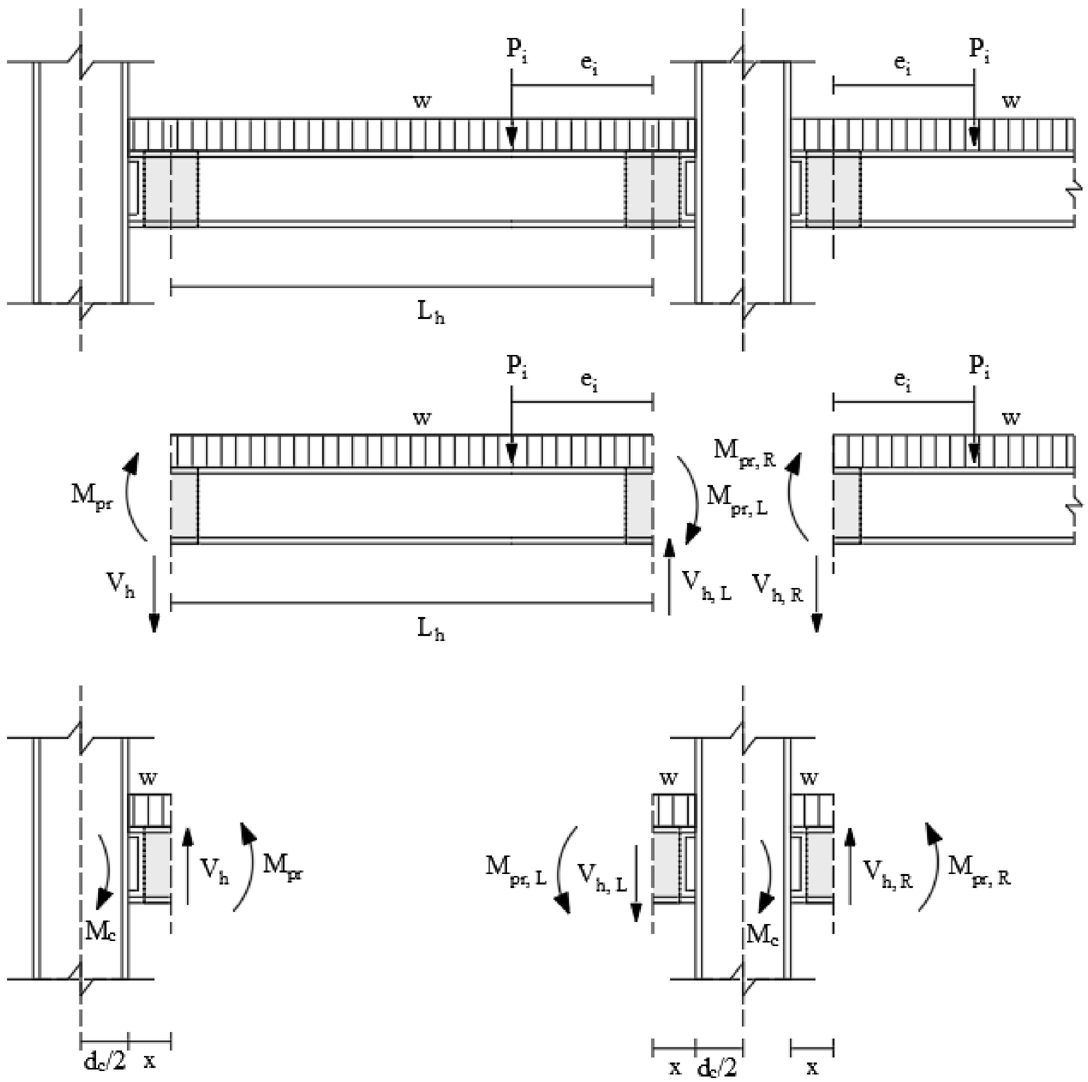

Figure 5.1-3. Freebody diagram for MRF's column design

$$\sum M'_{rc} \geq M_c \tag{5.1.8}$$

$$M'_{rc} = 1.18\varphi M_{pc}\left(1 - \frac{C_f}{\varphi C_y}\right) \leq \varphi M_{pc} \tag{5.1.9}$$

Once the columns are designed to have appropriate resistance relative to their connecting beams, the member strength must be checked for: i) cross-section strength, ii) overall strength, and iii) lateral torsional buckling, according to the steel design requirements (CSA-S16-14).

Beams and columns are selected to have class 1 flanges and webs defined by Eqs. (5.1.10) and (5.1.11), respectively. Beams and columns are made of steel ASTM A572, grade 50 ($F_y = 345\ MPa$).

i) Flange Class 1

$$\frac{b}{2t} \leq \frac{145}{\sqrt{F_y}} \tag{5.1.10}$$

ii) Web Class 1

$$\frac{h}{w} \leq \frac{1100}{\sqrt{F_y}}\left(1 - 0.39\left(\frac{C_f}{\varphi C_y}\right)\right) \tag{5.1.11}$$

5.2 D-FSBF Buildings

5.2.1 Building Description

The addition of backup perimeter MRFs to the building's floor plan illustrated in Chapter 3, is shown in Figure 5.2-1 and the elevation representing the 2D numerical model developed for half of the building floor plan is presented in Figure 5.2-2. Gravity loads remain unchanged from the bare FSBF to the D-FSBF configurations. The models selected to be analyzed in this section, are designed to evaluate the overall performance of Dual FSBF structures, and their appropriate ductility factors. All columns in the SFRS are oriented to have bending about their strong axis. Gravity columns have variable orientations as shown in Figure 5.2-1. All sections for the FSBF system remain the same in the dual system and the backup perimeter MRF is designed for additional base shear representing 25% V. The Dual FSBF system was designed for R_d =4 and Ro = 1; however, slightly greater overstrength could be consider, such as 1.1. Further discussions on the selection of higher R_d value are presented later.

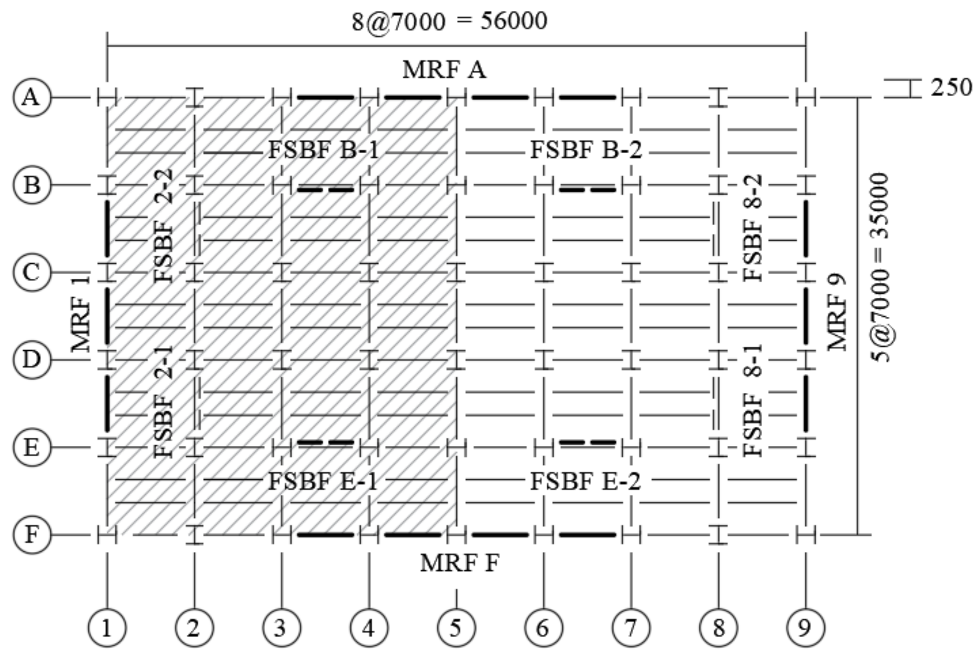

Figure 5.2-1. D-FSBF building floor plan

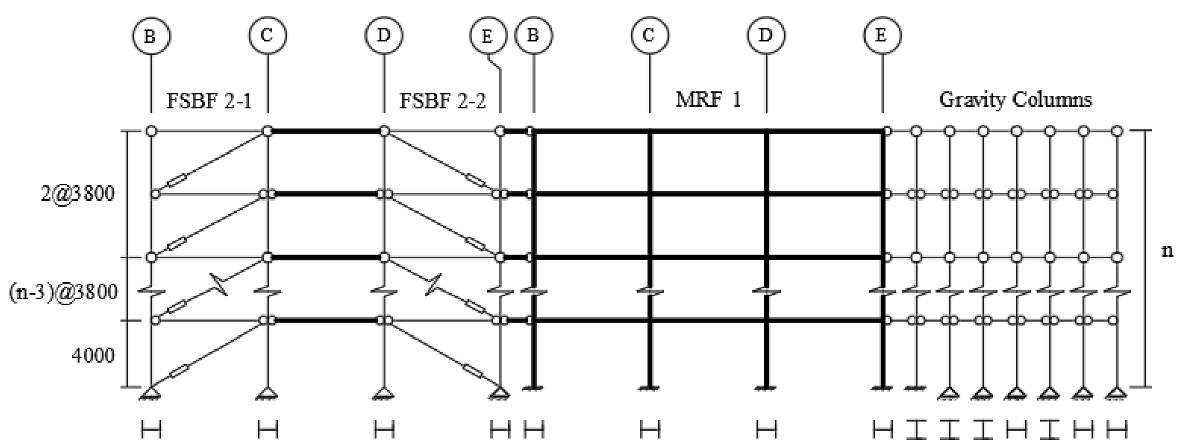

Figure 5.2-2. The 2-D OpenSees model of D-FSBF

Member sizes, connection geometries, and properties of PFDs defined in Chapter 3 for the bare FSBF system for 4-storey and 8-storey buildings remain the same for the D-FSBF systems presented herein and are provided in Table 5.2-1 and Table 5.2-2. The member sizes resulted for the backup MRF design are given for both buildings in Table 5.2-3.

Table 5.2-1. PFD slip forces and brace sections for 4- and 8-storey D-FSBF-I buildings (R_dR_0=4)

D-FSBF-I				
Storey	Slip Force (kN)		Brace members	
8	-	550	-	HSS177.8X177.8X9.5
7	-	850	-	HSS203.2X203.2X12.7
6	-	1100	-	HSS228.6X228.6X12.7
5	-	1350	-	HSS254X254X12.7
4	750	1500	HSS177.8X177.8X15.9	HSS254X254X12.7
3	1150	1650	HSS228.6X228.6X12.7	HSS254X254X15.9
2	1450	1750	HSS254X254X12.7	HSS254X254X15.9
1	1650	1800	HSS254X254X15.9	HSS254X254X15.9

Table 5.2-2. Column and beam sections of FSBF-I and FSBF-II as part of Dual FSBF-I and Dual FSBF-II of 4- and 8-storey buildings

Members of FSBF as part of Dual FSBF-I and Dual FSBF-II				
Storey	Columns of FSBF-I & FSBF-II		Beams of FSBF-I & FSBF-II	
	D-FSBF-I	D-FSBF-II	D-FSBF-I	D-FSBF-II
8	-	W310X86	-	W310X52
7	-	W310X86	-	W310X74
6	-	W310X202	-	W360X79
5	-	W310X202	-	W360X101
4	W310X117	W310X342	W310X74	W360X110
3	W310X117	W310X342	W310X129	W360X122
2	W310X283	W310X500	W310X129	W410X132
1	W310X283	W310X500	W310X143	W410X132

Table 5.2-3. Beam and column sections of backup MRF as part of Dual FSBF-I and Dual FSBF-II of 4- and 8-storey buildings

Storey	Members of backup MRF as part of Dual FSBF-I and Dual FSBF-II					
	Dual FSBF-I; Dual FSBF-II		Dual FSBF-I and Dual FSBF-II			
	MRF Beams		MRF Outer Columns		MRF Middle Columns	
	I	II	I	II	I	II
8	-	W310X32.7	-	W250X58	-	W250X58
7	-	W410X39	-	W250X58	-	W250X58
6	-	W410x54	-	W250X89	-	W250X89
5	-	W410X60	-	W250X89	-	W250X89
4	W360X33	W460X60	W250X80	W250X101	W310X129	W250X101
3	W360X64	W460X68	W250X80	W250X101	W310X129	W250X101
2	W360X79	W460X68	W250X101	W250X131	W310X158	W250X131
1	W360X79	W460X68	W250X101	W250X131	W310X158	W250X131

5.2.2 Nonlinear Response History Analysis of D-FSBF buildings

Research done by (Sahoo and Chao 2015), showed the effects of flexural stiffness compared to flexural strength of backup moment frames displaced in parallel with Buckling Restrained Braced Frames and its role in reducing residual drift. It was observed that flexural stiffness was the property that influenced the building's residual drift performance rather than strength. From this, ideally, the backup moment frame should be optimized for stiffness and not strength. The choice to design the frame using a strength-based parameter, 25%V, is an indirect method to assign the appropriate stiffnesses required to lower the residual drift. More research (Pettinga et al. 2007) suggests that by utilizing a stiffness-based approach for the reduction of residual drift, the proportion of base shear is more likely to be found within the range of 5-10% as opposed to 25%. For steel structures, this distinction between stiffness and strength-based approaches may be a distinction without a difference since the limited ranges of available member sizes may result in the optimal solution being outside the realm of possibility. Therefore, to be consistent with the NBCC and common engineering practice, the 25%V proportion was selected, and the appropriate frame stiffness is expected to be achieved indirectly by a strength-based methodology.

The efficacy of the backup moment frame is a combination of a small amount of added stiffness and load path redistribution, denoted herein as frame-action, and should not have a significant effect on the overall stiffness of the entire structure. This is reflected in the periods of the Dual FSBF-I (R_dR_0=4) systems provided in Table 5.2-4.

Table 5.2-4. Dynamic properties and seismic base shear of 4- and 8-storey Dual FSBF-I buildings

System	Empirical Fundamental Period, $2T_a$	First Mode Period, T_1 (OpenSees)	Seismic Weight, W	Base Shear (ESFP), V
	[s]	[s]	[kN]	[kN]
D-FSBF-I (4-st.)	0.770	0.614	31970	4595
D-FSBF-I (8-st.)	1.530	1.330	62847	5279

5.2.2.1 Ground Motions Selection

The selection of ground motions remains unchanged from Chapter 3. Because of small variation in the 1st mode period, the scaling factor used remain unchanged.

5.2.2.2 Modelling of Backup Moment Resisting Fames

Opensees framework contains elements that enable the user to have the ability to define MRF beams with hinge plasticity defined by the *beamWithHinges* element. This element contains two hinges at each end of the element that has a specified length, L_{pl}. The region outside of the defined hinge regions is defined as being linearly elastic. This element constrains distributed plasticity within the hinge length defined. A rigid link is defined from the centerline of the column to the column's face.

To define the MRF's beam section within the plastic hinge region, the flanges and web of I-shape section are discretized into fibers made of the nonlinear steel material, *Steel02*. The web of the beam is made of 30 horizontal fibers and each flange is discretized in 4 horizontal and 2x30 vertical fibers, such that 30 vertical fibers cover half of the flange, $(b_f - t_f)/2$. *Steel02* material is assigned to all fibers. Then, the *Fatigue* material wrapped to the nonlinear *Steel02* material is assigned to flange fibers as shown in Figure 2.5-3 and Eq. (2.5.3) of Chapter 2, in accordance with (Bosco and Tirca 2017).

Similarly, to the modelling of the FSBF, the columns are defined by a *ForceBeamColumn* element that have been subdivided into 8 elements over their height and discretized into 8 vertical and horizontal fibers in the flange and web, respectively, and 5 horizontal and vertical fibers in the flange and web, respectively. The distance between column centerline and beam's end, as shown in Figure 5.2-3, is defined by rigid links, with lengths relative to the depths of their respective members to capture the column connection eccentricity and the beam connection depth. *ZeroLength* elements define the beam to column face connections, where all degrees-of-freedom are restrained by very stiff rotational and translational stiffnesses to capture the rigid moment connection. Very small vertical and horizontal masses are lumped at the top beam-column nodes of each storey to have convergence of the mass matrix calculations. All masses are lumped to the beam-column nodes of the FSBF in parallel. The top beam-column nodes are slaved to the first column of the FSBF to create a rigid diaphragm by using the *equalDOF* functionality in OpenSees.

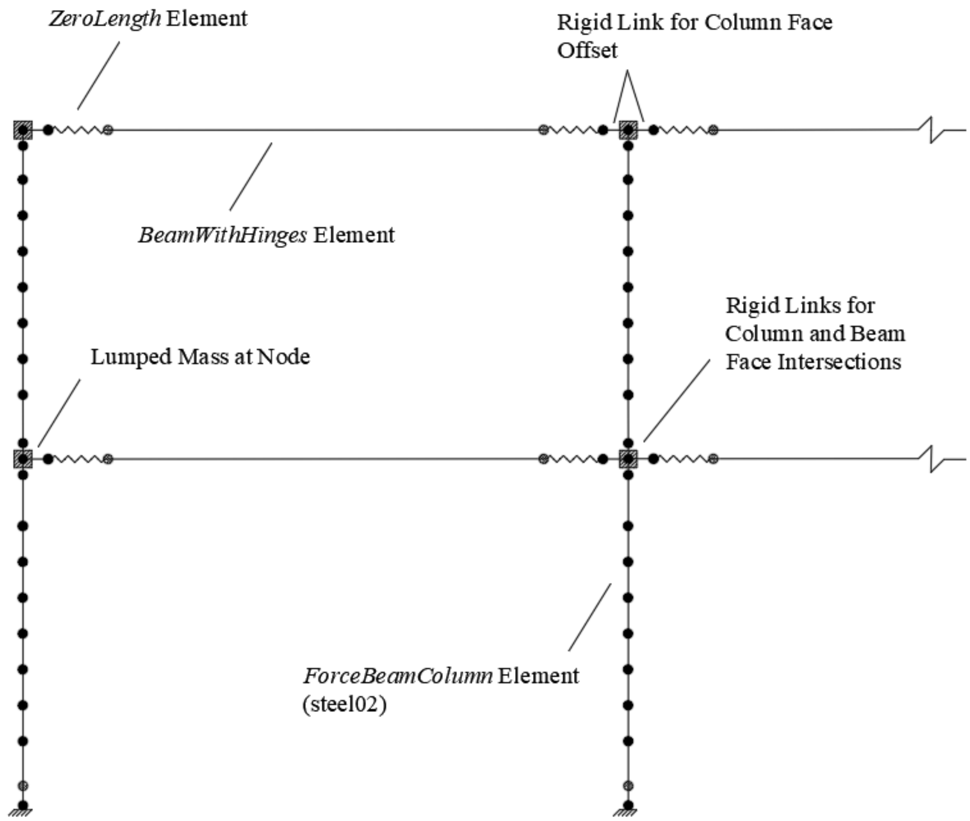

Figure 5.2-3. OpenSees model for backup MRF

All columns of the MRF are fixed at the base. Geometric nonlinearity is defined by the leaning gravity columns as previously described for the FSBF model.

5.2.2.3 Friction Sliding Braced Frame as a Dual System – Design Results

Previous research on BRBs as a Dual System (Kiggins and Uang 2006; Sahoo and Chao 2015) has shown that backup MRFs results in a marginal improvement in interstorey drift, however significant improvements are observed in residual drift. Conceptually, this is due to the frame-action behaviour of the backup MRF and the added redundancy in load paths. Residual drift is an important performance parameter to evaluate a structure's reparability (Erochko et al. 2011; McCormick et al. 2008) and in a structure's capability to resist aftershock damage (Yeo et al.

2005). This research suggests that residual drift above 0.5%h_s deems the structure to be irreparable. For the analysis herein, the residual drift criteria for the Reparability Limit State (RLS) is 0.5%h_s, which for the models shown in the previous chapters has not been achieved. This and the previous literature on BRBs justify and legitimize the research on FSBFs as a dual system to observe if similar results can be achieved.

5.3 Nonlinear response of 4-Storey – Dual Friction Sliding Braced Frame (D-FSBF-I) Building

As shown in Chapter 3, the 4-storey bare FSBF has a peak (Mean+SD) ISD under crustal and subduction GMs of 1.20%h_s and 3.37%h_s, respectively. When comparing these values with those resulting from D-FSBF-I (4-St.) building, plotted in Figure 5.3-1, which are 0.92%h_s under crustal and 1.33%h_s under subduction GMs, there is a 23% and 60% reduction, respectively. This suggests that D-FSBF-I (4-storey) is capable of decreasing the peak ISD and shows a uniformly distributed drift along the building height. As shown, the peak ISD is within the 2.5%h_s code limit.

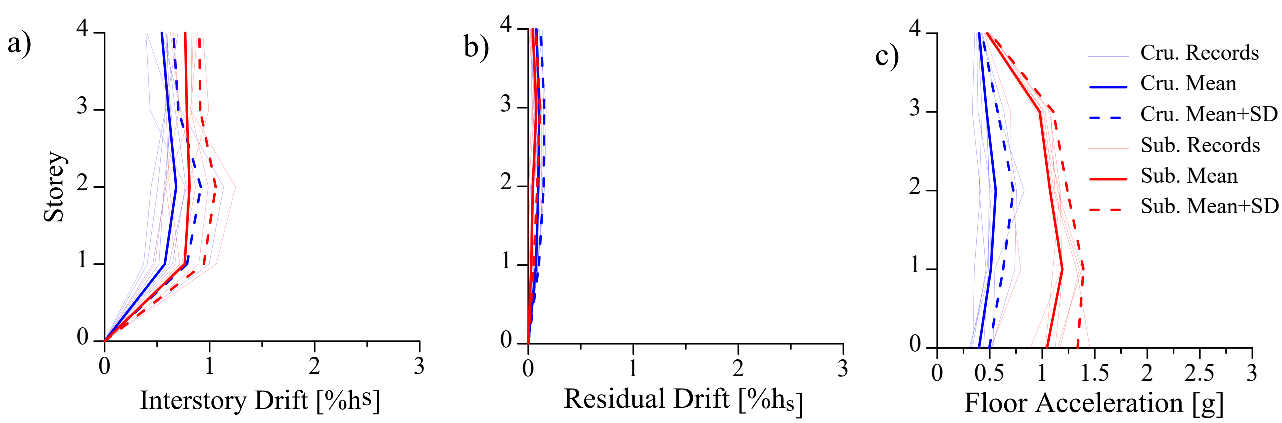

Figure 5.3-1. D-FSBF-I response at design level under crustal and subduction GMs: a) ISD, b) RISD and c) FA

For D-FSBF-I (4-storey), the peak RISD is 0.15%h_s and 0.11%h_s under crustal and subduction GM suites, respectively. When comparing with the peak (Mean+SD) RISD resulting from FSBF-CC-I (4-storey), the values presented in Figure 5.3-1 b) show a substantial decrease which is below the target for RLS of 0.5%h_s. The decrease in residual drift is much more significant than it is with interstorey drift. As previously observed, the FSBF-I (4-storey) and FSBF-CC-I (4-storey) buildings will not be reparable after a code-spectrum demand and are not recommended. The results obtained for D-FSBF-I (4-storey) building show an adequate behaviour. A comparison in terms of peak (Mean+SD) ISD and RISD under crustal and subduction GMs is given in Table 5.3-1 and in terms of peak (Mean+SD) FA in Table 5.3-2. The decrease in percentage between the dual system and the system under consideration, $\left(\frac{Dual-A}{A}\right)(100)$, where A is the system under evaluation, is also given.

Table 5.3-1. Comparison of peak (Mean+SD) ISD and RISD for all studied 4-storey buildings resulted under crustal and subduction GMs. at design level

SFRS	Peak (Mean+SD) ISD				Peak (Mean+SD) RISD			
	Crustal %h_s	Relative Decrease	Sub. %h_s	Relative Decrease	Crustal %h_s	Relative Decrease	Sub. %h_s	Relative Decrease
D-FSBF-I	0.92	-	1.33	-	0.15	-	0.11	-
FSBF-CC-I	1.19	22%	1.47	9.5%	0.62	76%	1.02	89%
FSBF-I	1.20	23%	3.37	60%	0.88	83%	3.13	97%

Table 5.3-2. Comparison of peak (Mean+SD) FA all studied 4-storey buildings resulted under crustal and subduction GMs. at design level

SFRS	Peak (Mean+SD) FA			
	Crustal (g)	Relative Decrease	Sub. (g)	Relative Decrease
D-FSBF-I	0.72	-	1.39	-
FSBF-CC-I	0.76	5.3%	1.22	-14%
FSBF-I	0.81	11%	1.25	-11%

Figure 5.3-2 shows the PFD behaviour and the backup MRF beam behaviour at Design Level under GMs #787-360 (crustal) and #MYG001 (subduction). Conceptually, if the design of the structure and device is appropriate, there should be no bearing experienced in the PFD, and the beams of the backup MRF should experience little to no non-linearity. The graphs shown in Figure 5.3-2 were taken at the floors with the highest interstorey drift. No bearing was experienced at any floor and no beam yielding was experienced at any floor level for both suites. Considering the floors that experienced the max. ISD, the maximum slip length demand of the PFD was 24mm and 31mm under #787-360 and #MYG001, respectively. The design slip length of the PFD at these floors was 87mm, and thus only 27% and 42% of the usable slip length was utilized, respectively. The drift time-history series plotted at all floors under #787-360 (crustal) and #FKS010 (subduction) GMs are provided in Figure 5.3-3. Meanwhile, in the same figure, the accelerograms of the aforementioned GMs and their Arias intensity are provided. The maximum drift values of each floor are achieved within the Trifunac duration time interval. The floors tend to be grouped together in groups of two throughout the ground motion's duration (columns of FSBF are continuous over two storeys), and the maximum values of the coupled floors are obtained at similar times and drifts.

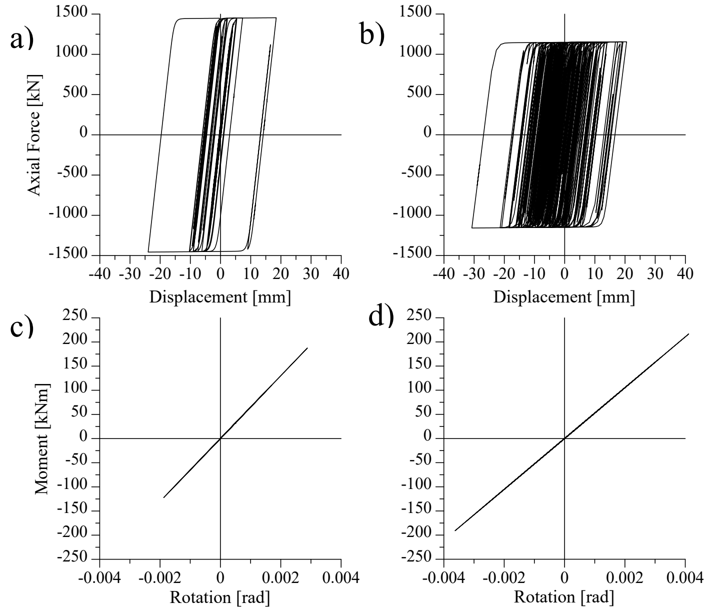

Figure 5.3-2. D-FSBF-I (4-storey) response at design level expressed in terms of hysteresis of PFD and MRF beam: a) response of PFD of 2nd floor under GM #787-360, b) response of PFD of 3rd floor under GM #MYG001, c) response of side MRF beam at 2nd floor under GM #787-360, and d) response of side MRF beam at 3rd floor under subduction GM #MYG001

Figure *5.3-4* and Figure *5.3-5* show the time-history series of axial force developed in PFDs at each floor and the energy dissipated by PFD at each floor of the 4-storey building model under a crustal and a subduction GM scaled to Design Level. In the case of crustal record #787-360, the PFD located at the first floor has dissipated the most energy. However, as per Figure *5.3-5*, the subduction ground motion #MYG001 demanded greater energy dissipation at the fourth floor. As depicted in Figure *5.3-5*, the force time-history series at the 4th floor show that PFDs reached the slip force in almost each cycle; hence it indicates that the PFD has spent most of its time slipping and thus dissipating a large amount of energy. The slip force of the design at the 4th floor is 750 kN compared to the first floor 1650 kN. Although it seems intuitive that the device with the largest slip force will result in the most energy dissipation, as is the case for the crustal GM #787-360, this is not necessarily true, as seen by the GM #MYG001.

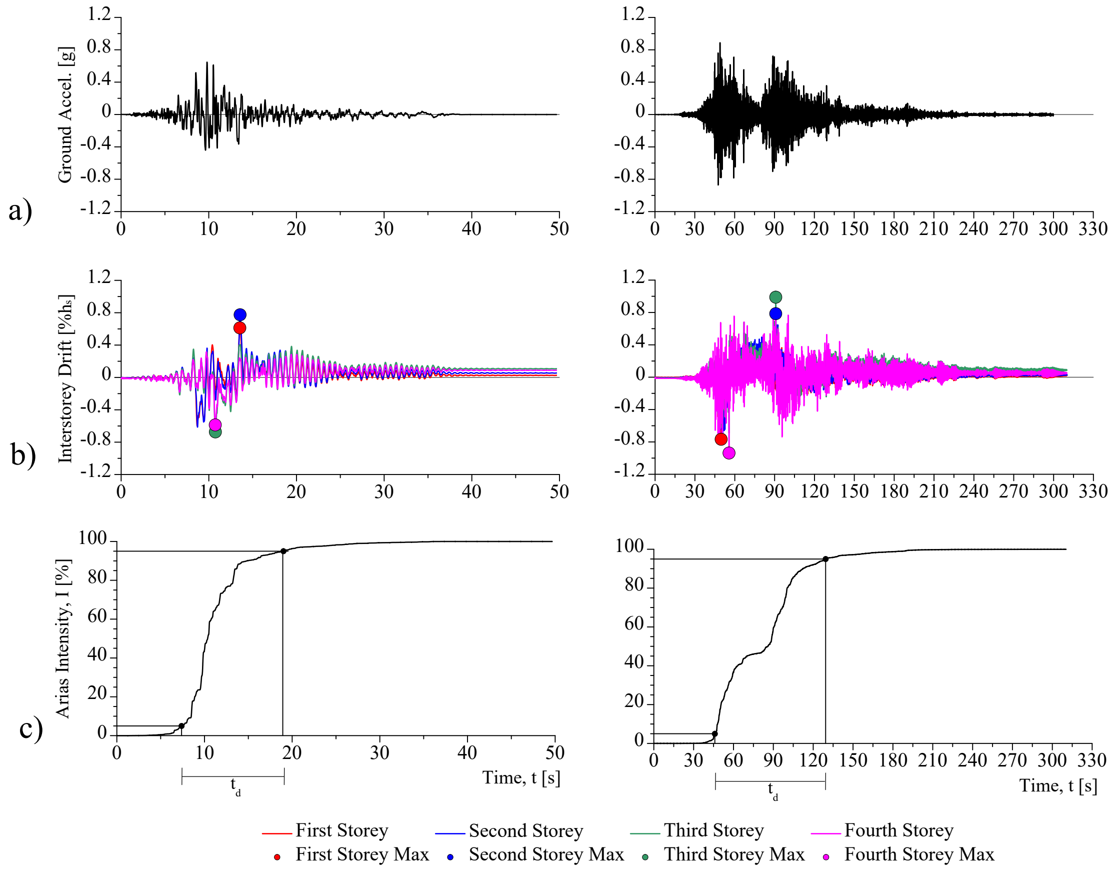

Figure 5.3-3. D-FSBF-I (4-storey) response under GM #787-360 (Left) and subduction GM #FKS010 (right): a) scaled accelerogram, b) D-FSBF-I interstorey drift time-history series of all floors and c) Arias intensity of GMs

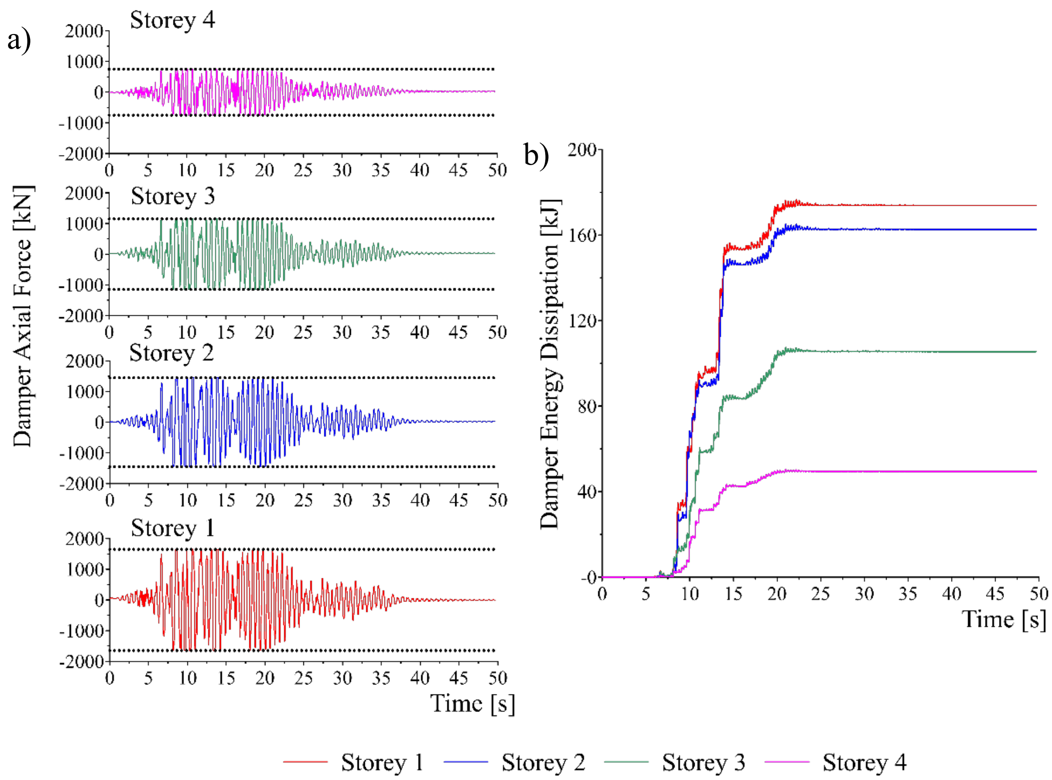

Figure 5.3-4. D-FSBF-I (4-storey) response under GM #787-360 scaled at Design Level: a) time-history series of axial force developed in PFD at each floor and b) PFDs energy dissipation

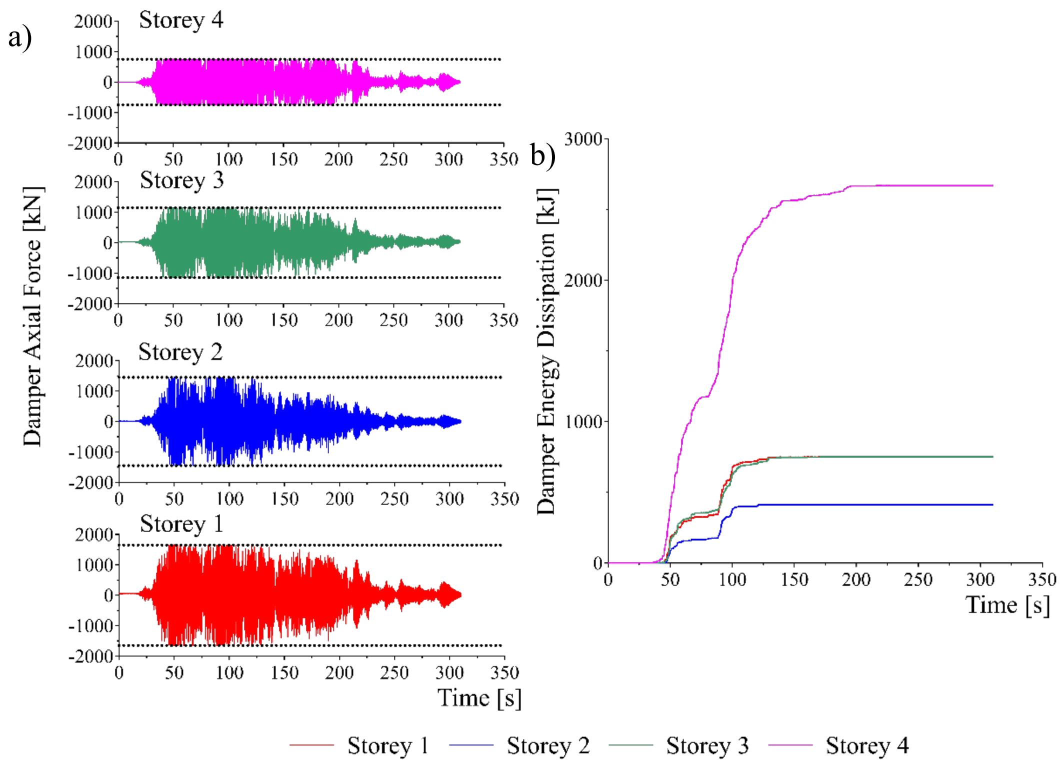

Figure 5.3-5. D-FSBF-I (4-storey) response under GM #MYG001 scaled at Design Level: a) time-history series of axial force developed in PFD at each floor and b) PFDs energy dissipation

5.4 Nonlinear Response of 8-Storey Dual Friction Sliding Braced Frame (D-FSBF-I) Building

In Chapter 3, it was shown that the 8-storey bare FSBF-I building was not able to withstand the seismic demand at Design Level for the majority of the crustal GMs and all of the subduction records. In Chapter 4 it was demonstrated how the continuous columns of FSBF-CC-I (8-storey) were able to improve the seismic response under crustal GMs but yielded an excessive interstorey drift of 3.80%h_s. The FSBF-CC-I (8-storey) system was unable to withstand the subduction GM suite. Employing the D-FSBF-I (R_dR_0=4) system for the 8-storey building, the response was considerably improved and the peak ISD is within the 2.5%h_s code limit. As depicted in Figure

5.4-1, the peak (Mean+SD) ISD is 1.61%h_s and 2.05%h_s under crustal and subduction GM suites, respectively. Furthermore, a peak (Mean+SD) RISD of 0.55%h_s and 0.69%h_s was recorded for the crustal and subduction GM suites, respectively. Thus, the Dual FSBF-I system employed for the 8-storey building responds well to ISD and RISD demand under both GM suites.

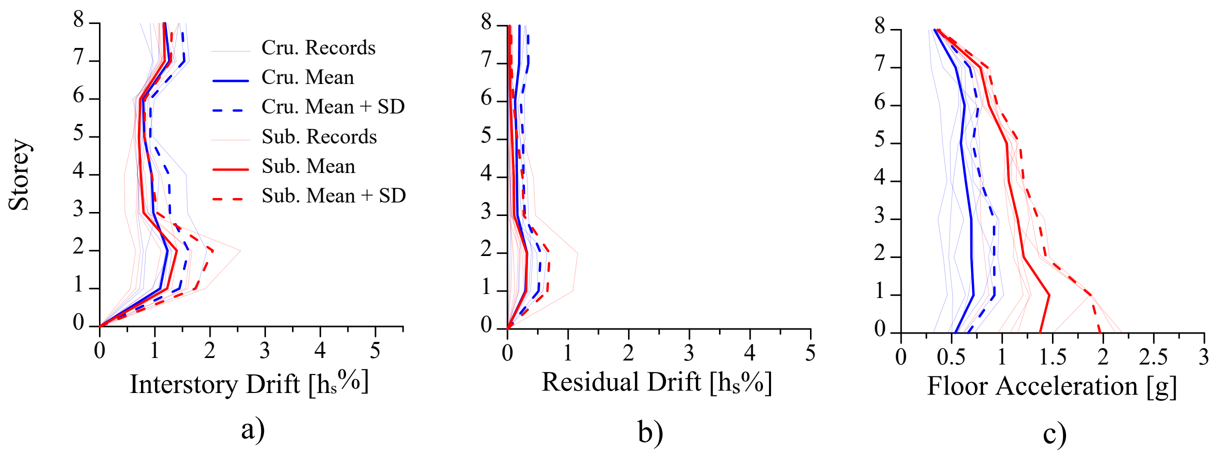

Figure 5.4-1. Response of 8-storey D-FSBF-I building under crustal and subduction GM suites scaled at design level: a) ISD, b) RISD, and c) FA

However, an increase in FA is observed due to the higher mode effects. Table 5.4-1 shows a comparison in term of peak (Mean+SD) ISD as resulted for all studied structural systems employed in the 8-storey building. A decrease in percentage between the dual system and the system under consideration $\left(\frac{Dual-A}{A}\right)(100)$, where A is the system under evaluation, is given. Although we see a decrease in ISD and RISD, there is a slight increase in floor acceleration (Table 5.4-2) which can prove to be important for acceleration sensitive non-structural components.

Figure 5.4-2 shows the hysteresis response of PFDs located at the floors with the largest ISD resulted under #838-90 (crustal) and #FKS010 (subduction) GMs, scaled at Design Level. As depicted, PFDs did not exhibited bearing, while, at the floor, the behaviour of the backup MRF's beam shows elastic response, which is the objective of the design to maintain an elastic restoring force to reduce residual drift.

Table 5.4-1. Comparison of peak (Mean+SD) ISD and RISD (design level) for all studied 8-storey buildings resulted under crustal and subduction GMs.

SFRS	Peak (Mean+SD) ISD				Peak (Mean+SD) RISD			
	Crustal $\%h_s$	Relative Decrease	Sub. $\%h_s$	Relative Decrease	Crustal $\%h_s$	Relative Decrease	Sub. $\%h_s$	Relative Decrease
D-FSBF-I	1.61	-	2.05	-	0.55	-	0.69	-
FSBF-CC-I	3.80	58%	Collapse	-	3.50	84%	Collapse	-
FSBF-I	Collapse	-	Collapse	-	Collapse	-	Collapse	-

Table 5.4-2. Comparison of peak (Mean+SD) FA (design level) for all studied 8-storey buildings resulted under crustal and subduction GMs

SFRS	Peak (Mean+SD) FA			
	Crustal (g)	Relative Decrease	Sub. (g)	Relative Decrease
D-FSBF-I	0.92	-	1.97	-
FSBF-CC-I	0.76	-21%	Collapse	-
FSBF-I	Collapse	-	Collapse	-

The maximum PFD displacement with respect to initial equilibrium position (0) is 25 mm and 35 mm for the crustal #838-90 and subduction #FKS010 GM, respectively. The usable stroke length of the PFDs was designed to be 87 mm with respect to the initial equilibrium position and thus only 29% and 40% of the stroke length was utilized at Design Level for #838-90 and #FKS010 GM, respectively.

Figure 5.4-3 shows the time-history series of ISD of all floors of 8-storey D-FSBF-I building under #838-90 and #FKS010 GMs, where a distinct higher mode effect where floors separate from the typical first mode shape for both GMs can be observed. Under the GM #838-90 it is observed that maximum drift of the 7th floor exceeds that of the first floor. This high ISD at the 7th floor explains the high energy dissipation of this floor as seen in Figure 5.4-4.

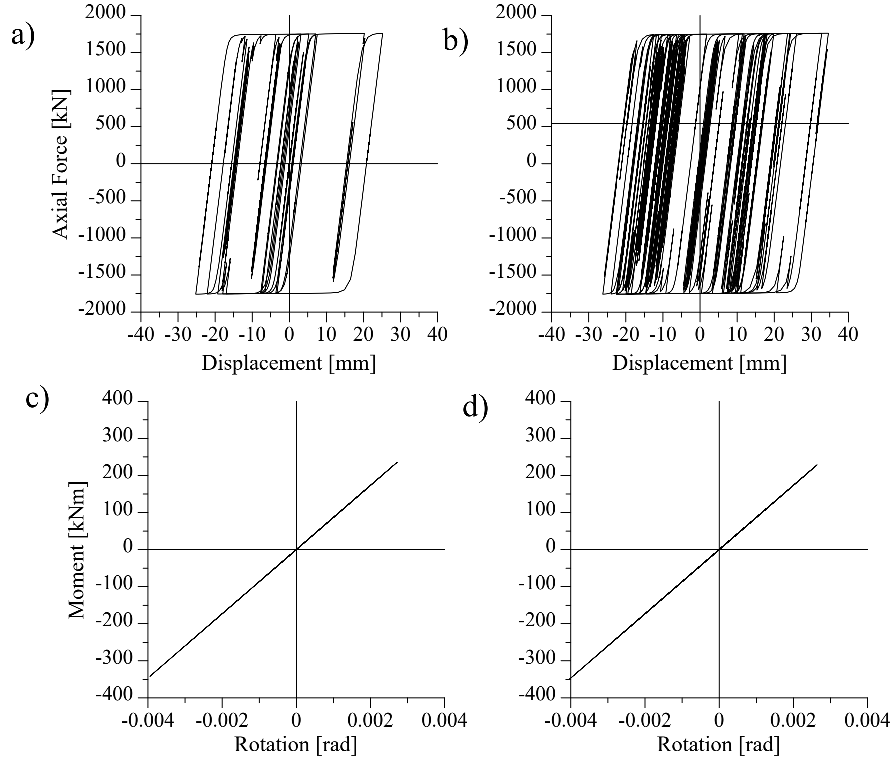

Figure 5.4-2. Response of 8-storey D-FSBF-I in terms of hysteresis of PFDs and MRF's beams under #838-90 and #FKS010 GM scaled at design level: a) PFD at 2nd floor under #838-90, b) PFD at 3rd floor under #FKS010, c) side MRF's beam at the 2nd floor under #838-90, and d) side MRF's beam at the 3rd floor under #FKS010.

Even with a relatively small F_{slip} = 850 kN required at the 7th floor compared to F_{slip} = 1800 kN at the 1st, the PFD of 7th floor exhibits the third highest energy dissipation. This should emphasize the importance of properly sizing the PFDs and avoiding the misconception that a larger PFD, in terms of its slip force, has a higher energy dissipative capacity. The more time that a PFD spends sliding the more energy the device can dissipate and thus the selection of the slip force should only be sized to appropriately accommodate for the expected forces in the braces and no larger to maximize sliding.

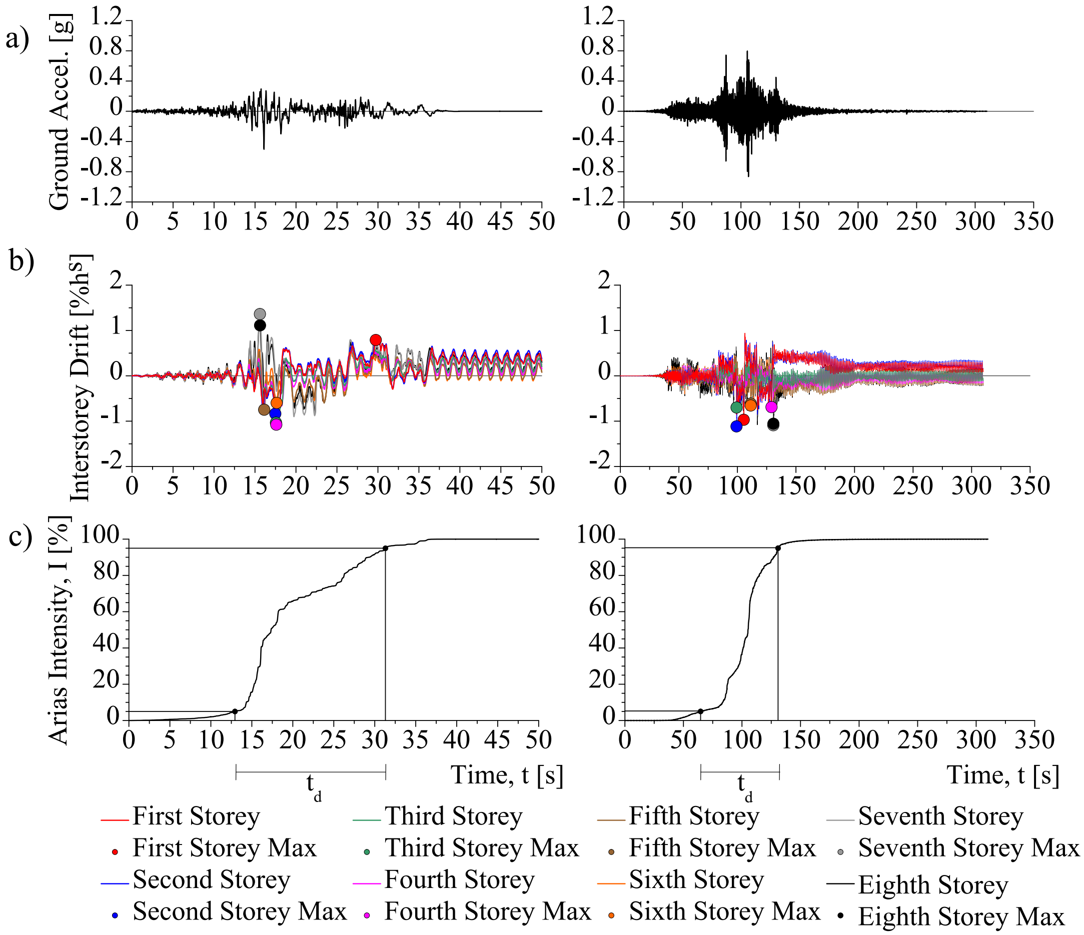

Figure 5.4-3. Response of 8-storey D-FSBF-I building under #838-90 (Left) and subduction #FKS010 GM (right): a) scaled accelerogram, b) time-history series of ISD at all floors and c) Arias intensity for GMs

Observing Figure 5.4-5 it can be seen that under #FKS010 GM, the PFD with the largest amount of total energy dissipated is at the 8th floor. Looking into the force time-history at the 8th floor, the PFD spends a large majority of its time at its slip force limit, thus representing a lot of time in the device's slipping phase. Under the crustal ground motion #838-90 in Figure 5.4-4 the 8th floor does not dissipate the most energy thus demonstrating the heavy dependence on the GM characteristics for the force distribution and displacements of the structure. The design of all of the PFDs at every floor have appropriate slip forces and lengths as shown by the building response under both GM suites.

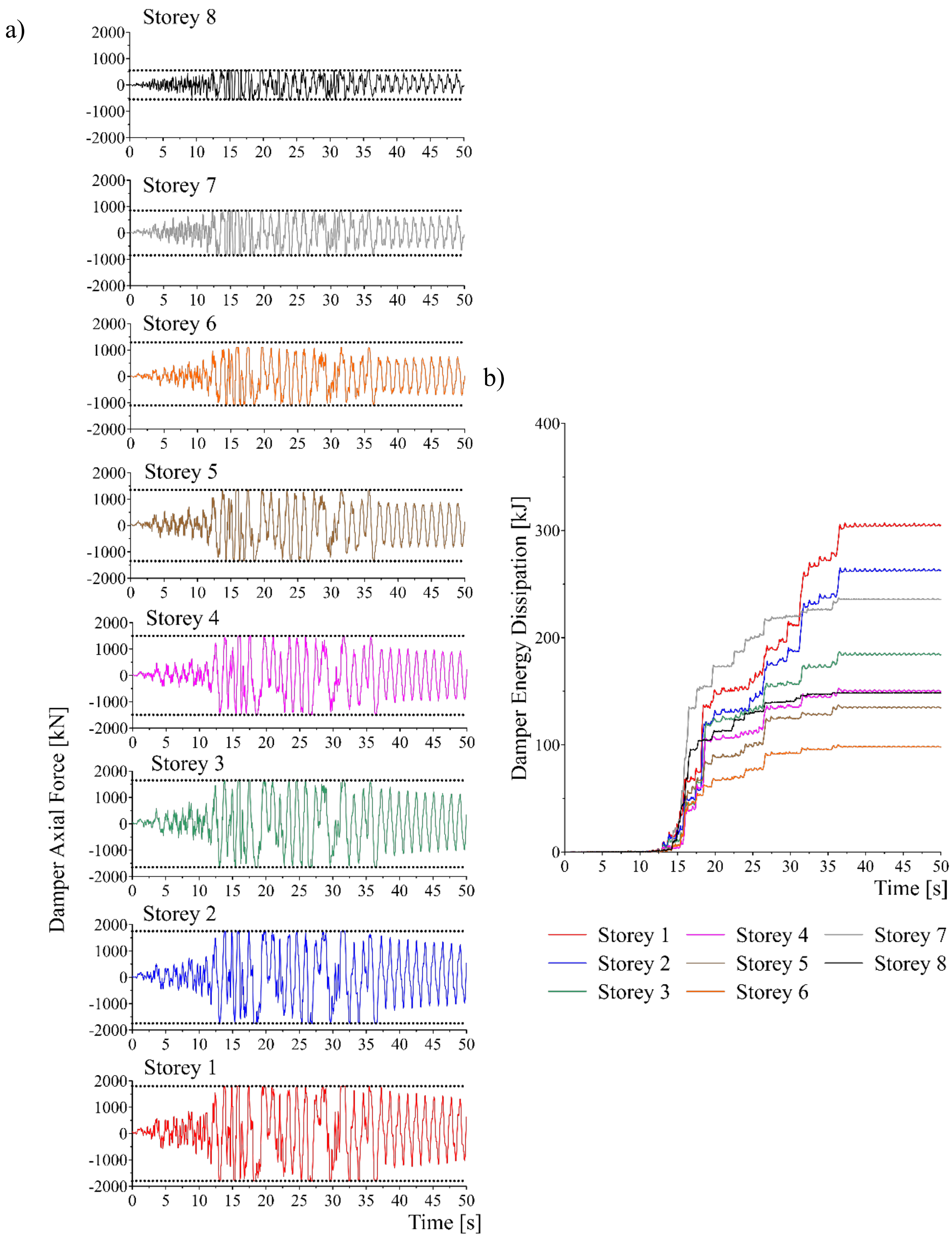

Figure 5.4-4. Response of 8-storey D-FSBF-I building in terms of: a) time-history axial force in damper installed in the left brace under scaled #838-90 GM at Design Level and b) the energy dissipation of PFDs installed at each floor

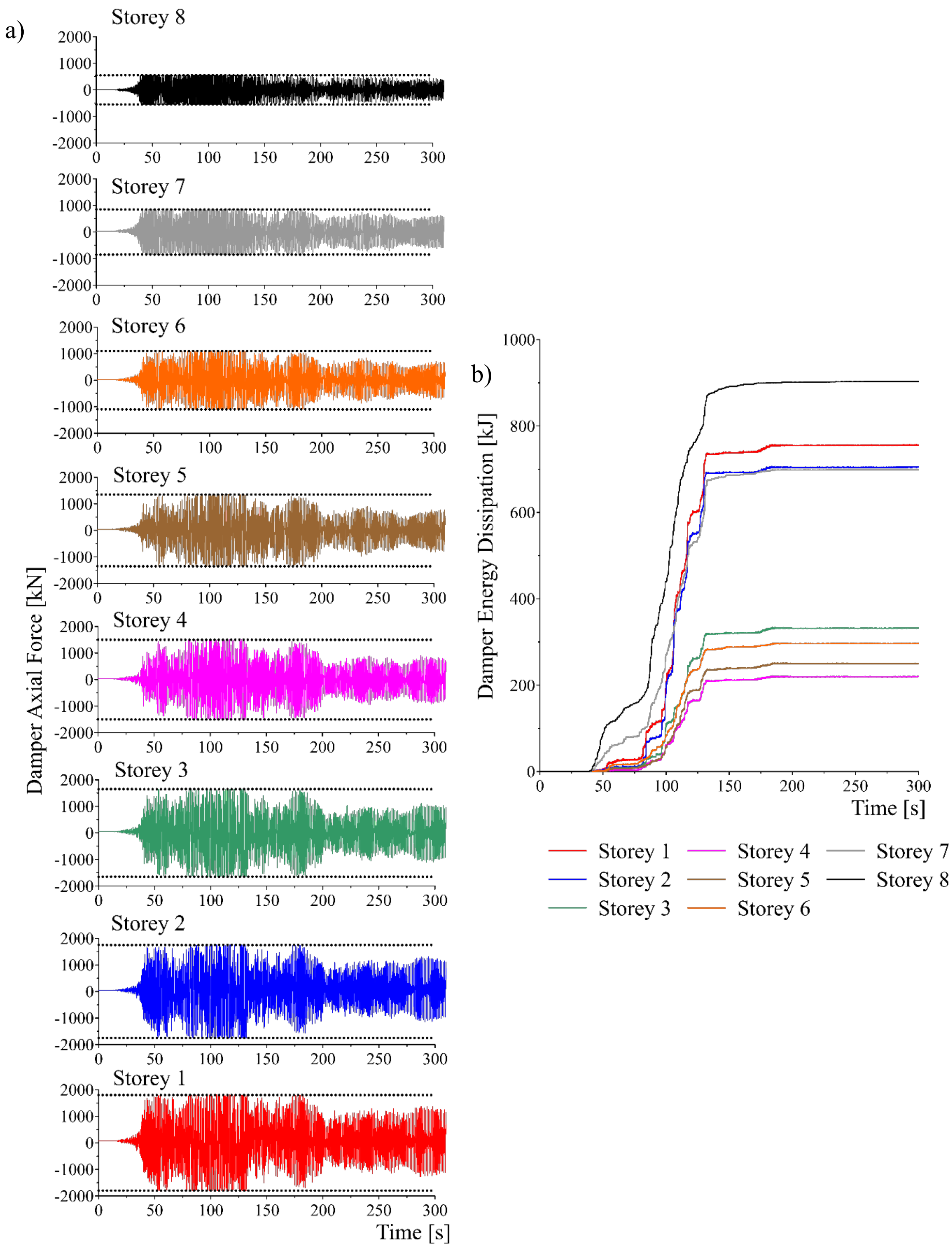

Figure 5.4-5. Response of 8-storey D-FSBF-I building in terms of: a) time-history axial force in damper installed in the left brace under scaled # FKS010 GM at Design Level and b) the energy dissipation of PFDs installed at each floor

5.5 Incremental Dynamic Analysis - Friction Sliding Braced Frame as a Dual System

5.5.1 Incremental Dynamic Analysis of 4-Storey D-FSBF-I building

Incremental Dynamic Analysis (IDA) has been conducted for 4-storey D-FSBF-I building. Collapse of the structure is defined by the model's inability to converge, or by the result of a very large increase in drift for a small increase in demand. For 4-storey D-FSBF-I model, the design spectral acceleration ordinate corresponding to T_1=0.614s is $S_a(T_1)$ = 0.679g. Figure 5.5-1 shows that the IDA curves present a stable response. As the demand increases beyond the D.L. (design level), the IDA curves show either a weaving or softening behaviour. First yielding of the backup MRF beams occurs at around 1.5%h_s ISD for both crustal and subduction GMs. The RLS of the median IDA occurs at 2.6%h_s ISD for crustal and subduction ground motions. It seems that 0.5%h_s RISD occurs at or slightly before the occurrence of 0.02 rad rotation of the MRF beams. Collapse of the median IDA curve occurs at 3.4%h_s and 3.55%h_s for crustal and subduction, respectively. It is worth mentioning that failure occurs after the PFD experiences bearing and the secondary ductile fuse reaches failure. When bearing of PFDs occur an increase in demand does not show an increase in ISD.

Figure 5.5-2 presents the IDA curves in terms of RISD under crustal and subduction GMs. As previously mentioned, 0.5%h_s RISDs occur at or slightly before 0.02rad is reached in MRF's beams. Collapse is then obtained after moderately increasing the demand past that of the demand that achieves 0.02 rad of beam rotation. This is consistent with the concept of the backup MRF, where elastic frame-action is used to achieve a reduction in residual drift. Once yielding of the beams is observed and once yielding exceeds 0.02 rad, the structure's response becomes less stable. For the 4-storey structure, D-FSBF-I, the RLS corresponds to an interstorey drift of 2.5%h_s.

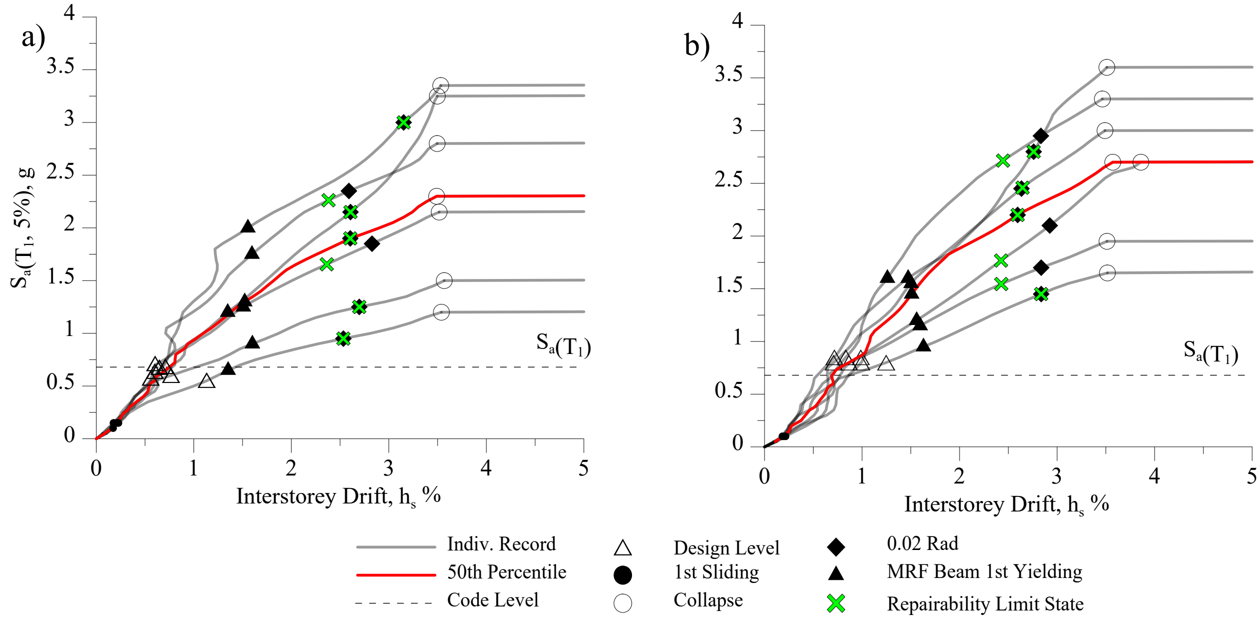

Figure 5.5-1. IDA curves of 4-storey D-FSBF-I building in terms of ISD resulted under: a) crustal GMs and b) subduction GMs

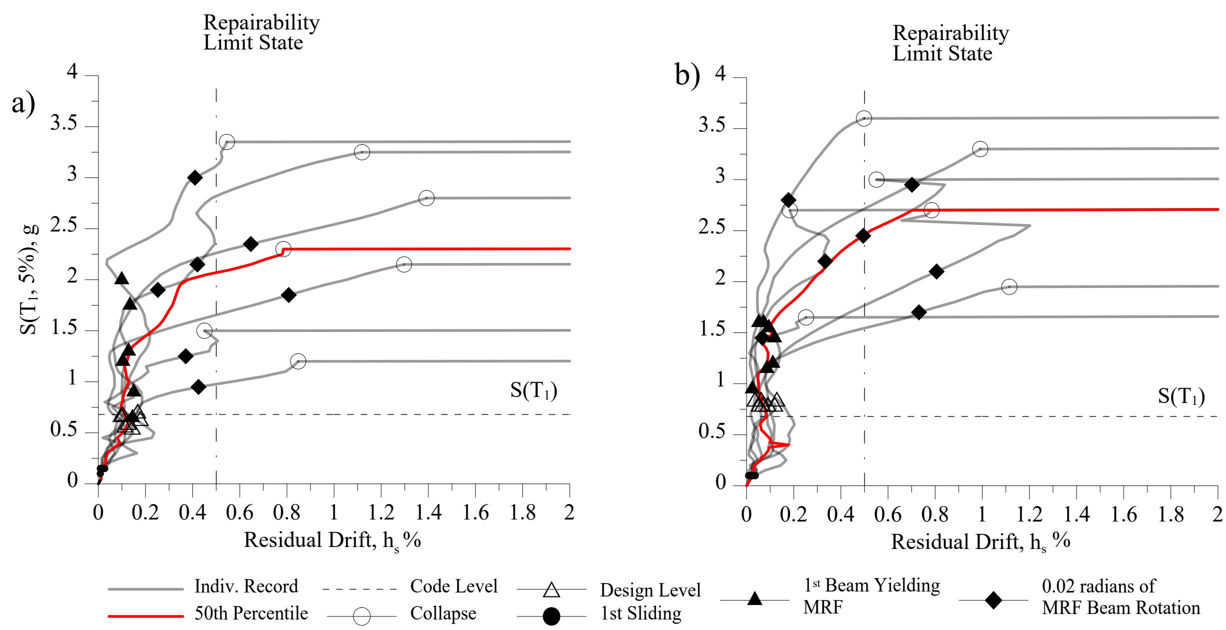

Figure 5.5-2. IDA curves of 4-storey D-FSBF-I building in terms of RISD resulted under: a) crustal GMs and b) subduction GMs

5.5.2 Incremental Dynamic Analysis of 8-storey D-FSBF-I building

The 8-storey D-FSBF-I building is subjected to a demand intensity of $Sa(T_1) = 0.375g$ at design level. As shown in Figure 5.5-3, Design Levels for each GM are clustered about the code demand for both subduction and crustal suites. When the 8-storey building was subjected to crustal GMs., the 1st yielding of the MRF beams occurred closer to design level demand; hence this behaviour differs from the 4-storey building. However, in the case of subduction record demand, the 1st yielding of the MRF beams occurred, in general, at higher intensity than that associated with design level. Since the RLS typically exists somewhere between the 1st yielding of the MRF beams and 0.02rad of rotation of the MRF beams, for 4 out of 7 crustal GMs and 3 out of 7 subduction GMs the RLS is close to the design level for the 8-storey D-FSBF-I building. The median ISD associated with 0.5%h_s RISD is 1.5%h_s and 2%h_s under crustal and subduction GM suites, respectively. The 0.02rad of MRF beam rotation corresponds to 2.5%h_s ISD for both crustal and subduction suites, as was also observed for the 4-storey D-FSBF-I building. Failure does not occur before 0.02rad of beam rotation was reached under all of the GMs in both GM suites. Thus, under crustal GMs, all IDAs show softening behaviour, while under subduction records two out of seven IDAs show hardening behaviour. Figure 5.5-4 presents the IDA curves in terms of RISD under subduction GMs. Median collapse occurs at a residual drift of 2.3%h_s and 2.1%h_s for crustal and subduction suites, respectively.

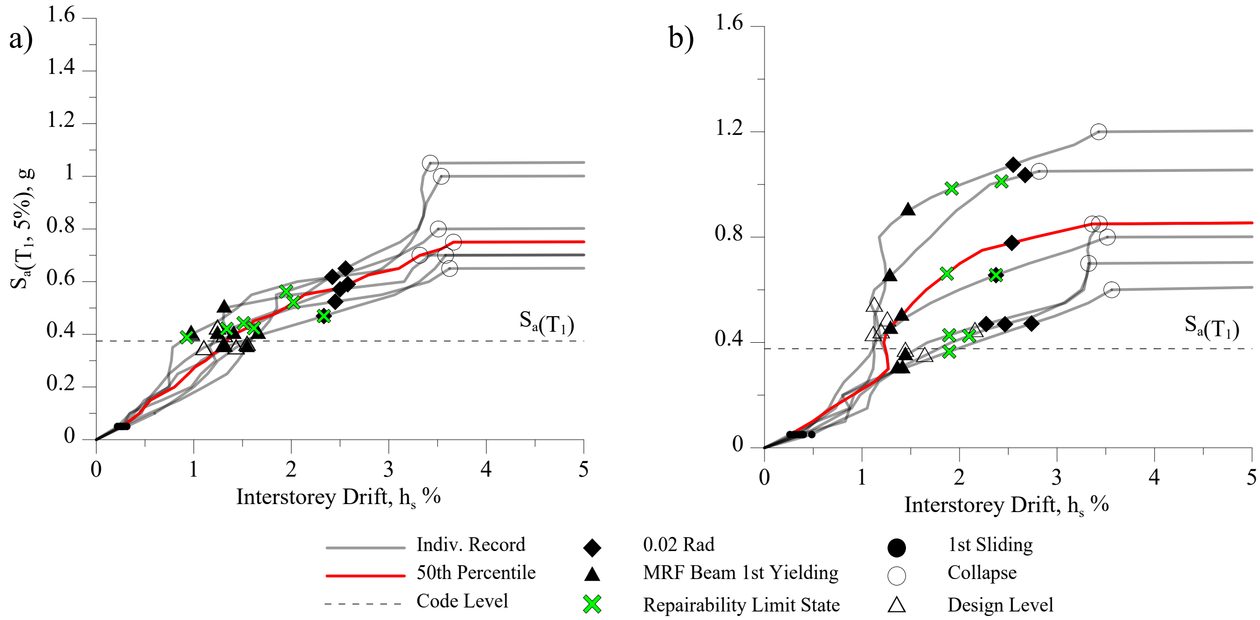

Figure 5.5-3. IDA curves of 8-storey D-FSBF-I building in terms of ISD resulted under: a) crustal GMs and b) subduction GMs

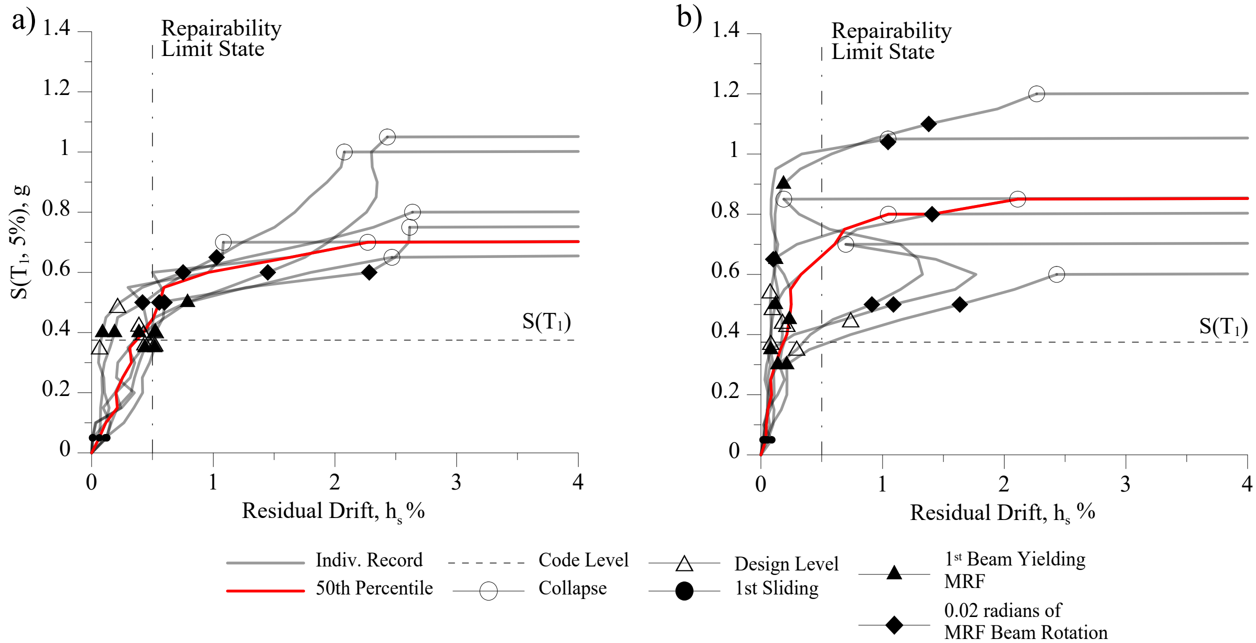

Figure 5.5-4. IDA curves of 8-storey D-FSBF-I building in terms of RISD resulted under: a) crustal GMs and b) subduction GMs

5.5.3 Relationship between interstorey drift and residual interstorey drift of D-FSBF-I buildings

To date, a well-fitted relationship between the ISD and RISD of a dual system has not been identified. In order to identify this relationship, if it is to exist, requires analysis on more building heights and configurations. However, preliminarily Figure 5.5-5 shows a scatter plot for 4-storey D-FSBF-I and 8-storey D-FSBF-I buildings to identify a relationship between the maximum ISD vs. the maximum RISD. Previous research on Dual systems for BRBs has been unable to find a direct relationship between ISD and RISD (Sahoo and Chao 2015). However, relationships were found for low-to-high rise buildings between storey stiffness (excluding the stiffness of BRBs) and storey residual drift. As part of the research herein, attempts have been made to reproduce these results for FSBFs as a Dual System, however no such relationship has been identified. Figure 5.5-5 is a plot of the maximum RISD vs. the maximum ISD for the 4-storey D-FSBF-I and 8-storey D-FSBF-I buildings under both GM suites taken from IDA. No obvious relationship is visible for low-to-mid rise buildings and thus further investigation, with more building heights, floor plans and brace configurations, should be considered to determine a usable relationship for preliminary design purposes. However, from Figure 5.5-5, it can be observed that, under crustal GMs, larger RISD than 0.5%h_s increases the likelihood that the building will experience 1%h_s ISD and more. Conversely, under subduction GMs, larger RISD than 0.5%h_s occurs for ISDs greater than 2%h_s. This behaviour can be influenced by the number of cycles and the ground motion mean period (e.g. larger GM period implies larger RISD in the building response).

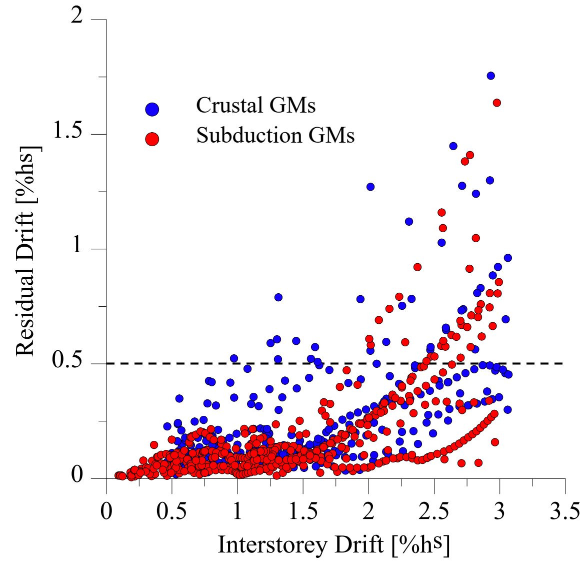

Figure 5.5-5. Scatter plot of maximum interstorey drift vs. maximum residual drift for 4-storey and 8-storey D-FSBF-I buildings

5.6 Brief Discussion on Ductility Factors for Friction Sliding Braced Frames as a Dual System

The purpose of this study was to identify the R_d factor for D-FSBF system that is required to carry out the design considering the force-based design approach. In this regard, by similarity with the BRBF system, two values were proposed such as R_d =4 and R_d=5, whereas R_0 =1.0 was considered. Both the 4-storey and 8-storey buildings were designed for values of R_dR_o equal to 4 and 5.

Figure 5.6-1 compares the (Mean+SD) values of ISD, RISD, and FA at each floor for 4-storey D-FSBF-I (R_dR_0 =4) and D-FSBF-II (R_dR_0=5) buildings under both crustal and subduction GM suites scaled to D.L. demand. For the 4-storey building designed with R_dR_0=4 and R_dR_0=5, comparing the peak (Mean+SD) ISD between D-FSBF-I and D-FSBF-II systems, it results that under crustal and subduction GM suites, the D-FSBF-II system yields 48% and 23% larger peak (Mean+SD)

ISD than the D-FSBF-I system, respectively. Similarly, under crustal and subduction GM suites, the D-FSBF-II system yields 7.3% and 23%, respectively, larger peak (Mean+SD) RISD than the D-FSBF-I system. The difference is smaller for FA under crustal GMs but a significant increase is observed under subduction GMs. However, for both dual systems and under both GM suites, the peak (Mean+SD) ISD is below 1.5%h_s and the peak (Mean+SD) RISD is below 0.5%$h_{s.}$

Similarly to the response of 4-storey buildings, Figure 5.6-2 compares the (Mean+SD) values of ISD, RISD, and FA at each floor of the 8-storey D-FSBF-I (R_dR_0 =4) and D-FSBF-II (R_dR_0=5) buildings under both crustal and subduction GM suites scaled to D.L. demand. For the 8-storey buildings, comparing the peak (Mean+SD) ISD resulted for D-FSBF-I and D-FSBF-II systems, it results that under crustal and subduction GM suites, the D-FSBF-II system yields 15% and 14%, respectively, larger peak (Mean+SD) ISD than the D-FSBF-I system. Subsequently, under crustal and subduction GM suites, the D-FSBF-II system yields 4.0% and 62%, respectively, larger peak (Mean+SD) RISD than the D-FSBF-I system. Then, comparing the peak (Mean+SD) FA resulted for D-FSBF-I and D-FSBF-II systems, it results that under crustal and subduction GM suites, the D-FSBF-II system yields 35% and 9.1%, respectively, larger peak (Mean+SD) FA than the D-FSBF-I system.

To investigate the overall response of buildings braced by a Dual system under crustal and subduction GM suites, the IDA analysis was performed and the median IDA curves are shown in Figure 5.6-3. As depicted, the 4-storey building shows a similar response under crustal GMs, regardless of R_dR_0 =4 or 5. However, under subduction records, when D-FSBF-II is employed, the difference in response increases and the system shows softening behaviour beyond D.L. For the 8-storey building, the median IDAs are almost similar regardless of R_dR_o value of 4 or 5.

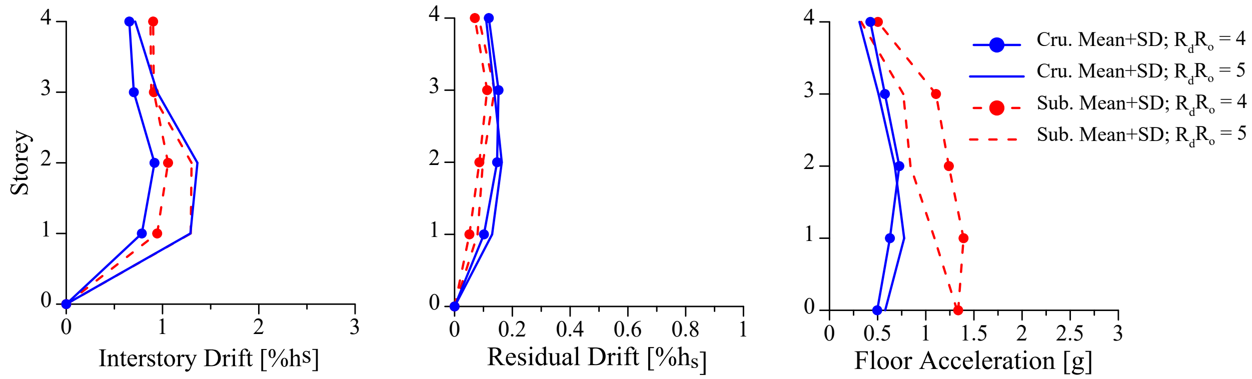

a) b) c)

Figure 5.6-1. Response of 4-storey D-FSBF-I and D-FSBF-II buildings at D.L. under crustal and subduction GM suites: a) (Mean+SD) ISD b) (Mean+SD) RISD and c) (Mean+SD) FA

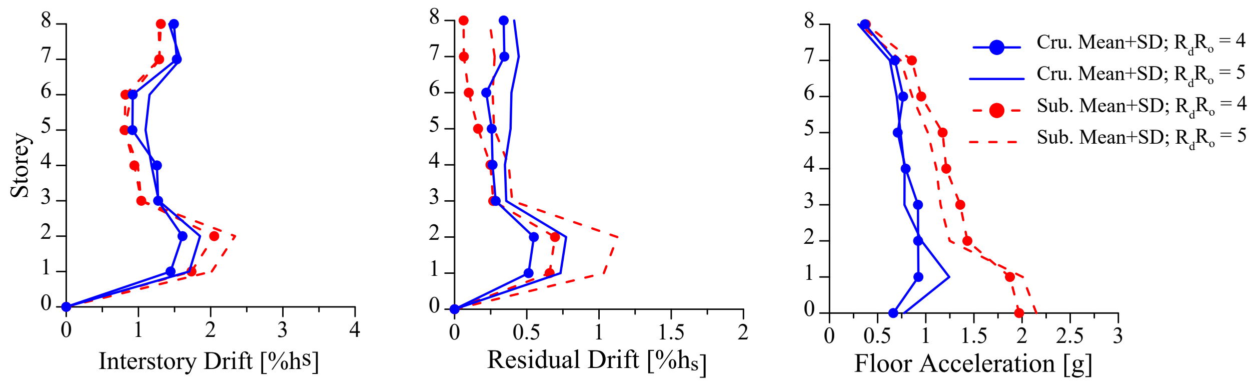

a) b) c)

Figure 5.6-2. Response of 8-storey D-FSBF-I and D-FSBF-II buildings at D.L. under crustal and subduction GM suites: a) (Mean+SD) ISD b) (Mean+SD) RISD and c) (Mean+SD) FA

It seems that the response of D-FSBF-I vs. D-FSBF-II diverge a bit past the code level but less significantly. The collapse points for the 8-storey structure are also relatively close for both the crustal and subduction suites. Between the 4 and 8-storey buildings, it is clear that the slopes of the IDA curves are steeper for the 4-storey than the 8-storey structure. Thus, a smaller increase in spectral acceleration results in a larger displacement for the 8-storey than for the 4-storey buildings.

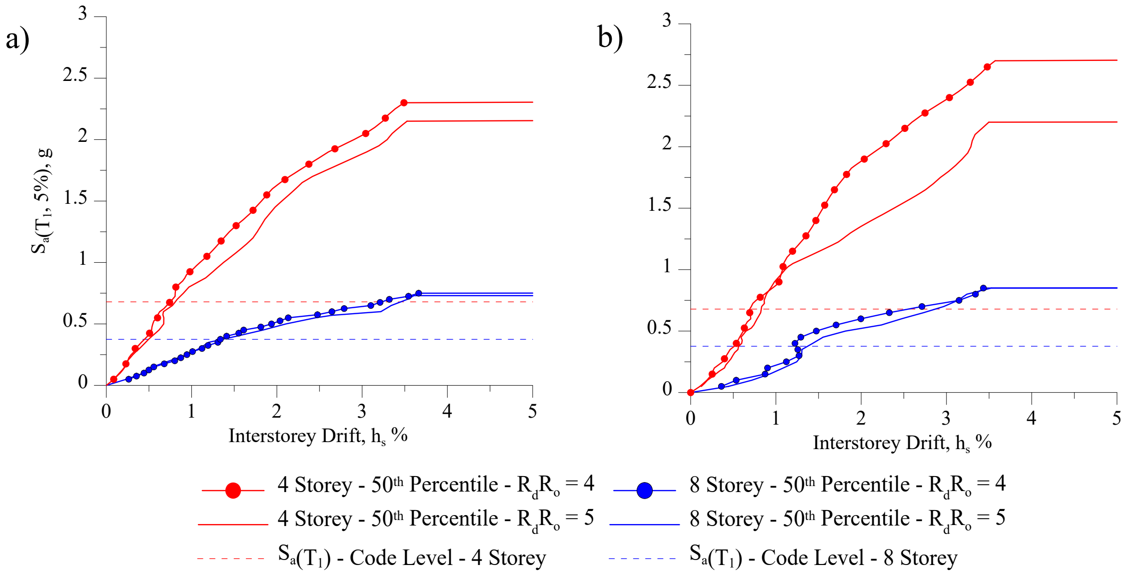

Figure 5.6-3. The 50th percentile IDA curves for 4-storey and 8-storey buildings braced by D-FSBF-I and D-FSBF-II under: a) crustal GMs and b) subduction GMs

The D-FSBF-II system is more flexible than the D-FSBF-I and reaches collapse at smaller intensity. Table 5.6-1 shows the total tonnage of steel for the SFRS that braces half of the floor plan area (MRF + FSBF) excluding the mass of the dampers and connections. As resulted, designing the 4-storey building considering R_dR_0=5 leads to 21.17% economy in terms of steel tonnage. An increase in ductility for low-rise buildings seems to show evidence for its justification.

For the 8-storey building, the difference in steel tonnage is only 6.65%. Seeing as the total amount of steel is a relatively small portion of the total construction costs of a building, it does not seem to be a reasonable to reduce the performance of the building for the gain. Thus, for 8-storey building braced by Dual FSBF system, R_dR_0=4 is recommended.

Table 5.6-1. Tonnage of steel used in the SFRS for different ductility factors and heights

No. Storeys	4	4	8	8
R_dR_o	4	5	4	5
Tonnage of Steel of the SFRS (tonnes)	30.51	24.05	68.94	64.33
Reduction of Steel Due to Higher Ductility	-	**21.17%**	-	**6.65%**

Chapter Six

Fragility Analysis and Collapse Safety

6.1 Fragility Analysis

Fragility analysis is a probabilistic measure, which permits the risk assessment of specific performance objectives to be quantified. Performance objectives can be defined qualitatively or quantitatively, however quantitative means, such as first yielding and plastic mechanism initiation, are sometimes difficult to identify for other performance levels (Wen et al. 2004).

6.1.1 Performance Levels and Limit States

In general, the four performance levels are: Operational (O), Immediate Occupancy (IO), Reparability (R) and Collapse Prevention (CP). All performance levels are determined based on quantitative parameters. An additional performance level could be beam hinging of the backup MRF, labelled herein as (BH), the suggested mapping of performance levels is shown in Table 6.1-1.

Table 6.1-1. Suggested damage mapping for performance levels

Performance Levels	Operational		Immediate Occupancy	Reparability	Collapse Prevention
Performance Ranges	No Structural Damage		Damage Control Range	Limited Safety Range	Collapse
Degree of Damage	None	Very Light Damage	Light Damage	Moderate Damage	Complete Damage
Damage Levels	Very Light		Light	Moderate	Severe
Suggested δ_{max}			0.7%hs	1.5–2.0%h_s	2.5–3.0%h_s
Suggested δ_{res}				0.5%h_s	2.0%h_s
Suggested θ_{max}				0.02rad	$<$0.03rad

Fragility Analysis herein is based on its scalar form (Abrahamson and Silva 1997; Baker and Cornell 2005; Zareian and Krawinkler 2007). The fragility curves calculated are based on the probability that a Performance Level is exceeded given a specific Intensity Measure, IM. This probabilistic model is assumed to be a lognormal cumulative distribution where the collapse of 50% of the ground motions is the distribution's median value and the aleatoric and epistemic uncertainties are given by β_{RR}, as per Eq. (2.7.6), and β_{RU} respectively (Ellington et al. 2007). As described in the literature review, to determine the aleatoric uncertainty, the seismic demand uncertainty $\beta_{D|S_a}$ must be evaluated. This is done through linear regression of a $ln(S_a)$ versus $\ln(\delta_{max})$. Performance levels are plotted for each GM, and the standard error is transformed into the seismic demand uncertainty. The capacity uncertainty is taken to be $\beta_c = 0.25$, and the modeling uncertainty (epistemic) is taken to be $\beta_{RU} = 0.20$.

6.1.2 Fragility Curves for 4-Storey Buildings

Following the procedure described for scalar form fragility curves in the literature review chapter, the constants a and b of the power-law function describing the relation between the intensity measure, $S_a(T_1)$, and the demand parameter, δ_{max}, are 1.903 and 1.255, respectively, for crustal GMs. The seismic demand uncertainty, $\beta_{D|S_a} = 0.271$ for crustal GMs, and is practically used to flatten the fragility curve about its median value. Observing the target Design Level that represents a demand with a 2%/50 years probability of exceedance, in Figure 6.1-1, the probability of exceedance for the crustal suite is 98%, 46%, and 7% for Performance Levels IO, R, and CP, respectively. From this, it can be concluded that for the 4-storey FSBF-I building, given Design Level IM, the R performance objective around half of the time and at least a quarter of the time the structure will experience severe damage.

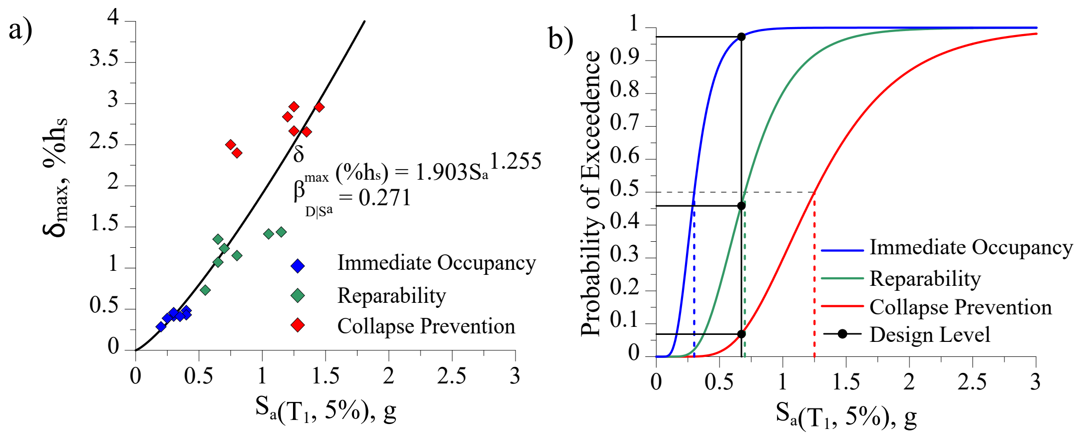

Figure 6.1-1. The 4-storey FSBF-I building: a) power law drift equation for seismic demand uncertainty and b) fragility curves for performance levels under crustal GMs

Considering the continuous column model of the 4-storey structure, FSBF-CC-I, in Figure 6.1-2, a moderate improvement can be observed over the 4-storey FSBF-I model. The relationship between the IM and Demand Parameter is defined by the power-law constants *a* and *b* equalling 1.705 and 1.142, respectively for crustal GMs and 1.850 and 0.932, respectively for subduction GMs. Considering the Design Level IM, the probability of exceeding the performance level given the IM is 93%, 29%, and 4% for crustal and 95%, 59%, 8% for subduction GMs for performance levels IO, R, and CP, respectively.

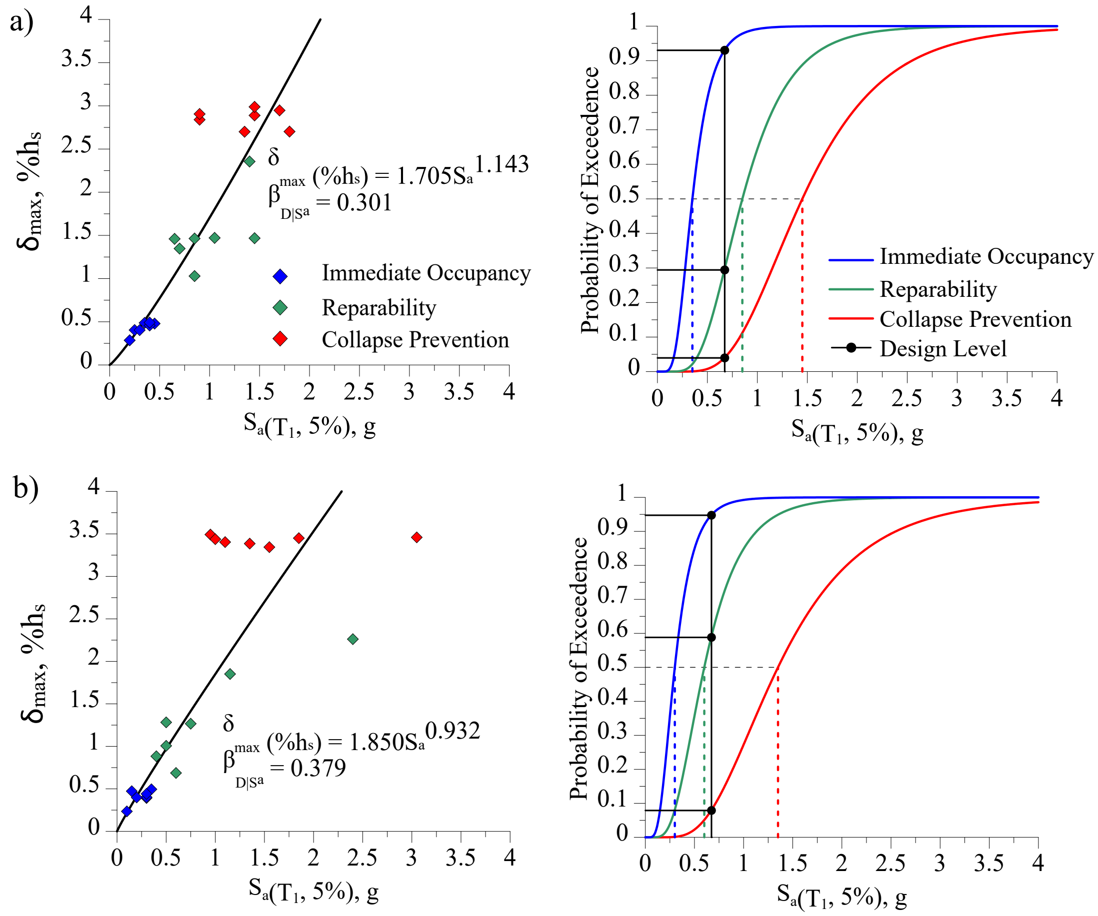

Figure 6.1-2. The power law drift equation for seismic demand uncertainty and fragility curves for performance levels of 4-storet FSBF-CC-I building under: a) crustal GMs b) subduction GMs

Regarding the dual system designed for the 4-storey building with the highest ductility, D-FSBF-II, a significant improvement is observed when comparing with the response of the bare FSBF-I and the bare FSBF-CC-I systems. The probability of exceeding the performance level given the Design Level IM is 88%, 7%, 1% for crustal GMs and 97%, 4%, 0% for subduction GMs for performance levels IO, R, and CP, respectively. This structure will thus have a significantly smaller probability of accumulating excess damage and thus will have limited costs in regard to necessary repairs after extreme events. It is worth noting that low probabilities of exceedance for the R performance level can also be viewed as having a low probability of exceeding the reparability limit state.

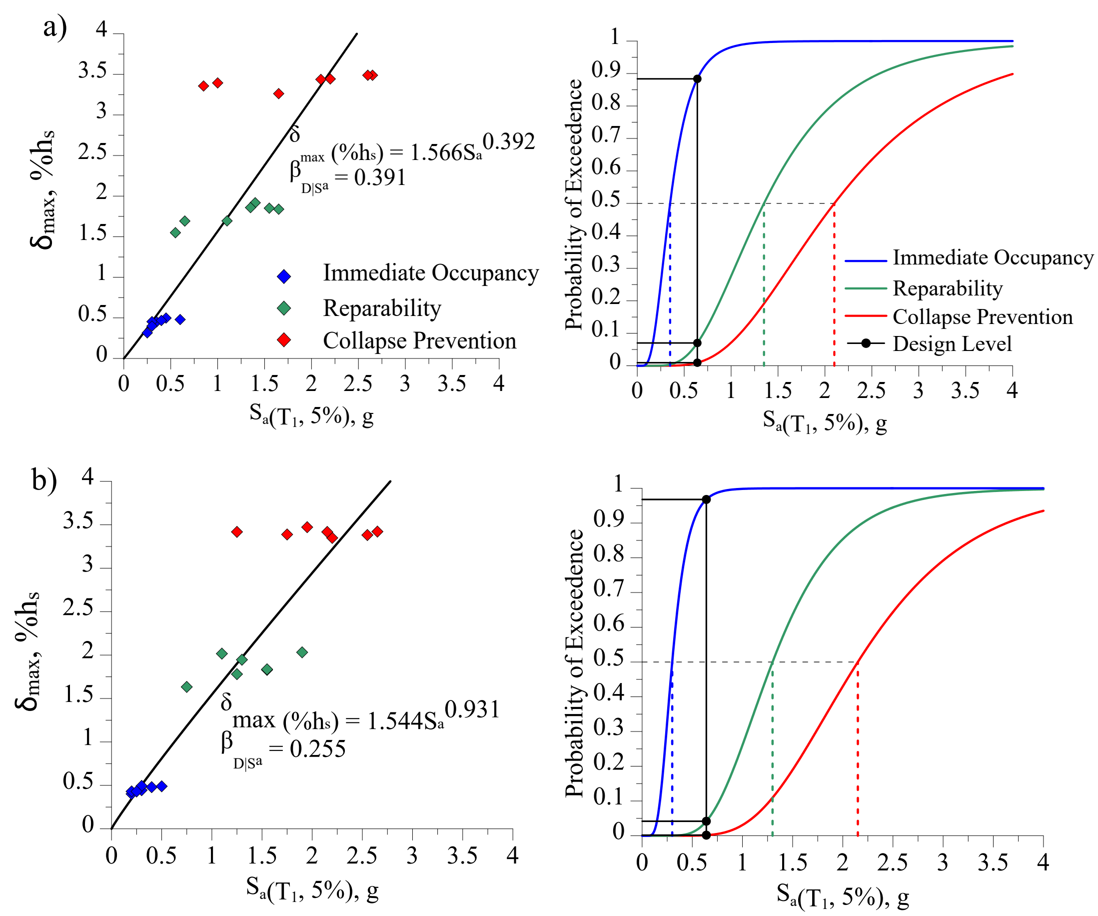

Figure 6.1-3. The power law drift equation for seismic demand uncertainty and fragility curves for performance levels of 4-storey D-FSBF-II building under: a) crustal GMs, b) subduction GMs

Out of the 4 braced systems such as: bare FSBF-I, bare FSBF-CC-I, D-FSBF-II and D-FSBF-I, the best results are provided by the D-FSBF-I system. In Figure 6.1-4, it is shown that the probability of the performance level to be exceeded considering the Design Level IM is 88%, 1%, 0% for crustal GMs and 94%, 1%, 0% for subduction GMs for performance levels IO, R, and CP, respectively. This improvement is only marginally better than that resulted for D-FSBF-II. Although these results are good, it may be a justification to prefer the higher ductility for low-rise buildings with dual systems a large statistical improvement is not observed between R_dR_o = 4 or 5 designs.

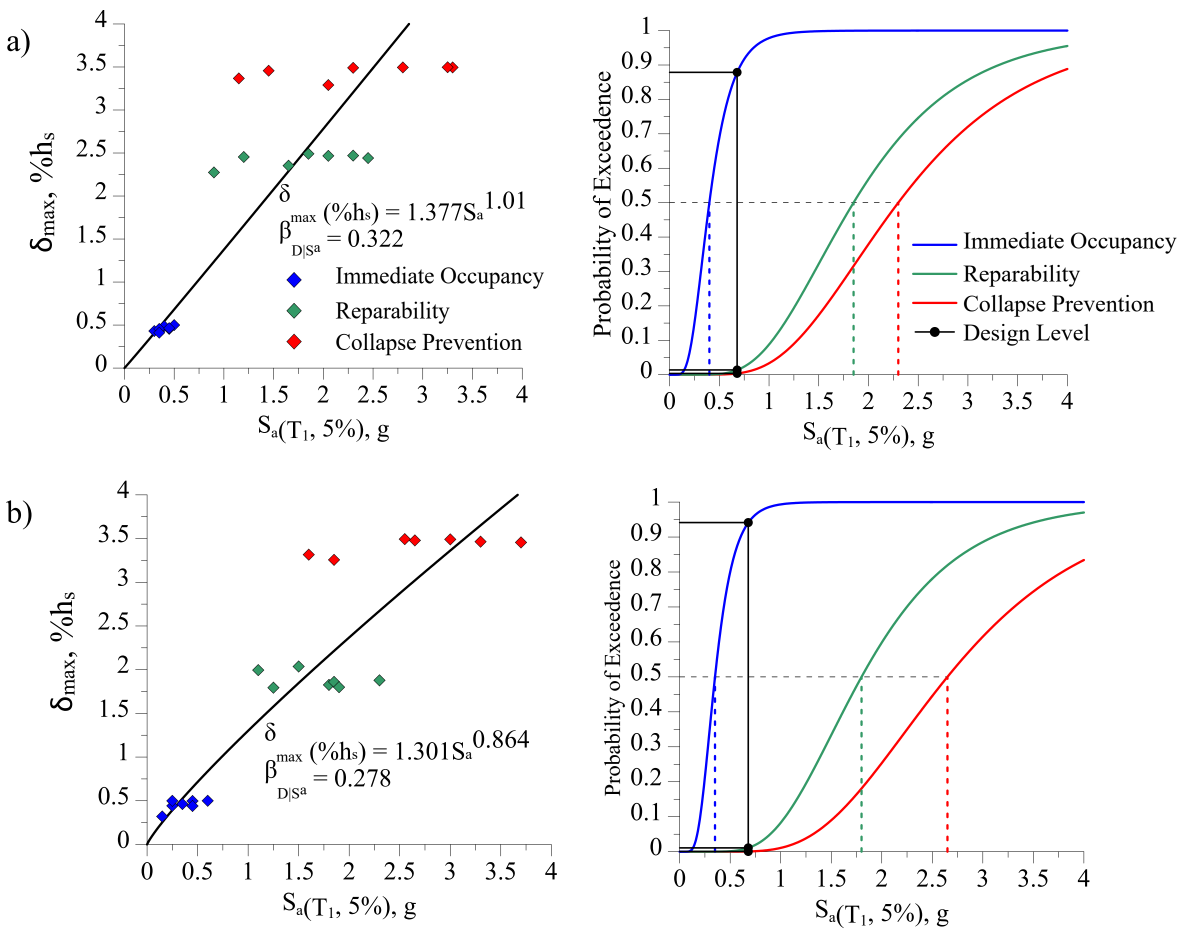

Figure 6.1-4. The building power law drift equation for seismic demand uncertainty and fragility curves for performance levels of 4-storey D-FSBF-I building under: a) crustal GMs, b) subduction GMs

6.1.3 Fragility Curves for 8-Storey Buildings

For 8-storey buildings it is not recommended to employ the bare FSBF-I and the bare FSBF-CC-I systems because both systems fail to meet the collapse safety criteria. For this reason, fragility analysis was carried out only for the 8-storey building braced with Dual FSBF system.

For the 8-storey D-FSBF-I, from Figure 6.1-5, it results that the probability of exceeding the performance level given the Design Level IM is 100%, 33%, 6% for crustal GMs and 100%, 13%, and 4% for subduction GMs, for performance levels IO, R, and CP, respectively. Thus, by observing R objective, it is more probable that the reparability limit state will not be exceed than the probability that it will be exceeded for this level of ductility.

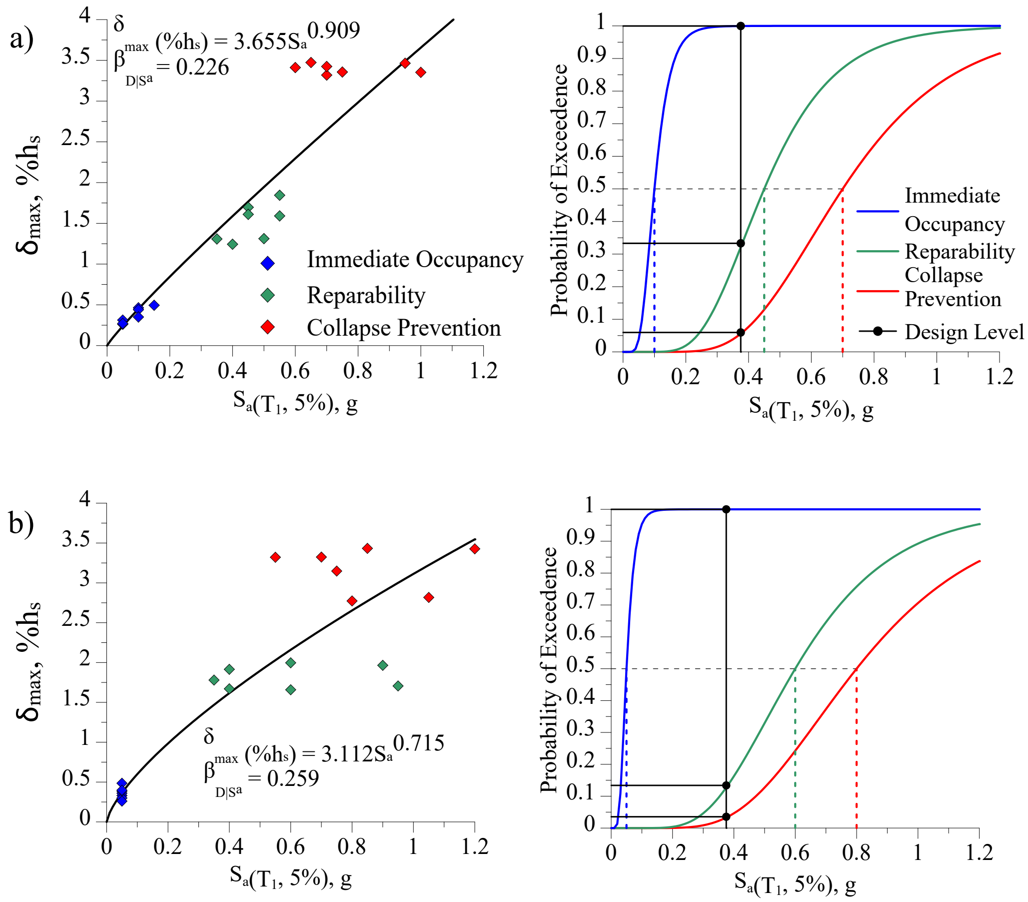

Figure 6.1-5. The power law drift equation for seismic demand uncertainty and fragility curves for performance levels of 8-storey D-FSBF-I building under: a) crustal GMs, b) subduction GMs

Figure 6.1-6 shows the fragility curve for the 8-storey building with higher ductility, D-FSBF-II. For this model, the probability of the performance level being exceeded for the Design Level IM is 100%, 29%, and 7% for crustal GMs and 100%, 31%, and 4% for subduction GMs for performance levels IO, R, and CP, respectively. It can be suggested from these results that a lower ductility factor would provide a better result for mid-rise buildings, however a value between 4 and 5 can also the justified for R_dR_o.

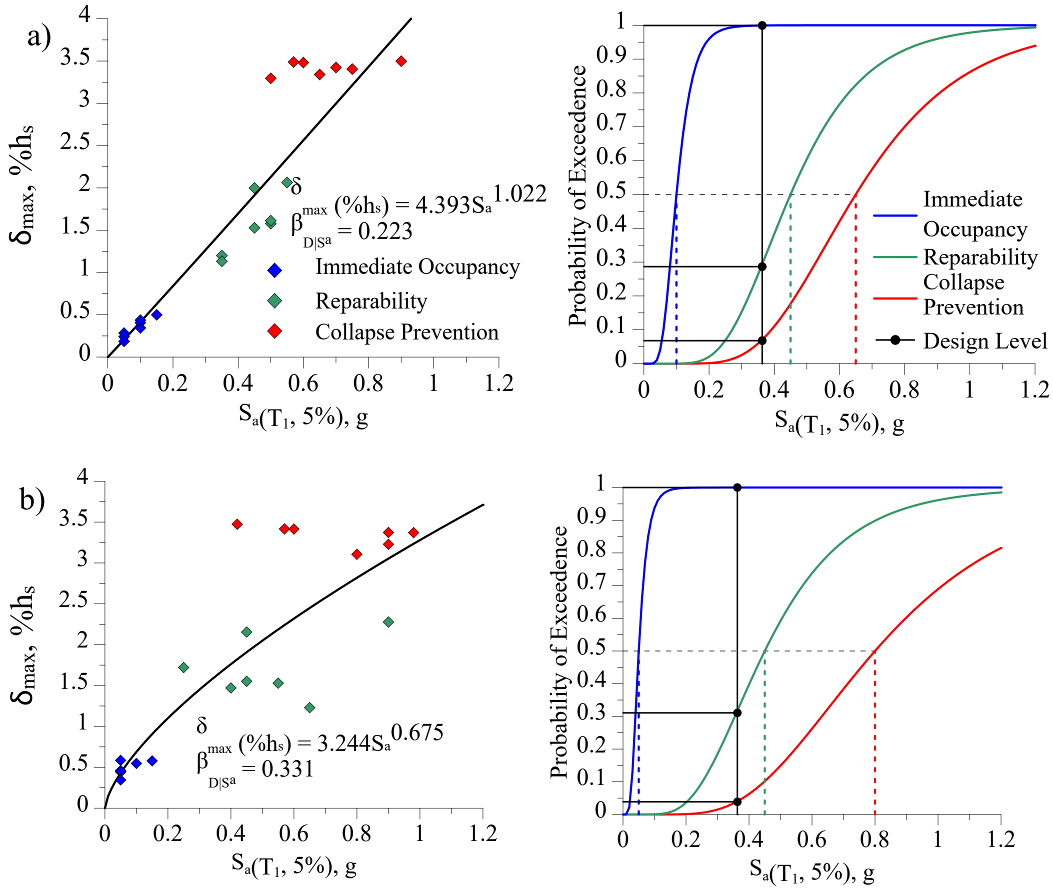

Figure 6.1-6. The power law drift equation for seismic demand uncertainty and fragility curves for performance levels of 8-storey D-FSBF-II building under: a) crustal GMs, b) subduction GMs

6.2 Collapse Safety Analysis

Collapse Safety Analysis is a probabilistic methodology developed for the performance assessment of a structure's ability to withstand dynamic loading with sufficient margin of safety. The development of this methodology is presented in FEMA P-695 (FEMA 2009) and expanded testing of the methodology was completed by NEHRP in 2010 (NEHRP 2010). This methodology permits researchers to evaluate the seismic performance factors including the ductility-related force modification factor, R_d. The response modification factor is determined by the acceptability of the collapse margin ratio. The building performance depends on the design, which is completed by the use of a multiplicative factor comprised of the overstrength and the response modification factor, R_dR_o.

According to FEMA P-695 (FEMA 2009), collapse safety analysis is done by means of IDA. The probability of collapse is measured through collapse margin ratios, the first of which is simply named the Collapse Margin Ratio, CMR as described by Eq. (6.2.1), where $\hat{S}_{CT}$, is the intensity at which 50% of the ground motions have resulted in collapse, and S_{MT} is the intensity for which the structure was designed.

$$CMR = \frac{\hat{S}_{CT}}{S_{MT}} \tag{6.2.1}$$

Rare earthquakes in the Western United States have shown distinct spectral shapes that differ from those found in modern codes which use design spectrums based on the structure's first period (Baker and Cornell 2006). This results in rare ground motions being less damaging than traditional design spectrums would dictate, thus a Spectral Shape Factor, SSF, is considered to increase the CMR accordingly. SSF is determined according to Table 7-1 in FEMA-P695 for different building archetypes and is based on the structure's first mode period of vibration and the structures period-based ductility, μ_T, as defined by Eq. (6.2.2), where δ_u is the structure's maximum ISD and $\delta_{y,eff}$ is the displacement at which first slipping of the damper occurs.

$$\mu_T = \frac{\delta_u}{\delta_{y,eff}} \tag{6.2.2}$$

This increase in CMR is referred to as the Adjusted Collapse Margin Ratio, ACMR, and is defined by Eq. (6.2.3). The ACMR is then compared to the Adjusted Collapse Margin Ratio value which has a 10% probability of collapse, $ACMR_{10\%}$. This probability of collapse is defined by an assumed lognormal distribution about the median value, $\hat{S}_{CT}$, and a lognormal standard deviation denoted by Eq. (6.2.4) equal to the total system collapse uncertainty, β_{TOT}. The total system uncertainty (β_{TOT}) is comprised of four statistically independent random variables, "record-to-record" uncertainty (RTR), "design requirement-related" uncertainty (DR), "test data-related" uncertainty (TD), and "modeling" uncertainty (MDL). All uncertainties, besides β_{RTR}, are rated on the following scale: (A) Superior, $\beta = 0.1$; (B) Good, $\beta = 0.2$; (C) Fair, $\beta = 0.35$; (D) Poor, $\beta = 0.5$. The "Record-to-record" uncertainty is also approximated as per Eq. (6.2.5) and is expressed as a function of period-based ductility μ_T. Acceptable values for $ACMR_{10\%}$ are given in Table 7-3 in FEMA P-695 (FEMA 2009) and should be exceeded by the calculated ACMR value for each index archetype $ACMR \geq ACMR_{10\%}$.

$$ACMR = SSF \; X \; CMR \tag{6.2.3}$$

$$\beta_{TOT} = \sqrt{\beta_{RTR}^2 + \beta_{DR}^2 + \beta_{TD}^2 + \beta_{MDL}^2} \tag{6.2.4}$$

$$\beta_{RTR} = \min \begin{bmatrix} 0.2 \\ 0.1 + 0.1\mu_T \leq 0.4 \end{bmatrix} \tag{6.2.5}$$

6.2.1 Collapse Safety for studied 4-storey and 8-storey Buildings

For all models studied herein, the period-based ductility, μ_T, was calculated, resulting in SSF values between 1.34 and 1.38 for 4-storey buildings and 1.55 and 1.57 for 8-storey buildings as shown in Table 6.2-1 and Table 6.2-2, respectively. The “record-to-record” uncertainty, β_{RTR}, was computed from fragility analysis as $\beta_{D|S_a}$. The “design requirement-related” uncertainty was taken as (A) Superior, $\beta_{DR} = 0.1$, the “test data-related” uncertainty was taken as (B) Good, $\beta_{TD} = 0.2$, and the “modeling” uncertainty was taken as (B) Good, $\beta_{MDL} = 0.2$. Total system uncertainty is thus calculated by $\beta_{TOT} = \sqrt{\beta_{D|S_a}^2 + \beta_{DR}^2 + \beta_{TD}^2 + \beta_{MDL}^2}$, and $ACMR_{10\%}$ is provided in Table 6.2-1 and Table 6.2-2 for the 4 and 8-storey buildings, respectively.

Table 6.2-1. Collapse safety analysis for 4-storey buildings under both ground motion suites

	Collapse safety of 4-storey buildings							
System Parameters	FSBF-I		FSBF-CC-I		D-FSBF-I		D-FSBF-II	
	Cru.	Sub.	Cru.	Sub.	Cru.	Sub.	Cru.	Sub.
S_{MT}	0.673	0.673	0.673	0.673	0.679	0.679	0.640	0.640
$\hat{S}_{CT}$	1.70	0.74	1.90	1.35	2.30	2.70	2.15	2.20
SSF	1.34	1.34	1.34	1.34	1.36	1.36	1.38	1.38
CMR	2.53	1.10	2.82	2.00	3.39	3.97	3.36	3.44
ACMR	3.39	1.47	3.78	2.69	4.61	5.42	4.62	4.73
$ACMR_{10\%}$	1.67	1.67	1.72	1.82	1.78	1.62	1.90	1.67
$ACMR/ACMR_{10\%}$	1.78	0.88	2.20	1.46	2.59	3.34	2.43	2.83
Pass/Fail	**Pass**	**Fail**	**Pass**	**Pass**	**Pass**	**Pass**	**Pass**	**Pass**

As resulted from Table 6.1-1, the margin of safety is achieved for all but one type of SFRS considered to brace the 4-storey building. Thus, the bare FSBF-I is not recommended, but the FSBF-CC-I is able to improve the building response. A large reserve capacity is observed when Dual FSBF system was employed to brace the 4-storey building. In terms of collapse, this reserved capacity does suggest that a larger ductility factor can be used for the design of these low-rise buildings, however reparability and other considerations may not justify this position. Furthermore, in terms of collapse safety, the bare FSBF-CC-I can be considered. However, using Dual FSBF systems, a reduction in ACMR of 13% is observed between D-FSBF-I and D-FSBF-II supporting the justification for higher ductility factors.

For the 8-storey building, sufficient margin of safety is not achieved when bare FSBF-I and bare FSBF-CC-I are employed. An improvement between the continuous columns and non-continuous columns models is observed but still failed to meet the passing criteria. However, using the Dual FSBF system, the response is significantly improved. It is well known that PFDs are displacement dependent and dissipate larger amounts of energy when the system exhibits large displacements. This phenomenon will occur mostly under crustal ground motions characterized by longer mean period (T_m) than under the subduction records where $T_m \sim 0.2$s. Thus, both D-FSBF-I and D-FSBF-II possess adequate collapse safety margin and are recommended for middle-rise buildings designed in the subduction zone region.

Table 6.2-2. Collapse safety analysis of 8-storey buildings under both ground motion suites

Collapse safety of 8-storey buildings								
System Parameters	FSBF		FSBF-CC		D-FSBF (4)		D-FSBF (5)	
	Cru.	Sub.	Cru.	Sub.	Cru.	Sub.	Cru.	Sub.
S_{MT}	0.370	0.370	0.370	0.370	0.375	0.375	0.363	0.363
$\hat{S}_{CT}$	0.35	0.25	0.43	0.24	0.75	0.85	0.73	0.85
SSF	1.56	1.56	1.56	1.56	1.55	1.55	1.57	1.57
ACMR	1.48	1.05	1.79	1.01	3.10	3.52	3.16	3.68
$ACMR_{10\%}$	1.90	1.90	1.90	1.90	1.62	1.67	1.62	1.78
$ACMR/ACMR_{10\%}$	0.78	0.56	0.94	0.53	1.92	2.11	1.95	2.07
Pass/Fail	**Fail**	**Fail**	**Fail**	**Fail**	**Pass**	**Pass**	**Pass**	**Pass**

Chapter Seven

Conclusions and Future Work

7.1 Conclusions

Dual FSBF systems benefit from the vertical continuity, hence the elastic frame-action, and a second load path provided by the backup MRF. Similar to other SFRSs, the seismic ductile fusses (PFDs) should dissipate the input energy and prevent the increase of forces in the adjacent structural members. However, PFDs sustain larger axial forces than the designed slip force, F_{slip}. To solve this drawback, a second ductile fuse is required to control the axial force transferred from PFD to the frame by means of gusset plate that is designed to experience bolt tear-out along the two bolt holes of the connection, when loaded beyond a defined force magnitude. This study investigated the behaviour of friction device-supportive HSS brace installed to brace a 4 and 8-storey prototype buildings located on Site Class C, in Vancouver, B.C., Canada. A force-based design methodology compatible with current Canadian codes and standard; NBCC 2015 and CSA S16/14 was used in design. A bare friction sliding braced frame (FSBF), a bare FSBF with continuous columns (FSBF-CC), and a Dual FSBF system where designed for R_dR_d = 4 and 5 and were modelled in OpenSees. Seismic performance of the buildings were assessed through nonlinear time-history analysis under two suites of ground motions: short duration crustal ground motions and long duration subduction ground motions. Incremental dynamic analysis was then completed to judge the overall structure response and failure modes. Lastly, collapse assessment was completed in accordance with FEMA P-695 and fragility analysis for performance levels such as: immediate occupancy (IO), reparability (R), and collapse prevention (CP) and the collapse safety was assessed for all systems. The following findings are reported from the study herein:

- The bare FSBF-I (R_dR_0=4) is not recommended to brace the 4-storey and 8-storey building located in subduction zone regions. The 4-storey FSBF-I building design was sufficient at design level for the crustal ground motions. For subduction ground motions, the 4-storey FSBF-I building does not pass the serviceability limit state, nor does it pass the reparability limit state of 0.5%h_s residual drift. The 8-storey building could not withstand the demand scaled to design level. The 4-storey FSBF-I building passes the collapse safety criteria under crustal GMs but fails under subduction GMs. Thus, using the bare FSBF-I is not recommended to brace even low-rise buildings in subduction zone regions.

- Continuous columns prototypes, FSBF-CC-I (R_dR_0=4), saw marginal improvements compared to the bare FSBF-I systems. The strength of 4-storey building, at design level demand, was sufficient in limiting the interstorey drift within the code limit under both crustal and subduction GM suites. However, at design level, the 4-storey building braced by FSBF-CC-I, still suffers from large residual interstorey drift especially under the subduction GM suite, which negatively affects the reparability of the structure after an earthquake event. Although the 4-storey FSBF-CC-I building passed the collapse safety criteria, the braced frame system does not pass the reparability criteria at design level and is not recommended to brace the 4-storey building.

- The FSBF-CC-I (R_dR_0=4) employed to brace the 8-storey prototype building fails to sustain the demand under all ground motions from the subduction GM suite scaled to design level. Under the scaled crustal GMs, the 8-storey FSBF-CC-I building experienced unacceptable transient and permanent interstorey drifts and fails under the subduction GM suite scaled to design level demand. The 8-storey FSBF-CC-I building did not pass the collapse safety criteria under both GM suites and the FSBF-CC-I system is not recommended to brace middle-rise buildings in subduction zone regions.

- Employing Dual systems, D-FSBF-I (R_dR_0=4) and D-FSBF-II (R_dR_0=5), leads to significant improvements in building response such as the interstorey drift and residual interstorey drift for both the 4-storey and 8-storey buildings. The backup MRF, designed to additional 25%V, possesses sufficient stiffness to provide elastic frame-action to the structure. Beams present in the backup MRF possess sufficient strength to not achieve failure before the induced failure of the friction devices and remain elastic at design level for both 4-storey and 8-storey buildings.

- The 4-storey D-FSBF-I and D-FSBF-II buildings possess sufficient strength and respond to serviceability limit state (interstorey drift within the 2.5%h_s code limit) and reparability criteria (residual interstorey drift below 0.5%h_s) under both GM suites scaled to design level. As determined by IDA, the reparability limit state occurs at higher intensities than the design level demand. Columns and beams of FSBF, as part of Dual system, show elastic behaviour that demonstrate the capacity design of the structure to be sufficient. Using D-FSBF-II is more economical, and the collapse safety criteria pass with sufficient safety margin. Employing D-FSBF-II system also leads to steel weight reduction of about 20%.

- For the 8-storey building, employing the D-FSBF-II (R_dR_0=5) system is less desirable because the reparability criteria is not satisfied (RISD > 0.5%hs) under both GM suites scaled to design level. Although both 8-storey D-FSBF-I and D-FSBF-II buildings pass the collapse safety criteria, the D-FSBF-I system is recommended for middle-rise buildings. Employing D-FSBF-I instead of D-FSBF-II results in a steel weight increase of about 7%.

- The energy dissipated by the friction devices was found to be highest in the devices located at the bottom floor of the structure for D-FSBF systems under crustal ground motions while the upper floor devices were the most solicited under subduction ground motions. This is explained by the characteristics of ground motions possessing large spectral ordinates in the short period range that excite the higher modes. Dual systems see sufficient stroke length in the friction devices at all floor levels to not have bearing occur near design level and only prior to failure under both crustal and subduction GM suites.

- Friction device model developed in OpenSees is sufficient in demonstrating the stable hysteretic behaviour seen from full-scale experimental testing. Furthermore, bearing phase modelling presents structures with the ability to observe the effects of sudden increased loads in the devices prior to failure.

- Fragility Analysis was conducted including aleatoric and epistemic uncertainties by considering the values retrieved by IDA. Probability of collapse at design level is significantly reduced for buildings braced by D-FSBF systems. For the 4-storey D-FSBF-II (R_dR_o = 5) building, at design level, the probability of collapse is 7% and 4% for crustal and subduction ground motions, respectively. For lower ductility, R_dR_o = 4, the corresponding probability of collapse is 1% for crustal and subduction ground motions. For 8-storey dual systems, the probability of collapse at design level is 33% and 13% under crustal and subduction, respectively for R_dR_o = 4. For higher ductility, the probability of collapse is 29% and 31% under crustal and subduction GMs.

7.2 Future Work

During the completion of the research herein, assumptions have had to be made which deserve further investigation. The following recommendations are made for future research regarding this topic:

- Buildings of higher heights should be considered.

- Design of buildings incorporating PFDs should be also conducted in moderate seismic zones in order to investigate their seismic response.

- Gusset plate tensile failure should be modelled in OpenSees and included in the overall structural models to observe the effects of the ductile secondary fuse.

- More in depth analysis of column base fixity of the backup MRF and a modelling of low-cycle fatigue of columns that can capture plastic hinging of columns and column shortening.

- More experimental evidence on the long-term efficacy of friction sliding devices including the devices' ability to maintain slip force over time, device wear after earthquake events, and failure mechanism.

References

Abrahamson, N. A., and Silva, W. J. (1997). "Empirical response spectral attenuation relations for shallow crustal earthquakes." *Seismological Research Letters*, 68(1), 94–109.

Aiken, I. D., Kelly, J. M., and Pall, A. (1988). "Seismic response of a nine-story steel frame with friction damped cross-bracing." *9th World Conference Earthquake Engineering*, Tokyo, Japan.

ASCE. (2000). *Minimum design loads for buildings and other structures*. *ANSI/ASCE Standard*.

ASCE. (2013). *ASCE 41-13 - Seismic Evaluation and Retrofit of Existing Buildings*. *American Society of Civil Engineers*.

Astaneh-Asl, A. (1998). *Seismic behavior and design of gusset plates for braced frames*. *Structural Steel Educational Council - Technical Information & Product Service*.

Atkinson, G. M., and Goda, K. (2011). "Effects of seismicity models and new ground-motion prediction equations on seismic hazard assessment for four Canadian cities." *Bulletin of the Seismological Society of America*, 101(1), 176–189.

Baker, J. W., and Cornell, A. (2006). "Spectral shape, epsilon and record selection." *Earthquake Engineering and Structural Dynamics*, 35, 1077–1095.

Baker, J. W., and Cornell, C. A. (2005). "A vector-valued ground motion intensity measure consisting of spectral acceleration and epsilon." *Earthquake Engineering and Structural*

Dynamics, 34(10), 1193–1217.

Balazic, J., Guruswamy, G., Elliot, J., Pall, R. T., and Pall, A. (2011). “Seismic Rehabilitation of Justice Headquarters Building Ottawa , Canada.” *12th World Conference on Earthquake Engineering*, 1–8.

Bertero, V. (1977). “Strength and deformation capacities of buildings under extreme environments.” *Structural Engineering and Structural Mechanics*, 211–215.

Bosco, M., and Tirca, L. (2017). “Numerical simulation of steel I-shaped beams using a fiber-based damage accumulation model.” *Journal of Constructional Steel Research*, Elsevier Ltd, 133, 241–255.

Bowden, F. P., and Tabor, D. (2001). *The Friction and Lubrication of Solids*. Oxford University Press.

Bruneau, M., and MacRae, G. (2017). *A Seismic Shift in Building Structural Systems: Reconstructing Christchurch*.

Chopra, A. K. (2012). *Dynamics of structures : theory and applications to earthquake engineering*. Pearson.

Clifton, C., Bruneau, M., Macrae, G., Leon, R., and Fussell, A. (2011). “Steel Building Damage from the Christchurch Earthquake Series of 2010/2011.” *Journal of the Structural Engineering Society New Zealand Inc.*, 24(2).

CSA S16. (2014). *S16-14 - Design of Steel Structures*. *Canadian Standards Association*.

Ellington, B. R., Celik, O. C., and Kinali, K. (2007). “Fragility assessment of building structural systems in Mid-America." *Earthquake Engineering and Structural Dynamics*, 36(13), 1–6.

Erochko, J., Christopoulos, C., Tremblay, R., and Choi, H. (2011). "Residual Drift Response of SMRFs and BRB Frames in Steel Buildings Designed according to ASCE 7-05." *Journal of Structural Engineering*, 137(5), 589–599.

FEMA. (2000). *FEMA 356 Prestandard and commentary for the seismic rehabilitation of buildings*.

FEMA. (2003). *FEMA 450. NEHRP Recomended Provisions for Seismic Regulations for New Buildings and Other Structures*.

FEMA. (2009). *Quantification of building seismic performance factors*. *FEMA P695*, Washington, DC.

Filiatrault, A. (1985). "Performance and Evaluation of Friction Damped Braced Frames under Simulated Earthquake Loads." University of British Columbia.

Filiatrault, A., Tremblay, R., and Kar, R. (2000). "Performance Evaluation of Friction Spring Seismic Damper." *Journal of Structural Engineering*, 126(4), 491–499.

Fitzgerald, T. F., Anagnos, T., Goodson, M., and Zsutty, T. (1989). "Slotted Bolted Connections in Aseismic Design for Concentrically Braced Connections." *Earthquake Spectra*, 5(2).

Giberson, M. F. (1969). "Two Nonlinear Beams With Definitions of Ductility." *Journal of the Structural Division*, American Society of Civil Engineers, 95(2), 137–157.

Jaisee, S., Yue, F., and Ooi, Y. H. (2021). "A state-of-the-art review on passive friction dampers and their applications." *Engineering Structures*, Elsevier, 235, 112022.

Ji, X., Kato, M., Wang, T., Hitaka, T., and Nakashima, M. (2009). “Effect of gravity columns on mitigation of drift concentration for braced frames.” *Journal of Constructional Steel Research*, Elsevier Ltd, 65(12), 2148–2156.

Joyner, W. B., and Boore, D. M. (1981). “Peak horizontal acceleration and velocity from strong-motion records including records from the 1979 imperial valley, California, earthquake.” *Bulletin of the Seismological Society of America*, 71(6), 2011–2038.

Kiggins, S., and Uang, C. M. (2006). “Reducing residual drift of buckling-restrained braced frames as a dual system.” *Engineering Structures*, 28(11), 1525–1532.

Lignos, D. G., Asce, A. M., Krawinkler, H., and Asce, M. (2011). “Deterioration Modeling of Steel Components in Support of Collapse Prediction of Steel Moment Frames under Earthquake Loading.”

Ludema, K. C., Arbor, A., Carlisle, S., and Schwartz, S. (1997). *Friction, wear, lubrication: a textbook in tribology*. *Choice Reviews Online*.

Lukkunaprasit, P., Wanitkorkul, A., and Filiatrault, A. (2004). “Performance Deterioration of Slotted-Bolted Connection Due to Bolt Impact and Remedy by Restrainers.” *13th World Conference on Earthquake Engineering*.

Macrae, G. A., Kimura, Y., and Roeder, C. (2004). “Effect of Column Stiffness on Braced Frame Seismic Behavior.” *Journal of Structural Engineering*, 130(3), 381–391.

McCormick, J., Aburano, H., Ikenaga, M., and Nakashima, M. (2008). “Permissible Residual Deformation Levels for Building Structures Considering both Safety and Human Elements.” *The 14th World Conference on Earthquake Engineering*, 8.

Morales, J. D. (2011). “Numerical Simulations of Steel Frames Equipped with Friction-Damped Diagonal- Bracing Devices.” Concordia University, Montreal, Canada.

National Research Council Canada. (2015). “NBCC 2015.” *Government of Canada*.

NEHRP. (2010). *Evaluation of the FEMA P-695 Methodology for Quantification of Building Seismic Performance Factors NEHRP Consultants Joint Venture A partnership of the Applied Technology Council and the Consortium of Universities for Research in Earthquake Engineering*.

Nims, D. K., Richter, P. J., and Bachman, R. E. (1993). “The use of the energy dissipating restraint for seismic hazard mitigation.” *Earthquake Spectra*, SAGE PublicationsSage UK: London, England, 9(3), 467–489.

Ohira, M. (2020). “Effects of Connections Detailing and Friction Dissipation Devices on the Seismic Response of a Hospital Steel Braced Frame Building.” Concordia University, Montreal, Quebec, Canada.

Pall, A. S., and Marsh, C. (1982). “Response of Friction Damped Braced Frames.” *Journal of the Structural Division*, American Society of Civil Engineers, 108(6), 1313–1323.

Pall, A. S., Marsh, C., and Fazio, P. (1980). “Friction joints for seismic control of large panel structures.” *Journal - Prestressed Concrete Institute*, 25(6), 38–61.

Pasquin, C., Leboeuf, N., and Pall, T. (2004). “Friction dampers for seismic rehabilitation of Eaton Building, Montreal.” *13th World Conference on Earthquake Engineering*, Vancouver, BC, Canada.

PEER/ATC 72-1. (2010). *Modeling and acceptance criteria for seismic design and analysis of* *tall buildings*. *Applied Technology Council*, Redwood City, CA.

Pettinga, D., Christopoulos, C., Pampanin, S., and Priestley, N. (2007). “Effectiveness of simple approaches in mitigating residual deformations in buildings.” *Earthquake Engineering & Structural Dynamics*, John Wiley & Sons, Ltd, 36(12), 1763–1783.

Qing, C., and Driver, R. G. (2008). *End tear-out failures of bolted tension members*. *University of Alberta*.

Ribeiro, F. L. A., Barbosa, A. R., Asce, M., Scott, M. H., and Neves, L. C. (2015). “Deterioration Modeling of Steel Moment Resisting Frames Using Finite-Length Plastic Hinge Force-Based Beam-Column Elements.” *Journal of Structural Engineering*, 141(2).

Roik, K., Dorka, U., and Dechent, P. (1988). “Vibration control of structures under earthquake loading by three-stage friction-grip elements.” *Earthquake Engineering & Structural Dynamics*, 16(4), 501–521.

Sahoo, D. R., and Chao, S.-H. (2015). “Stiffness-Based Design for Mitigation of Residual Displacements of Buckling-Restrained Braced Frames.” *Journal of Structural Engineering*, 141(9), 04014229.

Scott, M. H., and Ryan, K. L. (2013). “Moment-Rotation Behavior of Force-Based Plastic Hinge Elements.” *Earthquake Spectra*, 29(2), 597–607.

Song, J., and Der Kiureghian, A. (2006). “Generalized Bouc–Wen Model for Highly Asymmetric Hysteresis.” *Journal of Engineering Mechanics*, 132(6), 610–618.

Symans, M. D., Charney, F. A., Whittaker, A. S., Constantinou, M. C., Kircher, C. A., Johnson, M. W., and McNamara, R. J. (2008). “Energy Dissipation Systems for Seismic

Applications: Current Practice and Recent Developments." *Journal of Structural Engineering*, 134(1), 3–21.

Tirca, L., Serban, O., Lin, L., Wang, M., and Lin, N. (2016). "Improving the Seismic Resilience of Existing Braced-Frame Office Buildings." *Journal of Structural Engineering*, 142(8), 1–14.

Tirca, L., Serban, O., Tremblay, R., Jiang, Y., and Chen, L. (2018). "Seismic Design, Analysis, and Testing of a Friction Stell Braced Frame System for Multi-Storey Buildings in Vancouver." *Key Engineering Materials*, 763, 1077–1086.

Uriz, P., and Mahin, S. A. (2008). *Toward Earthquake-Resistant Design of Concentrically Braced Steel-Frame Structures*. *Pacific Earthquake Engineering Research Center*.

Vamvatsikos, D., and Cornell, C. A. (2001). "Incremental Dynamic Analysis." *Earthquake Engineering and Structural Dynamics*, 31(3), 491–514.

Wang, Y. (2018). "Seismic Performance of Steel Buildings with Braced Dual Configuration and Traditional Frame Systems through Nonlinear Collapse Simulations School of Graduate Studies Master of Applied Science (Civil Engineering)." Concordia University, Montreal, Canada.

Wen, Y. K. (1980). "Equivalent linearization for hysteretic systems under random excitation." *Journal of Applied Mechanics, Transactions ASME*, 47(1), 150–154.

Wen, Y. K. (1989). "Methods of random wibration for inelastic structures." *Applied Mechanics Reviews*, 42(2), 39–52.

Wen, Y. K., Ellingwood, B. R., and Bracci, J. (2004). *Vulnerability function framework for* *consequence-based engineering*. *Mid-America earthquake center project*.

Whittaker, A. S. (1990). *An experimental study of the behavior of dual steel systems*. *University of California at Berkeley*.

Yeo, G. L., Cornell, C. A., and University, D. of C. and E. E. S. (2005). *Stochastic Characterization and Decision Bases under Time-Dependent Aftershock Risk in Performance-Based Earthquake Engineering*.

Zareian, F., and Krawinkler, H. (2007). "Assessment of probability of collapse and design for collapse safety." *Earthquake Engineering and Structural Dynamics*, 36(13), 1901–1914.